

Ohta–Kawasaki energy for amphiphiles: asymptotics and phase-field simulations

Qiang Du* James M. Scott† Zirui Xu‡

Abstract

We study the minimizers of a degenerate case of the Ohta–Kawasaki energy, defined as the sum of the perimeter and a Coulombic nonlocal term. We start by investigating radially symmetric candidates which give us insights into the asymptotic behaviors of energy minimizers in the large mass limit. In order to numerically study the problems that are analytically challenging, we propose a phase-field reformulation which is shown to Gamma-converge to the original sharp interface model. Our phase-field simulations and asymptotic results suggest that the energy minimizers exhibit behaviors similar to the self-assembly of amphiphiles, including the formation of lipid bilayer membranes.

MSC 2020: 35B36, 35Q92, 49Q20

Keywords: variational model, nonlocal model, Gamma-convergence, phase-field model, pattern formation

Contents

1	Introduction	2
1.1	Background and motivation	2
1.2	Results in the existing literature	4
1.3	Our contributions	5
2	Radially symmetric candidates	7
2.1	Liposome candidates	7
2.2	Micelle candidates	8
2.3	Optimal candidates	9
3	Rescaled energy functional	10
3.1	Detailed asymptotics of liposome candidates	11
3.2	Conjectures about the Gamma-limits	13

*Department of Applied Physics and Applied Mathematics, and Data Science Institute, Columbia University, New York, NY 10027, USA. Email: qd2125@columbia.edu.

†Department of Applied Physics and Applied Mathematics, Columbia University, New York, NY 10027, USA. Email: jms2555@columbia.edu.

‡Department of Applied Physics and Applied Mathematics, Columbia University, New York, NY 10027, USA. Email: zx2250@columbia.edu. Corresponding author.

4	Phase-field reformulation	15
4.1	Diffuse interface energy	16
4.2	The sharp interface Gamma-limit	17
4.2.1	Compactness result	18
4.2.2	Liminf inequality	20
4.2.3	Limsup inequality	22
4.2.4	Convergence of global minimizers	25
4.3	Equivalence to the original problem	26
4.3.1	Justification for the relaxation	26
4.3.2	Justification for boundary conditions	27
5	Phase-field simulations	30
5.1	Simulations in 2-D	31
5.2	Simulations in 3-D	33
6	Discussion	37
A	Helfrich and Willmore energies	39
B	Calculations of radially symmetric candidates	40
C	Asymptotics with 1-Wasserstein distance	46

1 Introduction

1.1 Background and motivation

As soft condensed matter, amphiphiles are known to form various structures in aqueous environments. An amphiphilic molecule usually consists of a hydrophilic head and a hydrophobic tail connected by a covalent bond. Consequently, amphiphiles spontaneously arrange themselves in water in such a way that the hydrophobic tails are segregated from water, protected by the hydrophilic heads. Soft matter systems tend to self-assemble into lower-dimensional structures such as surfaces, curves and points, giving rise to sheet-like membranes, polymer networks and colloidal dispersions, respectively [56, Pages 107 and 108]. One particularly important example is the bilayer membrane formed by lipids in water, which exhibits both rigidity and fluidity in that the membrane resists deformation while allowing rapid lateral diffusion of lipid molecules within each monolayer. The elasticity of the membrane is very different from those of solid materials such as aluminum foil and plastic film. The membrane is soft, which is a crucial property for biological cells and artificial liposomes. The typical energies required to bend a membrane are small enough for thermal fluctuations at room temperature to be important [8, Pages 3 and 4]. Indeed, the bending elasticity of membranes is only a high-order effect, as will be discussed in Section 3.2.

At the macroscopic level, the Helfrich energy introduced in 1973 proved to be a successful continuum model for describing the elasticity of the lipid bilayer membrane (see Appendix A). In this model, the membrane is treated as a two-dimensional surface of zero thickness, with its energy given by the surface integral of a quadratic function in the principle curvatures. However, the actual membrane is of a bilayer structure and nonzero thickness (usually a few nanometers). In order to gain a detailed knowledge at

the microscopic level, an atomistic molecular dynamics simulation was carried out in 1992 [16]. Albeit accurate, such a simulation was time-consuming and thus restricted to a relatively small spatio-temporal scale ($60 \text{ nm}^3 \times 0.2 \text{ ns}$), rendering the physical processes of interest out of reach¹. Since our primary interest is not in individual atoms but rather in the collective behaviors of large numbers of atoms, it is natural to group several neighboring atoms into a single bead, leading to the so-called coarse-graining methods, which reduce the degrees of freedom and accelerate the computation [36, 8, 45, 55].

On an even coarser scale, a smooth density function is often used to represent the spatial distribution of each type of atoms or atom groups at the mesoscopic level. In 1986, Ohta and Kawasaki derived a density functional theory from statistical physics to explain the mesoscopic periodic patterns formed by diblock copolymers [13]. This theory was later generalized to triblock copolymers [53, 68] as well as mixtures of diblock copolymers and homopolymers [14]. The latter generalization was recently shown to be capable of modeling the lipid bilayer membrane along with its fusion processes [32], and we study a special case of such a generalization in this paper.

We focus on the sharp interface limit (also known as the strong segregation limit). In our energy, we let U and V denote the regions occupied by the hydrophobic tails and hydrophilic heads of the lipids, respectively. The rest of the space is occupied by water. As their names suggest, the hydrophobic tails are insoluble in water, while the hydrophilic heads are assumed to be miscible with water. Therefore, the interfacial tension exists only on the interface of U , but not on the V -water interface. An additional Coulombic term accounts for the covalent bonding between the hydrophobic tails and hydrophilic heads. This energy has been studied in the small mass regime in connection with the spherical micelle formed by amphiphilic surfactants in water [6]. In the large mass regime, although the question remains largely open, it is believed that the energy minimizers might resemble the lipid bilayer membrane [6, Page 4]. In fact, a variant of this energy (which makes use of the 1-Wasserstein distance) has been proposed to model the lipid bilayer membrane at the mesoscopic level [50, 43].

For two subsets U, V of \mathbb{R}^n satisfying $U \cap V = \emptyset$, we study the minimization problem of the following energy

$$E(U, V) = \text{Per } U + \gamma N(U, V), \quad (1)$$

under the mass constraints $|U| = m$ and $|V| = \zeta m$, where γ, m and ζ are positive constants. The local term $\text{Per } U$ is the standard perimeter of U (which equals the surface area for smooth $U \subseteq \mathbb{R}^3$). The nonlocal term N is defined as follows

$$2N(U, V) = \int_U \int_U G(\vec{x} - \vec{y}) \, d\vec{y} \, d\vec{x} - \frac{2}{\zeta} \int_U \int_V G(\vec{x} - \vec{y}) \, d\vec{y} \, d\vec{x} + \frac{1}{\zeta^2} \int_V \int_V G(\vec{x} - \vec{y}) \, d\vec{y} \, d\vec{x},$$

where the Newtonian kernel $G(\vec{x} - \vec{y}) = (4\pi|\vec{x} - \vec{y}|)^{-1}$ if $n = 3$, and $G(\vec{x} - \vec{y}) = -\ln|\vec{x} - \vec{y}|/(2\pi)$ if $n = 2$. In this paper we are mainly concerned with the three-dimensional (3-D, i.e., $n = 3$) case which is physically most relevant, and we will also consider the 2-D case ($n = 2$) for comparison purposes. Note that the 1-D case ($n = 1$) with $G(x - y) = -|x - y|/2$ and $\zeta = 1$ has been solved in [62, Section 3]: any local minimizer

¹In recent years, there have been significant improvements using machine learning and neural networks, and the state-of-the-art for 1.27×10^8 atoms is 0.8 ns per day on 4560 nodes of the Summit supercomputer with 27360 GPUs [37]. If they use an NVIDIA A100 GPU like we do in this paper, it would take them 25.6 years instead of 1 day. To put things into perspective, there are about 5×10^6 and 10^9 lipid molecules in a $1 \mu\text{m}^2$ lipid bilayer and in the plasma membrane of a small animal cell, respectively, with a typical lipid molecule (phosphatidylcholine) consisting of 130 atoms. If we also take into account the surrounding solvent molecules, then the number of atoms would be raised to the power of 3/2 (assuming that the simulation box is a cube). Therefore, for our study, the atomistic molecular dynamics simulations seem out of reach, especially because of the relatively slow kinetics of soft matter systems.

consists of one or multiple non-overlapping bilayer(s), such as two bilayers $VUV0VUV$ (where 0 represents a layer of water of arbitrary thickness, and any U layer is twice as thick as any V layer), and the global minimizer selects the local minimizer whose U layers are of thickness close to $\sqrt[3]{12/\gamma}$. We expect those 1-D results can be generalized to $\zeta \neq 1$.

Intuitively, we can imagine that U and V uniformly carry equal amounts of positive and negative charges, respectively, so that the total electrostatic potential energy arising from the electrostatic interactions is given by $N(U, V)$. We define the associated electrostatic potential ϕ as

$$\phi(\vec{x}) = \int_U G(\vec{x}-\vec{y}) d\vec{y} - \frac{1}{\zeta} \int_V G(\vec{x}-\vec{y}) d\vec{y}, \quad \vec{x} \in \mathbb{R}^n. \quad (2)$$

According to [6, Equation (2.6)], by noticing $-\Delta\phi = \mathbf{1}_U - \mathbf{1}_V/\zeta$, we can rewrite N as

$$N(U, V) = \frac{1}{2} \int_{\mathbb{R}^n} \phi(\vec{x}) \left(\mathbf{1}_U - \frac{\mathbf{1}_V}{\zeta} \right) (\vec{x}) d\vec{x} = -\frac{1}{2} \int_{\mathbb{R}^n} \phi(\vec{x}) \Delta\phi(\vec{x}) d\vec{x} = \frac{1}{2} \int_{\mathbb{R}^n} |\nabla\phi(\vec{x})|^2 d\vec{x}, \quad (3)$$

where $-\nabla\phi$ is the electrostatic field.

We mainly focus on the minimizers of the energy E in the large mass regime $m \gg 1$ with γ fixed. Or equivalently, we can fix m and let $\gamma \gg 1$, thanks to the scaling properties of the local and nonlocal terms.

1.2 Results in the existing literature

Throughout this subsection we fix $\gamma = 1$ and let m vary. In Proposition 1.1 we recall some existing results in 3-D ($n = 3$). It is believed that these results can be generalized to other dimensions $n \geq 2$ [6, Section 3.1].

Proposition 1.1. The following properties of E are known in the literature for $\zeta = 1$, and their proofs can be generalized to any $\zeta > 0$:

- ① For any $m > 0$, the global minimizer exists [6, Theorem 3.1].
- ② The global minimizer satisfies the regularity property [6, Theorem 3.2], i.e., there is a representative of (U, V) such that U and V are both open and bounded with finitely many connected components, and that ∂U is of differentiability class C^∞ .
- ③ The global minimizer satisfies the screening property [6, Theorem 2.1], i.e., there is a representative of (U, V) such that $\phi > 0$ in $U \cup V$, and that $\phi = 0$ in $\mathbb{R}^3 \setminus (U \cup V)$.
- ④ There exists $m_0 > 0$ such that a spherical micelle (see Definition 2.5 and Figure 3-c) is the unique global minimizer for $m < m_0$, and that it is not a global minimizer for $m > m_0$ [6, Theorem 3.5].
- ⑤ The global minimum of E has a lower bound and an upper bound. As $m \rightarrow \infty$, both bounds scale linearly with m [62, Section 4].

Next we give a brief review of existing studies for various ζ .

The case of $\zeta = 1$

In the large mass regime $m \gg 1$, only some qualitative properties of the energy minimizers are known in the literature, e.g., there is a uniform bound on the mean curvature of ∂U for the global minimizer for $m \geq 1$ [6, Page 9]. The exact global minimizer is unknown and is conjectured in several works (see [6, Figure 2(c) and Page 9] and [61, Bottom of Page 78]) to resemble a planar bilayer membrane, cut off at large distance.

In the literature there is a variant of the energy (1), with the nonlocal term N replaced by the 1-Wasserstein distance. For this variant, as $m \rightarrow \infty$, it is energetically preferable for U and V to form a closed bilayer membrane with an approximately uniform thickness [50, 43]. In [61, Bottom of Page 21] van Gennip mentioned a failed attempt to generalize this result from such a variant to the problem (1).

The case of $\zeta \ll 1$

In the limit of $\zeta \rightarrow 0$, the problem (1) reduces to the so-called surface charge model [7, Section 6]. For the global minimizer, the negative charge is concentrated on the surface of U , and acts like a Faraday shield canceling out the positive charge carried by U , i.e., we have $\phi = 0$ on $\mathbb{R}^3 \setminus \bar{U}$.

As mentioned above, for $\zeta = 1$ and $m \gg 1$ the global minimizer should locally resemble the bilayer membrane shown in Figure 3-a, where a layer of V of approximately uniform thickness surrounds U . For $\zeta \leq 1$ and $m \gg 1$, it is natural to expect that the global minimizer takes on a similar bilayer membrane structure, with the thickness of the V layer converging to 0 as $\zeta \rightarrow 0$.

The case of $\zeta \gg 1$

In the limit of $\zeta \rightarrow \infty$, the mass of V becomes infinitely large, and the negative charge carried by V becomes infinitely dilute, therefore the problem (1) reduces to the liquid drop model [69] where we only consider the positive charge carried by U . It is widely believed that the infimum of the energy in the liquid drop model is attained by a ball for $m \ll 1$, and is approached by many equally large distant balls for $m \gg 1$.

Therefore, for $\zeta \gg 1$, it is natural to expect the global minimizer to be a micelle for $m \ll 1$, and to be the union of many equally large non-overlapping micelles for $m \gg 1$.

1.3 Our contributions

We now summarize our main contributions and then outline the overall structure of the rest of this paper.

As mentioned in Section 1.2, regarding the global minimizer for $\zeta = 1$ and $m \gg 1$, several works (e.g., [6, Figure 2(c) and Page 9] and [61, Bottom of Page 78]) documented the belief that U is approximately a large disk with a radius of order \sqrt{m} and with a thickness of order 1, and that V is of an approximately uniform thickness surrounding U , as can be seen from our numerical simulations in Figure 9. However, our numerical results indicate that such a disk-shaped membrane has higher energy than a liposome (see Definition 2.1) for $\zeta = 1$ and $m \gg 1$. In Figure 9, the disk-shaped membrane is slightly thicker near its rim, and thus the rim carries an energy penalty of order \sqrt{m} , proportional to the circumference. Therefore for the disk-shaped membrane, the energy-to-mass ratio E/m converges with order $1/\sqrt{m}$, which is consistent with [62, Theorem 8]. Meanwhile, according to Corollary 2.2, the convergence rate for the liposome is $1/m$. Note that the infimum of E/m is attained in the limit of $m \rightarrow \infty$ [6, Proposition 8.3]. Our work suggests that the liposome is the global minimizer for $\zeta = 1$ and $m \gg 1$, since a sphere minimizes the Helfrich energy in Proposition 3.10.

In the existing literature, the equal mass case $\zeta = 1$ has been the focal point of most studies (e.g., [7, 6, 61, 64, 63, 62], except for a 1-D study [14]). In this paper we consider the general cases $\zeta \in (0, \infty)$. As mentioned in the paragraph following (1), the 1-D results should be qualitatively the same for different ζ . But as we will illustrate in Figure 3, as ζ increases, the optimal morphology in 3-D should undergo transitions from the bilayer membrane to cylindrical micelle to spherical micelle. As mentioned in Section 1.2, in the large mass regime, it is natural to expect that for sufficiently large ζ , the global minimizer consists of many spherical micelles which are scattered and non-overlapping, as depicted in Figure 3-c. Meanwhile, for intermediately large ζ , it is natural to expect the global minimizer to resemble a cylindrical micelle, see Figure 3-b.

In Sections 2.1 and 3.1, we use asymptotic analysis to study the energy minimizer among radially symmetric liposome candidates for $\zeta > 0$ and $m \gg 1$. An important finding is that the inner V layer is slightly thicker but has slightly less mass compared to the outer V layer. Interestingly, we notice that such slight differences also exist in a variant model (at least in 2-D), where the Coulombic nonlocal term N is replaced by the 1-Wasserstein distance, as mentioned in Remark 3.6-③. If we impose equal mass on the inner and outer V layers at the expense of optimality, then the energy in our model will increase on the same order as the bending energy, as mentioned in Remark 3.6-②.

For a general bilayer membrane which is not necessarily radially symmetric, up to a suitable rescaling, we can consider its Gamma-limit with vanishing thickness as $\gamma \rightarrow \infty$. Under the conjecture that its energy converges to the Helfrich energy, in Proposition 3.10 we calculate the bending and Gaussian moduli using our asymptotic results for 2-D and 3-D radially symmetric liposome candidates (note that a 2-D circular liposome may be viewed as a 3-D cylindrical bilayer which resembles a very long tube [65, Middle of Figure 1]). Our calculation reveals that for small ζ , the Gaussian modulus is positive, and thus the optimal structure may resemble triply periodic minimal surfaces (TPMS) which exist ubiquitously in copolymer systems and biological specimens (see Remark 3.11).

In Figure 1 we summarize the conjectured candidates for 3-D global minimizers in the large mass regime, with the parameters ζ_i to be defined later. For $\zeta < \zeta_1$, we believe that the local structure of the global minimizer resembles a bilayer membrane, and that its global structure is a liposome ($\zeta_0 < \zeta < \zeta_1$) or approximately a TPMS ($\zeta < \zeta_0$). For $\zeta_1 < \zeta < \zeta_2$, its local structure resembles a cylindrical micelle, and its global structure resembles a circular ring. For $\zeta > \zeta_2$, the global minimizer consists of many scattered droplets of spherical micelles.

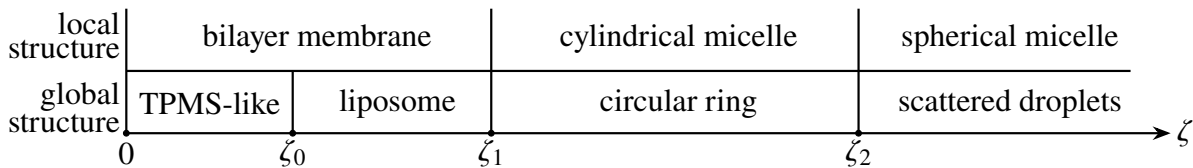


Figure 1: Our conjectures about the 3-D global minimizer for $m \gg 1$.

In Section 5, we present numerical evidence for our conjectures. The numerical simulations are based on a phase-field reformulation of the sharp interface model (1). In order to justify such a reformulation, we prove a Gamma-convergence result in Section 4. The novelty of the proof is that our phase-field energy is degenerate: only one of the two order parameters is penalized by the Dirichlet energy, and the potential well has non-isolated minimizers. The rest of this paper is organized as follows. In Section 2, we restrict ourselves to the simplest radially symmetric case and derive some asymptotic results. In order to better

present our asymptotic results, in Section 3 we rescale the energy and propose some conjectures. In Section 4 we present our phase-field reformulation and prove its Gamma-convergence to the sharp interface model. In Section 5 we present some numerical simulations. In Section 6, we conclude with remarks about future directions. In Appendix A we provide some background knowledge on the Helfrich and Willmore energies. In Appendix B, we present the detailed calculations in the radially symmetric case. In Appendix C, we recall the results in a variant model where the Coulombic nonlocal term is replaced by the 1-Wasserstein distance, in order to make it convenient for readers to draw comparisons.

2 Radially symmetric candidates

In this section, we only consider radially symmetric candidates, thus reducing the variational problem to a finite-dimensional optimization problem which can be analyzed asymptotically. We obtain the asymptotic expansions of the minimum energy and the optimal layer thickness, thus laying the foundation for further studies of non-radially-symmetric cases. In Sections 2.1 and 2.2, we consider two types of candidates, namely liposome and micelle, as depicted in Figure 2, and then draw comparisons in Section 2.3.



Figure 2: Left: a portion of a liposome candidate. Right: a portion of a micelle candidate. Both are radially symmetric.

2.1 Liposome candidates

Liposome candidates are concentric rings or shells as shown on the left of Figure 2. More specifically, we have the following definition.

Definition 2.1. We say (U, V) is a liposome candidate, if $U, V \subseteq \mathbb{R}^n$ satisfy

- ① $U = B(R_2) \setminus B(R_1)$ and $V = (B(R_3) \setminus B(R_2)) \cup (B(R_1) \setminus B(R_0))$ for some $0 < R_0 < R_1 < R_2 < R_3$, where $B(R_i)$ is an n -dimensional ball of radius R_i centered at the origin O .
- ② R_i satisfies the following mass constraints

$$R_3^n - R_0^n = (\zeta + 1)(R_2^n - R_1^n), \quad (4)$$

$$R_2^n - R_1^n = \begin{cases} m/\pi, & n = 2, \\ 3m/(4\pi), & n = 3. \end{cases} \quad (5)$$

Corollary 2.2. [of Theorem B.3] With ζ and γ fixed, as $m \rightarrow \infty$, the minimizer of $E(U, V)$ among the liposome candidates satisfies

$$(R_1 - R_0, R_2 - R_1, R_3 - R_2) \rightarrow \sqrt[3]{3/(\gamma\zeta + \gamma)}(\zeta, 2, \zeta), \quad (6)$$

with the following asymptotics

$$\frac{E(U, V)}{m} = \begin{cases} \sqrt[3]{\gamma \frac{\zeta+1}{8/9}} + \frac{8\pi^2}{5} \frac{\zeta^2+4\zeta+1}{\gamma(\zeta+1)m^2} + O\left(\frac{1}{m^3}\right), & \text{for } n = 2, \\ \sqrt[3]{\gamma \frac{\zeta+1}{8/9}} + \frac{4\pi}{15m} \frac{\zeta^2+4\zeta+16}{(\gamma(\zeta+1)/3)^{2/3}} + O\left(\frac{1}{m^{3/2}}\right), & \text{for } n = 3. \end{cases}$$

Corollary 2.3. [of Proposition B.4] Under the additional assumption that the inner and outer V layers have the same mass [61, Equation (5.16)], i.e., $R_3^n - R_2^n = R_1^n - R_0^n$, with ζ and γ fixed, as $m \rightarrow \infty$, the minimizer of $E(U, V)$ among the liposome candidates still satisfies (6), with the following asymptotics

$$\frac{E(U, V)}{m} = \begin{cases} \sqrt[3]{\gamma \frac{\zeta+1}{8/9}} + 24\pi^2 \frac{2\zeta^2+8\zeta+7}{5\gamma(\zeta+1)m^2} + O\left(\frac{1}{m^3}\right), & \text{for } n = 2, \\ \sqrt[3]{\gamma \frac{\zeta+1}{8/9}} + \frac{4\pi}{5m} \frac{7\zeta^2+28\zeta+32}{(\gamma(\zeta+1)/3)^{2/3}} + O\left(\frac{1}{m^{3/2}}\right), & \text{for } n = 3. \end{cases}$$

Remark 2.4.

- ① The additional assumption in Corollary 2.3 was used in [61, Pages 83 and 84]. Albeit not the optimal choice, it was thought to be only slightly non-optimal. Our calculations show that the leading-order term of the energy remains the same under this additional assumption, but that the next-order term (corresponding to the bending energy) becomes 6 to 21 times as large, depending on n and ζ . In other words, the bending energy can be decreased by dropping this additional assumption and allowing the inner and outer V layers to have different masses.
- ② From (6) we know that $R_{i+1} - R_i$ converges to a constant as $m \rightarrow \infty$. This can serve as an illustration that the lipid bilayer has an intrinsically preferred thickness, which is consistent with [62, Remark 4]. In the large mass regime $m \gg 1$, the bilayer should be of thickness of order 1.

2.2 Micelle candidates

Definition 2.5. In Definition 2.1, if $R_0 = R_1 = 0$, then (U, V) is called a micelle candidate. (Note that for $n = 2$, in some literature [1] the terminology core-shell is used instead.)

Proposition 2.6. The energy (1) of a micelle candidate is $E(U, V) = \text{Per } U + \gamma N(U, V)$, where

$$\text{Per } U = \begin{cases} 2\pi\sqrt{m/\pi}, & n = 2, \\ 4\pi(3m/(4\pi))^{2/3}, & n = 3, \end{cases}$$

and

$$N(U, V) = \begin{cases} \pi\zeta^{-2}(\zeta+1)((\zeta+1)\ln(\zeta+1)-\zeta)(m/\pi)^2/8, & n = 2, \\ \pi\zeta^{-2}(\zeta+1)(4\zeta+6-6(\zeta+1)^{2/3})(3m/(4\pi))^{5/3}/15, & n = 3. \end{cases} \quad (7)$$

Proof. Proposition 2.6 is a consequence of Proposition B.1 with $R_0 = R_1 = 0$ and

$$R_3^n/(\zeta+1) = R_2^n = \begin{cases} m/\pi, & n = 2, \\ 3m/(4\pi), & n = 3. \end{cases}$$

□

Corollary 2.7. For a micelle candidate, if $n = 2$, then E/m attains its minimum at

$$m = 4\pi \left(\gamma(\zeta+1)((\zeta+1) \ln(\zeta+1) - \zeta)/\zeta^2 \right)^{-2/3}, \quad \text{and} \quad \min_{m>0} \frac{E}{m} = \frac{3}{2} \sqrt[3]{\gamma\zeta^{-2}(\zeta+1)((\zeta+1) \ln(\zeta+1) - \zeta)};$$

if $n = 3$, then E/m attains its minimum at

$$m = 20\pi\zeta^2 (\gamma(\zeta+1))^{-1} / (2\zeta+3-3(\zeta+1)^{2/3}), \quad \text{and} \quad \min_{m>0} \frac{E}{m} = \frac{9}{2} \sqrt[3]{\gamma\zeta^{-2}(\zeta+1)(2\zeta+3-3(\zeta+1)^{2/3})/15}.$$

Remark 2.8.

- ① Due to the screening property (see Proposition 1.1-③), for the disjoint union of non-overlapping components, the energy is simply the sum of the energy for each connected component. Therefore, in the large mass regime $m \gg 1$, we can construct a candidate consisting of many non-overlapping micelles, each of which has a mass close to the optimal mass given in Corollary 2.7 (similar to the construction mentioned in [62, Page 96]). Such a candidate will attain the optimal energy-to-mass ratio asymptotically as $m \rightarrow \infty$. In fact, our energy in Proposition 2.6 is of a similar form to [12, Equation (6.1)]. Using the same approach as [12, Proof of Lemma 6.2], we can prove that the optimal way to allocate the mass m is as follows: let m_i (assuming $m_i > 0$) be the mass of each connected component, then all but one m_i (say, $\{m_i\}_{i \neq 1}$) must be equal, with $m_1 = O(1)$. Therefore, in the large mass limit $m \rightarrow \infty$, the optimal way to allocate the mass yields asymptotically the same energy-to-mass ratio as Corollary 2.7.
- ② According to [62, Theorem 8], we can regard a 2-D micelle as the limiting case of an infinitely long 3-D cylindrical micelle, with asymptotically the same energy-to-mass ratio.
- ③ We have also considered the candidates with $R_0 = 0$ and $R_1 > 0$, and they always have higher energy-to-mass ratios than the liposome candidates in the large mass limit, according to our calculations. Therefore, they are omitted in our discussions.

2.3 Optimal candidates

We now compare the candidates that are considered in Sections 2.1 and 2.2. By comparing the leading-order term of E/m in Corollaries 2.2 and 2.7, we are led to the belief that in the large mass regime in 3-D, as ζ increases, the preferred morphology should be successively bilayer membrane, cylindrical micelle, and spherical micelle, as shown in Figure 3. This picture is qualitatively consistent with the predictions by other theories [4, Section 1.3.2.3].

Conjecture 2.9. Let $n = 3$. For any fixed $\gamma > 0$ and $\zeta > \zeta_0$ (where ζ_0 is defined in Remark 3.11-②, for reasons that will be mentioned therein), we have $\inf_{U,V} E(U,V)/m \rightarrow c(\zeta) \sqrt[3]{\gamma}$ as $m \rightarrow \infty$, where

$$c(\zeta) = \begin{cases} \sqrt[3]{9(\zeta+1)/8}, & \text{if } 0 < \zeta \leq \zeta_1, \\ \frac{3}{2} \sqrt[3]{\zeta^{-2}(\zeta+1)((\zeta+1) \ln(\zeta+1) - \zeta)}, & \text{if } \zeta_1 < \zeta \leq \zeta_2, \\ \frac{9}{2} \sqrt[3]{\zeta^{-2}(\zeta+1)(2\zeta+3-3(\zeta+1)^{2/3})/15}, & \text{if } \zeta_2 < \zeta < \infty. \end{cases}$$

Here $\zeta_1 \approx 1.81696$ is the unique nonzero root of $\zeta + \zeta^2/3 = (\zeta+1) \ln(\zeta+1)$, and $\zeta_2 \approx 3.64572$ is the unique nonzero root of $5((\zeta+1) \ln(\zeta+1) - \zeta) = 9(2\zeta - 3(\zeta+1)^{2/3} + 3)$.

Remark 2.10.

- ① The piecewise function $c(\zeta)$ is plotted on the left of Figure 3, where ζ_1 and ζ_2 are also marked. As ζ increases, the minimum energy is attained on different branches indicated by different colors, and the preferred morphology should transition from bilayer membrane to cylindrical micelle to spherical micelle, which are illustrated by Figure 3-a, b and c, respectively.
- ② In [61, Section 5.3], van Gennip also compared the energy among the bilayer membrane, cylindrical micelle, and spherical micelle candidates. However, van Gennip only considered the case of $\zeta = 1$, and concluded that the bilayer membrane has the lowest energy among all the candidates. Our calculations reveal that cylindrical micelle and spherical micelle may have lower energy for $\zeta \neq 1$, and that amphiphiles can self-assemble into not only sheet-like membranes, but also polymer networks and colloidal dispersions.

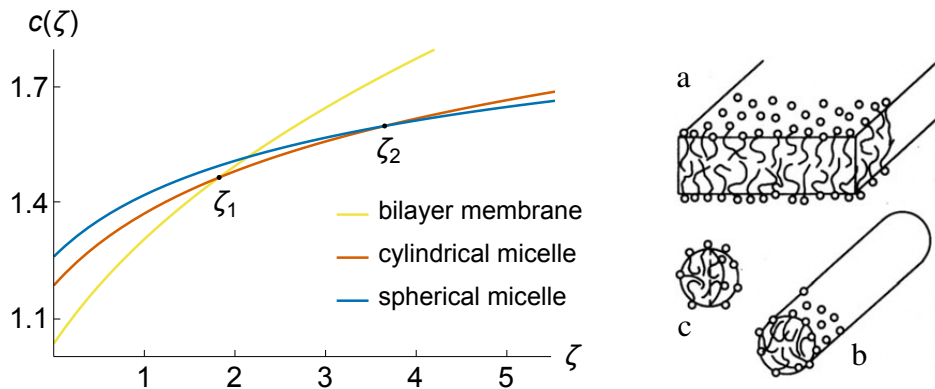


Figure 3: Left: Three branches of $c(\zeta)$. Right: a, bilayer membrane; b, cylindrical micelle; c, spherical micelle. The right image is reproduced from [4, Figure 1.6].

3 Rescaled energy functional

In Section 2, we have briefly presented some asymptotic results as $m \rightarrow \infty$. In order to make it convenient and rigorous to translate our asymptotic results within the Gamma-convergence framework, in this section

we rescale the energy functional so that the minimizer converges in Radon measure to lower-dimensional structures (surfaces, curves and points). In Section 3.1, we elaborate on the asymptotic results of the liposome candidates for the rescaled energy, and in Section 3.2, we propose some conjectures about Gamma-convergence of the rescaled energy.

Definition 3.1. Analogous to [50], we define a rescaled version of (1):

$$F_\rho(u, v) = \begin{cases} \rho^{1-d} \text{Per } U + \rho^{-2-d} N(U, V), & \text{if } (u, v) \in K_\rho, \\ \infty, & \text{otherwise,} \end{cases}$$

where d can be chosen from $\{1, 2, 3\}$ as needed, $U = \text{supp}(u)$ and $V = \text{supp}(v)$. Moreover,

$$K_\rho = \{(u, v) \in BV(\mathbb{R}^n; \{0, \rho^{-d}\}) \times L^2(\mathbb{R}^n; \{0, \rho^{-d}\}) : vu = 0 \text{ a.e., } \int u = m, \int v = \zeta m\}.$$

Proposition 3.2. Denote U_ρ to be the dilation of U with a scale factor of $1/\rho$, i.e., $\vec{x} \in U \Leftrightarrow U_\rho \ni \vec{x}/\rho$, and similarly for V_ρ . Then we have $|U_\rho|/\int u = \rho^{d-n} = |V_\rho|/\int v$ and $\rho^{d-n} F_\rho(u, v) = \text{Per } U_\rho + N(U_\rho, V_\rho)$, where $u = \mathbf{1}_U/\rho^d$ and $v = \mathbf{1}_V/\rho^d$.

Proof. Use the scaling properties of the perimeter and Newtonian potential. \square

Remark 3.3. According to Proposition 3.2, F_ρ is equivalent to E up to a rescaling, and thus the results in Proposition 1.1 also apply to F_ρ : for any $\zeta, m, \rho > 0$ and for any d , the global minimizer of F_ρ exists and satisfies the screening property.

3.1 Detailed asymptotics of liposome candidates

Throughout this subsection, we let $d = 1$. We consider liposome candidates given by $U = B(R_2) \setminus B(R_1)$ and $V = (B(R_3) \setminus B(R_2)) \cup (B(R_1) \setminus B(R_0))$ for some $0 < R_0 < R_1 < R_2 < R_3$ satisfying $R_3^n - R_0^n = (\zeta + 1)(R_2^n - R_1^n)$ and

$$R_2^n - R_1^n = \begin{cases} m\rho/\pi, & n = 2, \\ 3m\rho/(4\pi), & n = 3, \end{cases}$$

where $B(R_i)$ is an n -dimensional ball of radius R_i centered at the origin O (see also Definition 2.1).

Corollary 3.4. [of Proposition 3.2 and Theorem B.3.] Let $d = 1$, with ζ and m fixed, as $\rho \rightarrow 0$, the minimizer of F_ρ among the liposome candidates has the following asymptotics if $n = 2$,

$$\begin{aligned} \frac{F_\rho(u, v)}{m} &= \sqrt[3]{\frac{\zeta+1}{8/9}} + 8\pi^2 \rho^2 \frac{\zeta^2+4\zeta+1}{5(\zeta+1)m^2} + O(\rho^3), & R_2 - R_1 &= \rho \sqrt[3]{\frac{24}{\zeta+1}} + O(\rho^3), \\ (R_3^2 - R_2^2) - (R_1^2 - R_0^2) &= \frac{4\rho^2 \zeta(\zeta+2)}{\sqrt[3]{3(\zeta+1)^2}} + O(\rho^3), & \frac{R_1 + R_2}{2} &= \frac{m}{4\pi} \sqrt[3]{\frac{\zeta+1}{3}} + O(\rho^2), \\ R_1 - R_0 &= \rho \sqrt[3]{\frac{3\zeta^3}{\zeta+1}} + \frac{2\pi\rho^2}{m/\zeta} \frac{\zeta+2}{\zeta+1} + O(\rho^3), & R_3 - R_2 &= \rho \sqrt[3]{\frac{3\zeta^3}{\zeta+1}} - \frac{2\pi\rho^2}{m/\zeta} \frac{\zeta+2}{\zeta+1} + O(\rho^3), \end{aligned}$$

and has the following asymptotics if $n = 3$,

$$\begin{aligned} \frac{F_\rho(u, v)}{m} &= \sqrt[3]{\frac{\zeta+1}{8/9}} + \frac{4\pi\rho^2}{15m} \frac{\zeta^2+4\zeta+16}{((\zeta+1)/3)^{2/3}} + O(\rho^3), & R_2 - R_1 &= \rho \sqrt[3]{\frac{24}{\zeta+1}} + O(\rho^3), \\ (R_3^3 - R_2^3) - (R_1^3 - R_0^3) &= \frac{\rho^2 \sqrt{m} \zeta (\zeta+2)}{\sqrt{\pi}(\zeta+1)/6} + O(\rho^3), & \frac{R_1+R_2}{2} &= \frac{\sqrt[6]{(\zeta+1)/3}}{2\sqrt{2\pi/m}} + O(\rho^2), \\ R_1 - R_0 &= \rho \sqrt[3]{\frac{3\zeta^3}{\zeta+1}} + \frac{\sqrt{8\pi}(\zeta+2)\zeta\rho^2}{\sqrt{m}\sqrt[6]{3(\zeta+1)^5}} + O(\rho^3), & R_3 - R_2 &= \rho \sqrt[3]{\frac{3\zeta^3}{\zeta+1}} - \frac{\sqrt{8\pi}(\zeta+2)\zeta\rho^2}{\sqrt{m}\sqrt[6]{3(\zeta+1)^5}} + O(\rho^3). \end{aligned}$$

Corollary 3.5. [of Propositions 3.2 and B.4.] Under the additional assumption that the inner and outer V layers have the same mass [61, Equation (5.16)], i.e., $R_3^n - R_2^n = R_1^n - R_0^n$, let $d = 1$, with ζ and m fixed, as $\rho \rightarrow 0$, the minimizer of F_ρ among the liposome candidates has the following asymptotics if $n = 2$,

$$\begin{aligned} \frac{F_\rho(u, v)}{m} &= \sqrt[3]{\frac{\zeta+1}{8/9}} + 24\pi^2 \rho^2 \frac{2\zeta^2+8\zeta+7}{5(\zeta+1)m^2} + O(\rho^3), \\ R_1 - R_0 &= \rho \sqrt[3]{\frac{3\zeta^3}{\zeta+1}} + \frac{6\pi\rho^2}{m/\zeta} \frac{\zeta+2}{\zeta+1} + O(\rho^3), & R_2 - R_1 &= \rho \sqrt[3]{\frac{24}{\zeta+1}} + O(\rho^3), \\ R_3 - R_2 &= \rho \sqrt[3]{\frac{3\zeta^3}{\zeta+1}} - \frac{6\pi\rho^2}{m/\zeta} \frac{\zeta+2}{\zeta+1} + O(\rho^3), & \frac{R_1+R_2}{2} &= \frac{m}{4\pi} \sqrt[3]{\frac{\zeta+1}{3}} + O(\rho^2), \end{aligned}$$

and has the following asymptotics if $n = 3$,

$$\begin{aligned} \frac{F_\rho(u, v)}{m} &= \sqrt[3]{\frac{\zeta+1}{8/9}} + \rho^2 \frac{4\pi}{5m} \frac{7\zeta^2+28\zeta+32}{((\zeta+1)/3)^{2/3}} + O(\rho^3), \\ R_1 - R_0 &= \rho \sqrt[3]{\frac{3\zeta^3}{\zeta+1}} + \frac{\sqrt{8\pi}(\zeta+2)\zeta\rho^2}{\sqrt{m}\sqrt[6]{(\zeta+1)^5/3^5}} + O(\rho^3), & R_2 - R_1 &= \rho \sqrt[3]{\frac{24}{\zeta+1}} + O(\rho^3), \\ R_3 - R_2 &= \rho \sqrt[3]{\frac{3\zeta^3}{\zeta+1}} - \frac{\sqrt{8\pi}(\zeta+2)\zeta\rho^2}{\sqrt{m}\sqrt[6]{(\zeta+1)^5/3^5}} + O(\rho^3), & \frac{R_1+R_2}{2} &= \frac{\sqrt[6]{(\zeta+1)/3}}{2\sqrt{2\pi/m}} + O(\rho^2). \end{aligned}$$

Remark 3.6.

- ① Due to the curvature of the bilayer, the inner V layer is slightly thicker than the outer V layer (i.e., $R_1 - R_0 > R_3 - R_2$), and F_ρ is penalized for bending on the second order (i.e., the ρ^2 term corresponding to the bending energy).
- ② Under the equal mass assumption $R_3^n - R_2^n = R_1^n - R_0^n$, the second-order term of F_ρ is 6 to 21 times as large as that of the optimal liposome candidate whose inner V layer has slightly less mass than the outer V layer.
- ③ Under the equal mass assumption, the difference in the thickness between the inner and outer V layers is asymptotically three times that of the optimal liposome candidate, in both 2-D and 3-D. This relation is also true at least in 2-D even if the Coulombic nonlocal term N is replaced by the 1-Wasserstein distance (see Appendix C). It is therefore natural to wonder how universal this relation can be.

3.2 Conjectures about the Gamma-limits

We now propose some conjectures about the Gamma-limits of the energy functional $F'_\rho := (F_\rho - c(\zeta) m) / \rho^2$ as $\rho \rightarrow 0$. Throughout this subsection, d is chosen to be the codimension of the expected geometry of the global minimizer as shown in Figure 3:

$$d = \begin{cases} 1, & \text{if } 0 < \zeta \leq \zeta_1 \text{ and } n = 2, \\ 2, & \text{if } \zeta_1 < \zeta < \infty \text{ and } n = 2, \end{cases} \quad d = \begin{cases} 1, & \text{if } 0 < \zeta \leq \zeta_1 \text{ and } n = 3, \\ 2, & \text{if } \zeta_1 < \zeta \leq \zeta_2 \text{ and } n = 3, \\ 3, & \text{if } \zeta_2 < \zeta < \infty \text{ and } n = 3, \end{cases}$$

where ζ_1 and ζ_2 are defined in Conjecture 2.9.

Conjecture 3.7. Let $n = 2$ and $\rho \rightarrow 0$. For $\zeta \in (0, \zeta_1)$, the Gamma-limit of F'_ρ is the elastica functional defined for closed $W^{2,2}$ curves in \mathbb{R}^2 in the sense of Radon measure, similar to the elastica functional \mathcal{W} mentioned in [50, Theorem 4.1]. For $\zeta \in (\zeta_1, \infty)$, the Gamma-limit of F'_ρ is a mass partition functional defined for weighted Dirac delta point measures, similar to the mass partition functional E_0^{2d} mentioned in [12, Theorem 6.1] (see also the mass partition functional E_0 mentioned in [1, Theorem 4.2]).

Conjecture 3.8. Let $n = 3$ and $\rho \rightarrow 0$. For $\zeta \in (\zeta_0, \zeta_1)$, the Gamma-limit of F'_ρ is a quadratic form in the principal curvatures defined for closed surfaces in the sense of Radon measure, similar to [43, Conjecture 2.4]. For $\zeta \in (\zeta_1, \zeta_2)$, the Gamma-limit of F'_ρ is the elastica functional defined for closed $W^{2,2}$ curves in \mathbb{R}^3 in the sense of Radon measure, which is a 3-D generalization of [50, Theorem 4.1]. For $\zeta \in (\zeta_2, \infty)$, the Gamma-limit of F'_ρ is a mass partition functional defined for weighted Dirac delta point measures, similar to the mass partition functional E_0^{3d} mentioned in [12, Theorem 4.3].

If the first statement in Conjecture 3.7 and the second statement in Conjecture 3.8 are correct, then Proposition 3.9 tells us that the global minimizer should resemble a circle.

Proposition 3.9. Let C be a closed $W^{2,2}$ curve in \mathbb{R}^3 with a prescribed length, and let κ be its curvature, then the elastica functional $\int_C \kappa^2 ds$ is minimized when C is a circle.

Proof. The length of C is given by $\int_C 1 ds$ and is assumed to be fixed. By Cauchy–Schwarz inequality we have $\int_C 1^2 ds \int_C \kappa^2 ds \geq (\int_C |\kappa| ds)^2 \geq 4\pi^2$, where the second inequality is due to [67, Theorem 7.2.3] and becomes an equality if and only if C is a planar convex curve. \square

Proposition 3.10. Assuming the first statement in Conjecture 3.8 is correct, i.e., for $n = 3$ and $\zeta \in (\zeta_0, \zeta_1)$, the Gamma-limit of F'_ρ is of the following quadratic form (cf. Appendix A for Helfrich and Willmore energies)

$$\int_S (\lambda_1 H^2 + \lambda_2 K) dA, \quad (8)$$

where $H = (\kappa_1 + \kappa_2)/2$ (with κ_1 and κ_2 being principal curvatures, positive if S is a sphere), $K = \kappa_1 \kappa_2$, and $\lambda_1, \lambda_2 \in \mathbb{R}$. If the recovery sequence is given by a bilayer with the middle U layer of uniform thickness (similar to the construction in [43, Section 4]), then we have

$$\lambda_1 = \frac{4}{15} \frac{1+4\zeta+\zeta^2}{((\zeta+1)/3)^{2/3}}, \quad \lambda_2 = \frac{4-4\zeta-\zeta^2}{5((\zeta+1)/3)^{2/3}}. \quad (9)$$

Proof. According to Proposition B.2 and the Proof of Proposition B.1, the liposome candidates shown in Corollary 3.4 satisfy the screening property. For any fixed U , there exists a unique V satisfying the screening property [7, Remark 4.2], which is a necessary condition for a minimizer (Proposition 1.1-(3)). Therefore, for the Radon measure of a sphere in 3-D, the recovery sequence is by assumption given by radially symmetric liposome candidates in 3-D. According to [62, Theorem 8], the 2-D liposome candidate can be regarded as a 3-D cylindrical bilayer which resembles a very long tube [65, Middle of Figure 1]. For a sphere in 3-D with radius R , we have $K = 1/R^2$ and $H = 1/R$. According to Corollary 3.4, we have

$$\frac{4\pi}{15} \frac{\zeta^2 + 4\zeta + 16}{((\zeta + 1)/3)^{2/3}} = 4\pi R^2 (\lambda_1/R^2 + \lambda_2/R^2).$$

For a cylinder in 3-D with length L and radius R , we have $K = 0$ and $H = 1/(2R)$. Similarly, we have

$$8\pi^2 \frac{\zeta^2 + 4\zeta + 1}{5(\zeta + 1)m} L = 2\pi RL (\lambda_1/(2R)^2 + \lambda_2 \cdot 0).$$

In Corollary 3.4, the radius R of the 2-D liposome candidate can be approximated by $(R_1 + R_2)/2 \approx m\sqrt[3]{(\zeta + 1)/3}/(4\pi)$. Therefore the coefficients λ_1 and λ_2 can be determined. \square

Remark 3.11.

- ① By the Gauss–Bonnet formula, for closed surfaces in the same homotopy class (i.e., closed surfaces of the same genus g), we have $\int_S K \, dA = 4\pi(1 - g)$, therefore (8) can be reduced to the Willmore energy $\int_S H^2 \, dA$ as long as no topological change occurs.
- ② Define $\zeta_0 = 2(\sqrt{2} - 1) \approx 0.82843$. We are now ready to explain the requirement $\zeta > \zeta_0$ imposed in Conjectures 2.9 and 3.8. If such conjectures were also true for $\zeta < \zeta_0$, then we would still be able to prove (9) in Proposition 3.10. However, for $\zeta < \zeta_0$ we have $\lambda_2 > 0$. Therefore, the quadratic form in Proposition 3.10 is not positive semi-definite, and it is energetically more favorable to have zero mean curvature and negative Gaussian curvature. As pointed out by [52, Page 143], if λ_2 becomes positive, then it is preferable for a surface to have large genus g , or many “holes”. For example, triply periodic minimal surfaces shown in Figure 4 possess many “holes”. Since the quadratic form is indefinite, it is desirable for those triply periodic minimal surfaces to have infinitesimal lattice constants. However, we expect an equilibrium to be attained at a finitely small lattice constant (on the order of ρ) due to counteracting higher-order terms.
- ③ It surprised us to find that λ_2 can be positive for relatively small ζ . However, with hindsight we may come up with the following intuitive but non-rigorous explanation. For relatively large ζ , bending of the bilayer is penalized because there will be a slight difference in the thickness between the inner and outer V layers, as mentioned in Remark 3.6-(1). For relatively small ζ , such penalty may be relatively small because the V layers have vanishing thickness as $\zeta \rightarrow 0$. Meanwhile, the middle U layer may prefer saddle-splay deformations, because the U layer becomes more “spread out” in this way and thus the Coulombic repulsion within the U layer may decrease.
- ④ Our numerical simulations in Figure 12 support the observation in Remark 3.11-(2). More specifically, our numerical results indicate that a gyroid-like minimizer has lower energy-to-mass ratio than the planar bilayer for $\zeta = 0.6 < \zeta_0$, and thus the latter cannot be a global minimizer for $m \gg 1$. For $\zeta = 1 > \zeta_0$, our numerical results suggest the opposite.

- ⑤ Various cubic bicontinuous structures resembling triply periodic minimal surfaces can be observed in copolymer systems and biological specimens (see [18, 41] and [31, Section 4.1]), e.g., in the endoplasmic reticulum, Golgi apparatus and mitochondria [56, Bottom of Page 144]. Our finding provides a plausible explanation for such phenomena in the parameter regime $\zeta < \zeta_0$, and also demonstrates the ability of the Ohta–Kawasaki energy to capture such aspects of amphiphile self-assembly.

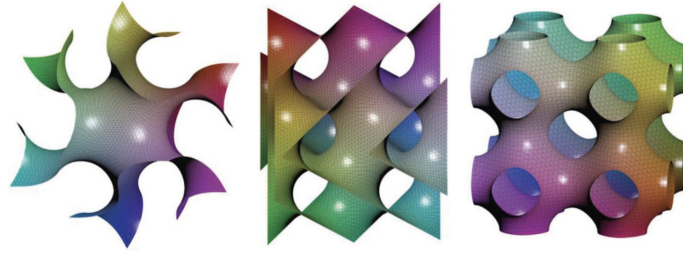


Figure 4: Triply periodic minimal surfaces. Left: gyroid. Middle: Schwarz diamond. Right: Schwarz primitive. Reproduced from [31, Figure 1].

Remark 3.12.

- ① Conjectures 3.7 and 3.8 states that our nonlocal problem Gamma-converges to a local problem. Our rationale behind those conjectures is as follows. According to the screening property (Proposition 1.1-③), each connected component of the minimizer satisfies the charge neutrality condition, and the total energy is just the sum of the energy for each connected component. Therefore we can consider each connected component separately. For each connected component, although the problem is nonlocal, the screening property may cause such nonlocality to decay sufficiently fast as $\rho \rightarrow 0$.
- ② Analogously, the screening property is also the reason that the electrostatic potential energy of a crystal is an extensive property. The electrostatic interactions are nonlocal, but an extensive property is local, i.e., it is proportional to the size of the crystal. In a variant model where the nonlocal term is given by the 1-Wasserstein distance, a similar phenomenon occurs: the nonlocal (or global) problem converges to the elastica bending energy which is a local problem [50, Section 9.3].

4 Phase-field reformulation

In order to provide some evidence for our conjectures in Section 3.2, we propose a phase-field reformulation which will be used for the numerical simulations in Section 5. We also prove the Gamma-convergence of our phase-field reformulation to a Gamma-limit, which is shown to be equivalent to the original problem (1).

The phase-field method [20] is a useful tool to study the motions of interfaces. The basic idea is to use a narrow but diffuse interface in place of the sharp interface, and the thickness of the interfacial layer is controlled by a diffuseness parameter ε . The interface is implicitly given by the level set of a smooth function, so there is no need to explicitly track the interface. Our phase-field reformulation is very similar to a previous work by two of us [69, Section III.A].

4.1 Diffuse interface energy

On a bounded domain $\Omega \subseteq \mathbb{R}^n$ with $|\Omega| \geq m + \zeta m$, we define the following phase-field functional

$$\mathcal{E}(u, v) = \mathcal{P}(u, v) + \gamma \mathcal{N}(u, v) + \mathcal{C}(u, v),$$

where \mathcal{P} is the diffuse interface version of the perimeter

$$\mathcal{P}(u, v) = \frac{\varepsilon}{2} \int_{\Omega} |\nabla u|^2 + \int_{\Omega} \frac{W(u, v)}{\varepsilon},$$

with the diffuseness parameter $\varepsilon > 0$, and the double-well potential W given by (see Figure 5)

$$2W(u, v)/27 := 4(u - u^2)^2/3 + \min\{v, 0\}^2 + \min\{1 - v, 0\}^2 + \min\{1 - u - v, 0\}^2, \quad (10)$$

which is to penalize violations of the three conditions: ① $u \in \{0, 1\}$; ② $0 \leq v \leq 1$; ③ $u + v \leq 1$. Since $|\nabla v|^2$ is not penalized in our energy, we choose a degenerate well for v instead of the classical double well $(v - v^2)^2$, in order to prevent v from being trapped in the local minima 0 and 1.

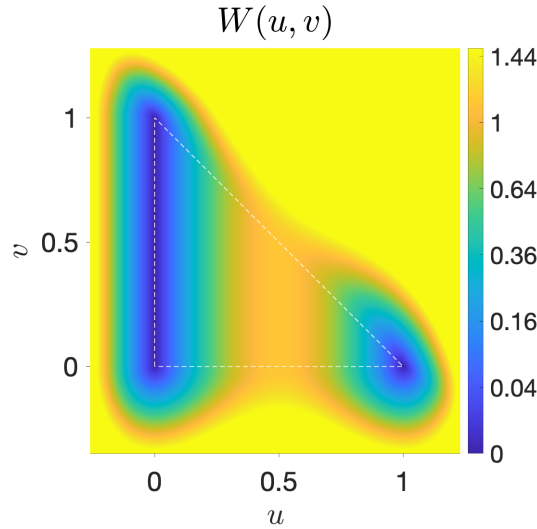


Figure 5: Visualization of W . For clarity a truncated version $\min\{W, 1.5\}$ is plotted.

We choose a function f which strictly increases on $[0, 1]$ satisfying $f(0) = 0$ and $f(1) = 1$. The simplest choice is the identity function $f(z) := z$, which will be used in this section for our proof of the Gamma-convergence. However, for our simulations in Section 5, we will choose f to be a nonlinear function in order to achieve the numerical efficiency as mentioned in [69, Section III.A]. As we will see later in Propositions 4.3 and 4.14, if (u, v) is a minimizer of \mathcal{E} for $\varepsilon \ll 1$, then u and v should be approximately 0 or 1 at most places in Ω . Therefore, the specific choice of f should have a vanishing effect on the minimizer of \mathcal{E} as $\varepsilon \rightarrow 0$.

With penalty coefficients $K_1, K_2 > 0$, the mass constraint term \mathcal{C} is defined as follows

$$2\mathcal{C}(u, v) = K_1 \left(m - \int_{\Omega} f(u) \right)^2 + K_2 \left(\zeta m - \int_{\Omega} f(v) \right)^2.$$

The nonlocal term \mathcal{N} is defined as follows

$$\begin{aligned} 2\mathcal{N}(u, v) &= \int_{\Omega} \int_{\Omega} f(u(\vec{x})) G(\vec{x}-\vec{y}) f(u(\vec{y})) \, d\vec{y} \, d\vec{x} - \frac{2}{\zeta} \int_{\Omega} \int_{\Omega} f(u(\vec{x})) G(\vec{x}-\vec{y}) f(v(\vec{y})) \, d\vec{y} \, d\vec{x} \\ &\quad + \frac{1}{\zeta^2} \int_{\Omega} \int_{\Omega} f(v(\vec{x})) G(\vec{x}-\vec{y}) f(v(\vec{y})) \, d\vec{y} \, d\vec{x}, \end{aligned}$$

where the nonlocal kernel G is the Green's function of negative Laplacian $-\Delta$. We consider two types of boundary conditions for G . The first type is no boundary conditions, under which G is the Green's function in the free space (i.e., the so-called fundamental solution). The second type is periodic boundary conditions, in which case we require Ω to be a rectangle ($n = 2$) or a rectangular cuboid ($n = 3$), and according to [12, Equations (2.1) and (2.2)], G is the periodic extension of the fundamental solution plus a continuous function, satisfying $\int_{\Omega} G = 0$. In Section 4.3.2, we justify that the above two types of boundary conditions are equivalent. In fact, for $n = 1$ such equivalence has already manifested itself in the striking similarity between Theorems 1 and 2 in [62] (note that $VUVU \cdots U$ therein is equivalent to $VUVU \cdots UV$, since an infinitesimal V block can be appended to the end without energy penalty, as long as V -0 interfaces are not penalized).

4.2 The sharp interface Gamma-limit

In this subsection, we aim to prove the Gamma-convergence of $\mathcal{E}_{\varepsilon}$ as $\varepsilon \rightarrow 0$ and $K_1, K_2 \rightarrow \infty$ (where the subscript ε is used to emphasize the dependence of \mathcal{E} on ε).

As mentioned before, in our proof of the Gamma-convergence, we let f be the identity function. As a first step, we let $K_1, K_2 \rightarrow \infty$, so that the admissible function space of $\mathcal{E}_{\varepsilon}$ is restricted to $\{u, v \in L^2(\Omega) : \int_{\Omega} v = \zeta \int_{\Omega} u = \zeta m\}$, and thus the constraint term \mathcal{C} vanishes. For convenience, in most parts of our proof of the Gamma-convergence, we do not explicitly incorporate the mass constraints, because it should be straightforward except in the proof of the limsup inequality (Proposition 4.7), where we do provide more details of the mass constraints. In addition, we have

$$\begin{aligned} 2\mathcal{N}(u, v) &= \int_{\Omega} \int_{\Omega} u(\vec{x}) G(\vec{x}-\vec{y}) u(\vec{y}) \, d\vec{y} \, d\vec{x} - \frac{2}{\zeta} \int_{\Omega} \int_{\Omega} u(\vec{x}) G(\vec{x}-\vec{y}) v(\vec{y}) \, d\vec{y} \, d\vec{x} \\ &\quad + \frac{1}{\zeta^2} \int_{\Omega} \int_{\Omega} v(\vec{x}) G(\vec{x}-\vec{y}) v(\vec{y}) \, d\vec{y} \, d\vec{x} \\ &= \int_{\Omega} \varphi(\vec{x}) (u(\vec{x}) - v(\vec{x})/\zeta) \, d\vec{x} = - \int_{\Omega} \varphi \Delta \varphi = \int_{\Omega} |\nabla \varphi|^2, \end{aligned} \tag{11}$$

where $\varphi = G * (u - v/\zeta)$, i.e., $\varphi(\vec{x}) = \int_{\Omega} G(\vec{x}-\vec{y}) (u(\vec{y}) - v(\vec{y})/\zeta) \, d\vec{y}$ for any $\vec{x} \in \Omega$. If we impose no boundary conditions on G (i.e., G is the fundamental solution), then φ satisfies $-\Delta \varphi = u - v/\zeta$; if we impose periodic boundary conditions on G , then φ satisfies $-\Delta \varphi = \text{constant} + u - v/\zeta$ and $\int_{\Omega} \varphi = 0$, where the constant is zero as long as $\int_{\Omega} v = \zeta \int_{\Omega} u$.

We assume that $\Omega \subseteq \mathbb{R}^n$ is an open bounded set with Lipschitz boundary. We extend the domain of definition of $\mathcal{E}_{\varepsilon}$ to $L^2(\Omega) \times L^2(\Omega)$:

$$\mathcal{E}_{\varepsilon}(u, v) = \begin{cases} \frac{\varepsilon}{2} \int_{\Omega} |\nabla u|^2 + \int_{\Omega} \frac{W(u, v)}{\varepsilon} + \gamma \mathcal{N}(u, v), & u \in W^{1,2}(\Omega), v \in L^2(\Omega), \int_{\Omega} v = \zeta \int_{\Omega} u = \zeta m, \\ \infty, & \text{otherwise.} \end{cases}$$

We want to prove that \mathcal{E}_ε Gamma-converges to the following functional defined on $L^2(\Omega) \times L^2(\Omega)$:

$$\mathcal{E}_0(u, v) = \begin{cases} |Du|(\Omega) + \gamma\mathcal{N}(u, v), & u \in BV(\Omega; \{0, 1\}), v \in L^2(\Omega; [0, 1]), vu = 0 \text{ a.e.}, \int_\Omega v = \zeta \int_\Omega u = \zeta m, \\ \infty, & \text{otherwise,} \end{cases}$$

where $|Du|$ is the absolute value of the distributional derivative of u . Note that \mathcal{E}_0 is a relaxed version of E , similar to [7, Equation (3.1)].

Our proof of the Gamma-convergence of \mathcal{E}_ε to \mathcal{E}_0 follows closely that of the classical Cahn–Hilliard energy functional given in [40]. The novelty of our proof lies in the degeneracy of the potential W shown in Figure 5, i.e., W has non-isolated minimizers $(u, v) \in \{0\} \times [0, 1]$. Furthermore, $|\nabla u|^2$ is penalized in our energy while $|\nabla v|^2$ is not. Sternberg [60, Section 2] also considered the case where W has non-isolated minimizers, but both $|\nabla u|^2$ and $|\nabla v|^2$ are penalized there. In the rest of this section, we consider an arbitrary sequence of diffuseness parameters $\{\varepsilon_k : k \in \mathbb{N}\} \subseteq \mathbb{R}_{>0}$ converging to 0. For brevity we abbreviate the subscript k and write \mathcal{E}_ε , which should be understood as $\mathcal{E}_{\varepsilon_k}$ for some $k \in \mathbb{N}$. We also write $\lim_{\varepsilon \rightarrow 0} \mathcal{E}_\varepsilon$ instead of $\lim_{k \rightarrow \infty} \mathcal{E}_{\varepsilon_k}$.

4.2.1 Compactness result

Definition 4.1. A sequence of functions $\{f_k : k \in \mathbb{N}\} \subseteq L^1(\Omega)$ is called equi-integrable (i.e., uniformly integrable) if: for any $\tau > 0$, there exists an $r > 0$, such that

$$\sup_{k \in \mathbb{N}} \int_{\{|f_k| \geq r\}} |f_k| < \tau.$$

Remark 4.2. In Definition 4.1, note that $\{f_1\}$ is always equi-integrable. Indeed, we can approximate f_1 using a simple function g so that $\int_\Omega |f_1 - g| < \tau/2$, and then choose r such that $\int_{\{|f_1| \geq r\}} |g| < \tau/2$, because $\max |g| < \infty$ and the Lebesgue measure of $\{|f_1| \geq r\}$ converges to 0 as $r \rightarrow \infty$. Similarly, any finite subset of $\{f_k : k \in \mathbb{N}\}$ is always equi-integrable, therefore we have an equivalent definition:

$$\limsup_{k \rightarrow \infty} \int_{\{|f_k| \geq r\}} |f_k| < \tau.$$

Proposition 4.3. As $\varepsilon \rightarrow 0$, if a sequence $\{(u_\varepsilon, v_\varepsilon)\} \subseteq W^{1,2}(\Omega) \times L^2(\Omega)$ satisfies

$$M := \sup_\varepsilon \mathcal{E}_\varepsilon(u_\varepsilon, v_\varepsilon) < \infty,$$

then there exists a subsequence $\{(u_\varepsilon, v_\varepsilon)\}$ (for brevity, this subsequence is not relabeled) and $(u_0, v_0) \in BV(\Omega; \{0, 1\}) \times L^2(\Omega; [0, 1])$ such that

$$u_\varepsilon \rightarrow u_0 \text{ in } L^2(\Omega), \quad v_\varepsilon \rightarrow v_0 \text{ in } L^2(\Omega), \quad v_0 u_0 = 0 \text{ a.e.}$$

Proof.

Step 1: We show that $u_\varepsilon^2 + v_\varepsilon^2$ is uniformly bounded in $L^1(\Omega)$ and equi-integrable. According to (10), there exists $R > 0$ such that $W(u, v) \geq u^2 + v^2$ whenever $u^2 + v^2 \geq R$. For any $r \geq R$, we have

$$\int_{\{u_\varepsilon^2 + v_\varepsilon^2 \geq r\}} (u_\varepsilon^2 + v_\varepsilon^2) \leq \int_{\{u_\varepsilon^2 + v_\varepsilon^2 \geq r\}} W(u_\varepsilon, v_\varepsilon) \leq \mathcal{E}_\varepsilon(u_\varepsilon, v_\varepsilon) \varepsilon \leq M\varepsilon,$$

which implies that $u_\varepsilon^2 + v_\varepsilon^2$ is equi-integrable. Moreover, since Ω is bounded, $\int_\Omega (u_\varepsilon^2 + v_\varepsilon^2)$ is bounded by $M\varepsilon + R|\Omega|$.

Step 2: We show that a subsequence of $\{u_\varepsilon\}$ converges pointwise a.e. to some $u_0 \in BV(\Omega; \{0, 1\})$ (by mimicking [40]). Denote $W_1(z) := \min\{|z - z^2|, 1\}$ and $\eta(z) := \int_0^z W_1(r) dr$. We have

$$M \geq \mathcal{E}_\varepsilon(u_\varepsilon, v_\varepsilon) \geq \int_\Omega |\nabla u_\varepsilon| \sqrt{W(u_\varepsilon, v_\varepsilon)} \geq \int_\Omega |\nabla u_\varepsilon| |u_\varepsilon - u_\varepsilon^2| \geq \int_\Omega |\nabla u_\varepsilon| W_1(u_\varepsilon) = \int_\Omega |\nabla \eta(u_\varepsilon)|.$$

Denote $\eta_\varepsilon = \eta(u_\varepsilon)$. Since $0 \leq W_1 \leq 1$ and $\eta(0) = 0$, we know $|\eta(z)| \leq |z|$ and thus $|\eta_\varepsilon| \leq |u_\varepsilon|$. According to Step 1, $\{u_\varepsilon\}$ and thus $\{\eta_\varepsilon\}$ are uniformly bounded in $L^2(\Omega)$ and thus in $L^1(\Omega)$. Therefore $\{\eta_\varepsilon\}$ is uniformly bounded in $BV(\Omega)$. According to [21, Theorem 5.5], there exists a subsequence $\{\eta_\varepsilon\}$ (not relabeled) and some $\eta_0 \in BV(\Omega)$ such that $\eta_\varepsilon \rightarrow \eta_0$ in $L^1(\Omega)$. A further subsequence $\{\eta_\varepsilon\}$ (not relabeled) converges pointwise a.e. to η_0 . Since $\eta(z)$ is strictly increasing and continuous in z , its inverse η^{-1} is continuous. Define $u_0 = \eta^{-1}(\eta_0)$, since $u_\varepsilon = \eta^{-1}(\eta_\varepsilon)$, we know that u_ε converges pointwise a.e. to u_0 . Moreover, by Fatou's lemma [25, Lemma 1.83-(i)] we have $\int_\Omega W_1(u_0)^2 \leq \liminf_{\varepsilon \rightarrow 0} \int_\Omega W_1(u_\varepsilon)^2$, where $\int_\Omega W_1(u_\varepsilon)^2 \leq \mathcal{E}_\varepsilon(u_\varepsilon, v_\varepsilon) \varepsilon \leq M\varepsilon$. Therefore $W_1(u_0)^2 = 0$ a.e., that is, $u_0 \in \{0, 1\}$ a.e. So $\eta_0 \in \{\eta(0), \eta(1)\}$ a.e. Since $\eta_0 \in BV(\Omega)$, we can write $\eta_0 = \eta(0)(1 - \mathbf{1}_U) + \eta(1)\mathbf{1}_U$ with a set $U \subseteq \Omega$ of finite perimeter. Hence, $u_0 = \mathbf{1}_U$ belongs to $BV(\Omega; \{0, 1\})$.

Step 3: We show that the subsequence of $\{u_\varepsilon\}$ obtained in Step 2 converges to u_0 in $L^2(\Omega)$. This is guaranteed by Vitali's convergence theorem [25, Theorems 2.22, 2.24 and 2.29], in view of Step 1.

Step 4: We show that a subsequence of $\{v_\varepsilon\}$ converges weakly in $L^2(\Omega)$ to some $v_0 \in L^2(\Omega)$. According to Step 1, $\{v_\varepsilon\}$ is uniformly bounded in $L^2(\Omega)$. By [25, Proposition 2.46-(iv)], it has a subsequence (not relabeled) such that $v_\varepsilon \rightharpoonup v_0$ in $L^2(\Omega)$ for some $v_0 \in L^2(\Omega)$.

Step 5: We show that $v_0 \in L^2(\Omega; [0, 1])$ and $v_0 u_0 = 0$ a.e. In view of Steps 2, 3 and 4, we can assume that the sequence $\{(u_\varepsilon, v_\varepsilon)\}$ satisfies $v_\varepsilon \rightharpoonup v_0$ in $L^2(\Omega)$, $u_\varepsilon \rightarrow u_0$ in $L^2(\Omega)$, and $u_\varepsilon \rightarrow u_0$ a.e. Our goal is to prove $\int_\Omega W(u_0, v_0) = 0$. Since $W(u, v)$ is continuous in u , by Fatou's lemma, we have the following

$$\int_\Omega W(u_0, v_0) \leq \liminf_{\varepsilon \rightarrow 0} \int_\Omega W(u_\varepsilon, v_0).$$

According to (10), $W(u, v)$ is convex in v , and we know $W_v(u, v) := \partial_v W(u, v) = 27(\min\{v, 0\} + \max\{v - 1, 0\} + \max\{v + u - 1, 0\})$, therefore we have

$$\int_\Omega W(u_\varepsilon, v_0) \leq \int_\Omega W(u_\varepsilon, v_\varepsilon) + \int_\Omega W_v(u_\varepsilon, v_0)(v_0 - v_\varepsilon),$$

where the first summand on the right-hand side can be bounded by $\mathcal{E}_\varepsilon(u_\varepsilon, v_\varepsilon) \varepsilon$, and the second summand can be split into

$$\int_\Omega W_v(u_0, v_0)(v_0 - v_\varepsilon) + \int_\Omega (W_v(u_\varepsilon, v_0) - W_v(u_0, v_0))(v_0 - v_\varepsilon),$$

where the first summand converges to 0 because $W_v(u_0, v_0) \in L^2(\Omega)$ and $v_\varepsilon \rightharpoonup v_0$ in $L^2(\Omega)$, and the absolute value of the second summand can be bounded by

$$\|v_0 - v_\varepsilon\|_{L^2(\Omega)} \cdot \|W_v(u_\varepsilon, v_0) - W_v(u_0, v_0)\|_{L^2(\Omega)}.$$

Since $\{v_\varepsilon\}$ is uniformly bounded in $L^2(\Omega)$, we know $\|v_0 - v_\varepsilon\|_{L^2(\Omega)}$ is uniformly bounded. Moreover, we have $|W_v(u_\varepsilon, v_0) - W_v(u_0, v_0)| \leq 27|u_\varepsilon - u_0|$, so $W_v(u_\varepsilon, v_0) \rightarrow W_v(u_0, v_0)$ in $L^2(\Omega)$. To summarize, we have proved $\int_\Omega W(u_\varepsilon, v_0) \rightarrow 0$ as $\varepsilon \rightarrow 0$. Therefore $W(u_0, v_0) = 0$ a.e. \square

4.2.2 Liminf inequality

Proposition 4.4. For any $u_0, v_0 \in L^2(\Omega)$ and $\{u_\varepsilon\}, \{v_\varepsilon\} \subseteq L^2(\Omega)$ such that both $u_\varepsilon \rightarrow u_0$ and $v_\varepsilon \rightarrow v_0$ in $L^2(\Omega)$, we have

$$\mathcal{E}_0(u_0, v_0) \leq \liminf_{\varepsilon \rightarrow 0} \mathcal{E}_\varepsilon(u_\varepsilon, v_\varepsilon).$$

Proof. We assume that the above right-hand side is finite (otherwise there is nothing to prove). Without loss of generality (by extracting a subsequence if necessary), we further assume that the liminf is actually a limit. By Proposition 4.3, we know $u_0 \in BV(\Omega; \{0, 1\})$, $v_0 \in L^2(\Omega; [0, 1])$, and $u_0 v_0 = 0$ a.e. We can also assume $\mathcal{E}_\varepsilon(u_\varepsilon, v_\varepsilon) < \infty$ for all ε , and thus $\{u_\varepsilon\} \subseteq W^{1,2}(\Omega)$.

Step 1: We first consider the case where $\gamma = 0$. Denote $W_1(z) := \min\{|z - z^2|, 1\}$, and $\eta(z) := \int_0^z W_1(r) dr$. Because $W_1(u)^2 \leq (u - u^2)^2 \leq W(u, v)/18$, we have

$$\mathcal{E}_\varepsilon(u_\varepsilon, v_\varepsilon) \geq \frac{\varepsilon}{2} \int_\Omega |\nabla u_\varepsilon|^2 + \frac{18}{\varepsilon} \int_\Omega W_1(u_\varepsilon)^2 \geq 6 \int_\Omega |\nabla u_\varepsilon| W_1(u_\varepsilon) = 6 \int_\Omega |\nabla \eta(u_\varepsilon)|.$$

Since $0 \leq W_1 \leq 1$, we know $|\eta(z) - \eta(r)| \leq |z - r|$ for any $z, r \in \mathbb{R}$. Denote $\eta_\varepsilon = \eta(u_\varepsilon)$ and $\eta_0 = \eta(u_0)$, then $\eta_\varepsilon \rightarrow \eta_0$ in $L^2(\Omega)$ and thus in $L^1(\Omega)$. According to [21, Theorem 5.2], we have

$$\liminf_{\varepsilon \rightarrow 0} \int_\Omega |\nabla \eta_\varepsilon| = \liminf_{\varepsilon \rightarrow 0} |D\eta_\varepsilon|(\Omega) \geq |D\eta_0|(\Omega).$$

Noticing $\eta_0 = \eta(1) u_0$ and $\eta(1) = 1/6$, we obtain

$$\liminf_{\varepsilon \rightarrow 0} \mathcal{E}_\varepsilon(u_\varepsilon, v_\varepsilon) \geq |Du_0|(\Omega) = \text{Per}_\Omega\{\vec{x} \in \Omega : u_0(\vec{x}) = 1\}.$$

Step 2: We now consider the case where $\gamma > 0$. We want to prove the following

$$\lim_{\varepsilon \rightarrow 0} \mathcal{N}(u_\varepsilon, v_\varepsilon) = \mathcal{N}(u_0, v_0).$$

Denote $w = u - v/\zeta$. From (11) we recall $2\mathcal{N}(u, v) = \int_\Omega \varphi w$, where $\varphi(\vec{x}) = G * w := \int_\Omega G(\vec{x} - \vec{y}) w(\vec{y}) d\vec{y}$. Denote $w_\varepsilon = u_\varepsilon - v_\varepsilon/\zeta$ and $w_0 = u_0 - v_0/\zeta$ with $\varphi_\varepsilon = G * w_\varepsilon$ and $\varphi_0 = G * w_0$, then

$$2|\mathcal{N}(u_\varepsilon, v_\varepsilon) - \mathcal{N}(u_0, v_0)| = \left| \int_\Omega \varphi_\varepsilon w_\varepsilon - \int_\Omega \varphi_0 w_0 \right| \rightarrow 0,$$

where we have used Lemma 4.6 and the fact that $w_\varepsilon \rightarrow w_0$ in $L^2(\Omega)$. \square

Lemma 4.5. Recall that G is the Green's function of $-\Delta$ under either no boundary conditions (i.e., the fundamental solution) or periodic boundary conditions. For $\eta \in L^2(\Omega)$, define $\psi(\vec{x}) = \int_\Omega G(\vec{x} - \vec{y}) \eta(\vec{y}) d\vec{y}$, then there is a constant $C \in \mathbb{R}_{>0}$ independent of η and \vec{x} , such that $|\psi(\vec{x})| \leq C \|\eta\|_{L^2(\Omega)}$.

Proof. According to the Cauchy–Schwarz inequality, we have

$$|\psi(\vec{x})|^2 = \left| \int_{\Omega} G(\vec{x}-\vec{y}) \eta(\vec{y}) \, d\vec{y} \right|^2 \leq \int_{\Omega} G(\vec{x}-\vec{y})^2 \, d\vec{y} \int_{\Omega} \eta(\vec{y})^2 \, d\vec{y} = \int_{\Omega} G(\vec{x}-\vec{y})^2 \, d\vec{y} \|\eta\|_{L^2(\Omega)}^2.$$

Therefore we only need to estimate $\int_{\Omega} G(\vec{x}-\vec{y})^2 \, d\vec{y}$.

Step 1: We first consider the case where G is the fundamental solution with $n = 3$. In such case, we have $G(\vec{x}-\vec{y}) = (4\pi|\vec{x}-\vec{y}|)^{-1}$. Inspired by [27, Page 159], we denote $R = \sqrt[3]{3|\Omega|/(4\pi)}$ so that $|\Omega| = |B(\vec{x}; R)|$, where $B(\vec{x}; R)$ is a ball of radius R centered at \vec{x} . Using the monotonicity of G , we obtain for any $\vec{x} \in \Omega$,

$$\int_{\Omega} \frac{d\vec{y}}{|\vec{x}-\vec{y}|^2} \leq \int_{B(\vec{x}; R)} \frac{d\vec{y}}{|\vec{x}-\vec{y}|^2} = 4\pi R = \sqrt[3]{48\pi^2|\Omega|}.$$

Step 2: We now consider the case where G is the fundamental solution with $n = 2$. In such case, we have $G(\vec{x}-\vec{y}) = -\ln|\vec{x}-\vec{y}|/(2\pi)$. Notice that for any $r \in \mathbb{R}_{>0}$, we have

$$(\ln r)^2 = -|\ln r| \ln r + 2(\max\{0, \ln r\})^2,$$

where the first summand monotonically decreases and can be bounded in a similar manner to Step 1, while the second summand monotonically increases and can be bounded in terms of $\ln \sup\{|\vec{x}-\vec{y}| : \vec{x}, \vec{y} \in \Omega\}$. Therefore, we can prove that $\int_{\Omega} (\ln|\vec{x}-\vec{y}|)^2 \, d\vec{y}$ is uniformly bounded in \vec{x} .

Step 3: We now consider the case where G is equipped with periodic boundary conditions. In this case $G(\vec{x}-\vec{y})$ is periodic, therefore $\int_{\Omega} G(\vec{x}-\vec{y})^2 \, d\vec{y}$ is independent of \vec{x} . According to [12, Equations (2.1) and (2.2)], G is the sum of the fundamental solution and a regular part, therefore $\int_{\Omega} G(\vec{x}-\vec{y})^2 \, d\vec{y}$ is finite. \square

Lemma 4.6. If $\eta_{\varepsilon} \rightharpoonup \eta_0$ in $L^2(\Omega)$, define $\psi_{\varepsilon}(\vec{x}) = \int_{\Omega} G(\vec{x}-\vec{y}) \eta_{\varepsilon}(\vec{y}) \, d\vec{y}$, and analogously for ψ_0 . Then

$$\left| \int_{\Omega} (\psi_{\varepsilon} \eta_{\varepsilon} - \psi_0 \eta_0) \right| \rightarrow 0 \quad \text{as } \varepsilon \rightarrow 0.$$

Proof. Notice that according to Lemma 4.5, we have $\psi_{\varepsilon}, \psi_0 \in L^{\infty}(\Omega)$. Moreover,

$$\begin{aligned} \left| \int_{\Omega} (\psi_{\varepsilon} \eta_{\varepsilon} - \psi_0 \eta_0) \right| &\leq \left| \int_{\Omega} (\psi_{\varepsilon} - \psi_0) \eta_{\varepsilon} \right| + \left| \int_{\Omega} \psi_0 (\eta_{\varepsilon} - \eta_0) \right| \\ &\leq \|\psi_{\varepsilon} - \psi_0\|_{L^2(\Omega)} \|\eta_{\varepsilon}\|_{L^2(\Omega)} + \left| \int_{\Omega} \psi_0 (\eta_{\varepsilon} - \eta_0) \right|, \end{aligned}$$

where $\left| \int_{\Omega} \psi_0 (\eta_{\varepsilon} - \eta_0) \right| \rightarrow 0$ and $\|\eta_{\varepsilon}\|_{L^2(\Omega)}$ has an upper bound independent of ε , because $\eta_{\varepsilon} \rightharpoonup \eta_0$ in $L^2(\Omega)$. In addition, we have

$$\begin{aligned} \lim_{\varepsilon \rightarrow 0} \|\psi_{\varepsilon} - \psi_0\|_{L^2(\Omega)}^2 &= \lim_{\varepsilon \rightarrow 0} \int_{\Omega} (\psi_{\varepsilon}(\vec{x}) - \psi_0(\vec{x}))^2 \, d\vec{x} = \int_{\Omega} \lim_{\varepsilon \rightarrow 0} (\psi_{\varepsilon}(\vec{x}) - \psi_0(\vec{x}))^2 \, d\vec{x} \\ &= \int_{\Omega} \lim_{\varepsilon \rightarrow 0} \left(\int_{\Omega} G(\vec{x}-\vec{y}) (\eta_{\varepsilon}(\vec{y}) - \eta_0(\vec{y})) \, d\vec{y} \right)^2 \, d\vec{x} = 0, \end{aligned}$$

where the last equality is again due to $\eta_{\varepsilon} \rightharpoonup \eta_0$ in $L^2(\Omega)$, and the second equality is due to the Dominated Convergence Theorem. To see why the Dominated Convergence Theorem applies, notice that according to Lemma 4.5, $|\psi_0(\vec{x})|$ is uniformly bounded in \vec{x} , and that $|\psi_{\varepsilon}(\vec{x})|$ is uniformly bounded in \vec{x} and ε , because $\|\eta_{\varepsilon}\|_{L^2(\Omega)}$ is uniformly bounded in ε . \square

4.2.3 Limsup inequality

Proposition 4.7. For any $u_0, v_0 \in L^2(\Omega)$, there exist $\{u_\varepsilon\}, \{v_\varepsilon\} \subseteq L^2(\Omega)$ such that both $u_\varepsilon \rightarrow u_0$ and $v_\varepsilon \rightarrow v_0$ in $L^2(\Omega)$, satisfying

$$\mathcal{E}_0(u_0, v_0) \geq \limsup_{\varepsilon \rightarrow 0} \mathcal{E}_\varepsilon(u_\varepsilon, v_\varepsilon).$$

Proof. We assume that the above left-hand side is finite (otherwise there is nothing to prove), therefore we have $u_0 \in BV(\Omega; \{0, 1\})$, $v_0 \in L^2(\Omega; [0, 1])$, and $u_0 v_0 = 0$ a.e.

Step 1: We first consider the case where $\gamma = 0$ and $n = 1$. We further assume $\Omega = [-1, 1]$ and $u_0 = \mathbf{1}_{[0,1]}$. Therefore $v_0(x) = 0$ for $x \in [0, 1]$ a.e. We take

$$u_\varepsilon(x) = (1 + \tanh(3x/\varepsilon))/2 \text{ for } x \in [-1, 1], \quad \text{and } v_\varepsilon = v_0 \mathbf{1}_{[-1, -\delta]} \text{ where } \delta = \varepsilon^{2/3}.$$

By Dominated Convergence Theorem, we have both $u_\varepsilon \rightarrow u_0$ and $v_\varepsilon \rightarrow v_0$, pointwise a.e. and thus in $L^2(\Omega)$. We can compute

$$\frac{1}{2} \int_{\Omega} |\nabla u_\varepsilon|^2 = \frac{1}{2} \int_{-1}^1 u'_\varepsilon(x)^2 dx = \frac{1}{4\varepsilon} \left(3 - \tanh^2\left(\frac{3}{\varepsilon}\right)\right) \tanh\left(\frac{3}{\varepsilon}\right).$$

In addition, we have

$$W(u_\varepsilon, v_\varepsilon) = 18(u_\varepsilon - u_\varepsilon^2)^2 + 27 \min\{1 - u_\varepsilon - v_\varepsilon, 0\}^2/2,$$

where the first summand has the following integral

$$\int_{\Omega} 18(u_\varepsilon - u_\varepsilon^2)^2 = \frac{\varepsilon}{4} \left(3 - \tanh^2\left(\frac{3}{\varepsilon}\right)\right) \tanh\left(\frac{3}{\varepsilon}\right),$$

and the second summand can be bounded as follows

$$\int_{\Omega} \min\{1 - u_\varepsilon - v_\varepsilon, 0\}^2 = \int_{-1}^{-\delta} \min\{1 - u_\varepsilon - v_0, 0\}^2 \leq \int_{-1}^{-\delta} u_\varepsilon^2,$$

where the inequality is due to $v_0 \leq 1$ a.e. Since u_ε increases monotonically, we have

$$\int_{-1}^{-\delta} u_\varepsilon^2 \leq (1 - \delta) u_\varepsilon^2(-\delta) \leq (1 - \tanh(3\delta/\varepsilon))^2 = \left(1 - \tanh(3\varepsilon^{-1/3})\right)^2.$$

Noticing $1 - \tanh z = 2/(e^{2z} + 1) < 2e^{-2z}$, we obtain $\int_{-1}^{-\delta} u_\varepsilon^2 = o(\varepsilon)$. To summarize, we have

$$\mathcal{E}_\varepsilon(u_\varepsilon, v_\varepsilon) = \frac{\varepsilon}{2} \int_{\Omega} |\nabla u_\varepsilon|^2 + \int_{\Omega} \frac{W(u_\varepsilon, v_\varepsilon)}{\varepsilon} \leq \frac{1}{2} \left(3 - \tanh^2\left(\frac{3}{\varepsilon}\right)\right) \tanh\left(\frac{3}{\varepsilon}\right) + o(1),$$

where the right-hand side converges to 1 as $\varepsilon \rightarrow 0$. Therefore $\mathcal{E}_0(u_0, v_0) = 1 \geq \limsup_{\varepsilon \rightarrow 0} \mathcal{E}_\varepsilon(u_\varepsilon, v_\varepsilon)$.

So far in our proof of the Gamma-convergence, we have not explicitly dealt with the mass constraints, which should be straightforward because the weak convergence in $L^2(\Omega)$ implies the convergence of the Lebesgue measure. However, we need to provide more details here. To make sure $\int_{\Omega} v_\varepsilon = \int_{\Omega} v_0$, we rescale v_ε defined above, i.e., we redefine $v_\varepsilon = v_0 \mathbf{1}_{[-1, -\delta]} \int_{-1}^0 v_0 / \int_{-1}^{-\delta} v_0$, where

$$\delta = \varepsilon^{2/3}, \quad \int_{-1}^0 v_0 = \zeta m, \quad \int_{-1}^{-\delta} v_0 = \zeta m - \int_{-\delta}^0 v_0 \geq \zeta m - \delta.$$

In this way, we have $v_\varepsilon \leq \zeta m / (\zeta m - \delta) = 1 + O(\varepsilon^{2/3})$ and thus $\varepsilon^{-1} \int_{\Omega} \min\{1 - v_\varepsilon, 0\}^2 \leq O(\varepsilon^{1/3})$. Therefore, after the above modification, v_ε satisfies the mass constraint while $\mathcal{E}_\varepsilon(u_\varepsilon, v_\varepsilon)$ increases only by order $\varepsilon^{1/3}$.

Step 2: We now consider the case where $\gamma = 0$ and $n > 1$. We assume $u_0 = \mathbf{1}_U$ for some open set $U \subseteq \mathbb{R}^n$ with ∂U being a nonempty compact hypersurface of differentiability class C^2 . We further assume $\mathcal{H}^{n-1}(\partial U \cap \partial \Omega) = 0$, where \mathcal{H} is the Hausdorff measure. We can rewrite $u_0 = g_0(d_U)$ where $g_0 = \mathbf{1}_{[0, \infty)}$, and d_U is the signed distance function defined by

$$d_U(\vec{x}) = \begin{cases} \inf \{|\vec{x} - \vec{y}| : \vec{y} \in \partial U\}, & \text{if } \vec{x} \in U, \\ -\inf \{|\vec{x} - \vec{y}| : \vec{y} \in \partial U\}, & \text{if } \vec{x} \notin U. \end{cases}$$

We take $u_\varepsilon = g_\varepsilon(d_U)$ and $v_\varepsilon = h_\varepsilon(d_U)v_0$, where $g_\varepsilon(z) := (1 + \tanh(3z/\varepsilon))/2$, and $h_\varepsilon := \mathbf{1}_{(-\infty, -\delta]}$ with $\delta = \varepsilon^{2/3}$. The function d_U is Lipschitz continuous and satisfies $|\nabla d_U| = 1$ a.e. in \mathbb{R}^n [17, Theorems 2.1 and 3.1]. Let l denote the size of the level set of d_U :

$$l(r) := \mathcal{H}^{n-1}(\{\vec{x} \in \Omega : d_U(\vec{x}) = r\}), \quad r \in \mathbb{R}.$$

By Lemma 4.8, we have

$$\begin{aligned} \mathcal{E}_\varepsilon(u_\varepsilon, v_\varepsilon) &= \frac{\varepsilon}{2} \int_{\Omega} |\nabla u_\varepsilon|^2 + \int_{\Omega} \frac{W(u_\varepsilon, v_\varepsilon)}{\varepsilon} \\ &= \int_{\Omega} \left(\frac{\varepsilon}{2} |\nabla u_\varepsilon|^2 + \frac{18}{\varepsilon} (u_\varepsilon - u_\varepsilon^2)^2 + \frac{27}{2\varepsilon} \min\{1 - u_\varepsilon - v_\varepsilon, 0\}^2 \right) \\ &\leq \int_{\Omega} \left(\frac{\varepsilon}{2} |\nabla u_\varepsilon|^2 + \frac{18}{\varepsilon} (u_\varepsilon - u_\varepsilon^2)^2 + \frac{27}{2\varepsilon} \min\{1 - u_\varepsilon - h_\varepsilon(d_U), 0\}^2 \right) \\ &= \int_{\Omega} \left(\frac{\varepsilon}{2} g'_\varepsilon(d_U)^2 + \frac{1}{\varepsilon} W(g_\varepsilon(d_U), h_\varepsilon(d_U)) \right) |\nabla d_U| \\ &= \int_{\mathbb{R}} \left(\frac{\varepsilon}{2} g'_\varepsilon(r)^2 + \frac{1}{\varepsilon} W(g_\varepsilon(r), h_\varepsilon(r)) \right) l(r) dr := \int_{\mathbb{R}} a_\varepsilon(r) l(r) dr. \end{aligned}$$

According to Step 1, we know $\int_{-1}^1 a_\varepsilon(r) dr \leq 1 + o(1)$. For any fixed $\tau > 0$, we have $a_\varepsilon(r) \rightarrow 0$ as $\varepsilon \rightarrow 0$ uniformly for $r \in \mathbb{R} \setminus (-\tau, \tau)$. Since Ω is bounded, by Lemma 4.8, $\int_{\mathbb{R}} l(r) dr = \int_{\Omega} |\nabla d_U| = |\Omega| < \infty$. Because ∂U is of differentiability class C^2 with $\mathcal{H}^{n-1}(\partial U \cap \partial \Omega) = 0$, we know that $l(r)$ is continuous at $r = 0$ satisfying $\lim_{r \rightarrow 0} l(r) = \mathcal{H}^{n-1}(\partial U \cap \Omega)$ [40, Lemma 5.8]. Therefore,

$$\limsup_{\varepsilon \rightarrow 0} \mathcal{E}_\varepsilon(u_\varepsilon, v_\varepsilon) \leq \limsup_{\varepsilon \rightarrow 0} (l(0) + o(1)) = \mathcal{H}^{n-1}(\partial U \cap \Omega) = \mathcal{E}_0(u_0, v_0).$$

We now show both $u_\varepsilon \rightarrow u_0$ and $v_\varepsilon \rightarrow v_0$ in $L^2(\Omega)$. To this end, we use $|\nabla d_U| = 1$ and Lemma 4.8 again to obtain

$$\int_{\Omega} (u_\varepsilon - u_0)^2 = \int_{\Omega} (g_\varepsilon(d_U) - g_0(d_U))^2 |\nabla d_U| = \int_{\mathbb{R}} (g_\varepsilon(r) - g_0(r))^2 l(r) dr.$$

As mentioned above, $\int_{\mathbb{R}} l < \infty$. Noticing $|g_\varepsilon - g_0| \leq |g_\varepsilon| + |g_0| \leq 2$ and $g_\varepsilon \rightarrow g_0$ pointwise a.e., by Dominated Convergence Theorem, we have $\int_{\Omega} (u_\varepsilon - u_0)^2 \rightarrow 0$. Similarly, we have $\int_{\Omega} (v_\varepsilon - v_0)^2 \rightarrow 0$.

In order to guarantee the mass constraint $\int_{\Omega} u_{\varepsilon} = m$, we can make some technical modifications to the above u_{ε} in a similar way to the classical Cahn–Hilliard energy functional [40, Equation (26)]. Similar to Step 1, we can also modify v_{ε} to guarantee the mass constraint $\int_{\Omega} v_{\varepsilon} = \zeta m$.

Step 3: We now remove the regularity assumption imposed on U in Step 2. By Lemma 4.9, there exists a sequence of open sets U_j with ∂U_j being a nonempty compact hypersurface of differentiability class C^2 and satisfying $\mathcal{H}^{n-1}(\partial U_j \cap \partial \Omega) = 0$, such that $\mathbf{1}_{U_j} \rightarrow \mathbf{1}_U$ in $L^2(\Omega)$ and $\text{Per}_{\Omega} U_j \rightarrow \text{Per}_{\Omega} U$. According to Step 2, for each fixed j we can find a sequence $\{u_{j,\varepsilon}\} \subseteq W^{1,2}(\Omega)$ and $\{v_{j,\varepsilon}\} \subseteq L^2(\Omega)$ such that both $u_{j,\varepsilon} \rightarrow \mathbf{1}_{U_j}$ and $v_{j,\varepsilon} \rightarrow (1 - \mathbf{1}_{U_j}) v_0$ in $L^2(\Omega)$ as $\varepsilon \rightarrow 0$, in addition to

$$\limsup_{\varepsilon \rightarrow 0} \mathcal{E}_{\varepsilon}(u_{j,\varepsilon}, v_{j,\varepsilon}) \leq \mathcal{H}^{n-1}(\partial U_j \cap \Omega) = \text{Per}_{\Omega} U_j.$$

Therefore we have

$$\limsup_{j \rightarrow \infty} \limsup_{\varepsilon \rightarrow 0} \mathcal{E}_{\varepsilon}(u_{j,\varepsilon}, v_{j,\varepsilon}) \leq \limsup_{j \rightarrow \infty} \text{Per}_{\Omega} U_j = \text{Per}_{\Omega} U.$$

Noticing

$$\lim_{j \rightarrow \infty} \lim_{\varepsilon \rightarrow 0} \|u_{j,\varepsilon} - u_0\|_{L^2(\Omega)} = \lim_{j \rightarrow \infty} \|\mathbf{1}_{U_j} - \mathbf{1}_U\|_{L^2(\Omega)} = 0,$$

and

$$\lim_{j \rightarrow \infty} \lim_{\varepsilon \rightarrow 0} \|v_{j,\varepsilon} - v_0\|_{L^2(\Omega)} = \lim_{j \rightarrow \infty} \|(1 - \mathbf{1}_{U_j}) v_0 - (1 - \mathbf{1}_U) v_0\|_{L^2(\Omega)} = 0,$$

we know

$$\limsup_{j \rightarrow \infty} \limsup_{\varepsilon \rightarrow 0} (\|u_{j,\varepsilon} - u_0\|_{L^2(\Omega)} + \|v_{j,\varepsilon} - v_0\|_{L^2(\Omega)}) = 0.$$

By Lemma 4.10, we have a diagonal sequence $\{u_{j_{\varepsilon}, \varepsilon}\}$ and $\{v_{j_{\varepsilon}, \varepsilon}\}$ such that both $u_{j_{\varepsilon}, \varepsilon} \rightarrow u_0$ and $v_{j_{\varepsilon}, \varepsilon} \rightarrow v_0$ in $L^2(\Omega)$, and

$$\limsup_{\varepsilon \rightarrow 0} \mathcal{E}_{\varepsilon}(u_{j_{\varepsilon}, \varepsilon}, v_{j_{\varepsilon}, \varepsilon}) \leq \text{Per}_{\Omega} U = \mathcal{E}_0(u_0, v_0).$$

Step 4: We now consider the case where $\gamma > 0$. According to Step 2 in the proof of Proposition 4.4, we have

$$\lim_{\varepsilon \rightarrow 0} \mathcal{N}(u_{\varepsilon}, v_{\varepsilon}) = \mathcal{N}(u_0, v_0).$$

□

Lemma 4.8. Coarea Formula for Lipschitz Functions [40, Theorem 1.14]. On an open set $\Omega \subseteq \mathbb{R}^n$, let $\psi : \Omega \rightarrow \mathbb{R}$ be Lipschitz continuous and let $\eta : \mathbb{R} \rightarrow \mathbb{R}$ be Borel measurable. If $\eta \circ \psi$ is integrable, then

$$\int_{\mathbb{R}} \eta(r) \mathcal{H}^{n-1}(\{\vec{x} \in \Omega : \psi(\vec{x}) = r\}) dr = \int_{\Omega} \eta(\psi) |\nabla \psi|.$$

Lemma 4.9. Approximation of a set of finite perimeter [40, Lemma 1.15]. If a bounded open set $\Omega \subseteq \mathbb{R}^n$ has Lipschitz boundary, and $U \subseteq \mathbb{R}^n$ has finite perimeter, then there exists a sequence of open sets U_j with ∂U_j being a nonempty compact hypersurface of differentiability class C^2 and satisfying $\mathcal{H}^{n-1}(\partial U_j \cap \partial \Omega) = 0$, such that $\mathbf{1}_{U_j} \rightarrow \mathbf{1}_U$ in $L^2(\Omega)$, $\text{Per}_{\Omega} U_j \rightarrow \text{Per}_{\Omega} U$, and $|U_j| = |U|$.

Lemma 4.10. Diagonalization Argument. If double-indexed sequences $\{a_{j,k}\} \subseteq \mathbb{R}$ and $\{b_{j,k}\} \subseteq \mathbb{R}$ satisfy

$$\limsup_{j \rightarrow \infty} \limsup_{k \rightarrow \infty} a_{j,k} \leq A, \quad \limsup_{j \rightarrow \infty} \limsup_{k \rightarrow \infty} b_{j,k} \leq B,$$

for some constants $A, B \in \mathbb{R}$. Then there exists a diagonal sequence $j_k \rightarrow \infty$ as $k \rightarrow \infty$ such that

$$\limsup_{k \rightarrow \infty} a_{j_k, k} \leq A, \quad \limsup_{k \rightarrow \infty} b_{j_k, k} \leq B.$$

Proof. Define

$$j_1^* = \min \left\{ j \in \mathbb{N} : \limsup_{k \rightarrow \infty} a_{j,k} \leq A+1 \text{ and } \limsup_{k \rightarrow \infty} b_{j,k} \leq B+1 \right\}.$$

We claim that j_1^* exists. Otherwise for each $j \in \mathbb{N}$, we have $j \in \mathcal{A} \cup \mathcal{B}$, where $\mathcal{A} := \{j \in \mathbb{N} : \limsup_{k \rightarrow \infty} a_{j,k} > A+1\}$ and $\mathcal{B} := \{j \in \mathbb{N} : \limsup_{k \rightarrow \infty} b_{j,k} > B+1\}$. Therefore $|\mathcal{A}| = \infty$ or $|\mathcal{B}| = \infty$. If $|\mathcal{A}| = \infty$, then $\limsup_{j \rightarrow \infty} \limsup_{k \rightarrow \infty} a_{j,k} \geq A+1$, which is a contradiction.

From the definition of j_1^* , we know that k_1^* (defined as follows) exists.

$$k_1^* := \min \left\{ k \in \mathbb{N} : \sup_{l \geq k} a_{j_1^*, l} \leq A+2 \text{ and } \sup_{l \geq k} b_{j_1^*, l} \leq B+2 \right\}.$$

Recursively, for $p = [2, \infty) \cap \mathbb{N}$, define

$$j_p^* = \min \left\{ j > j_{p-1}^* : \limsup_{k \rightarrow \infty} a_{j,k} \leq A+1/p \text{ and } \limsup_{k \rightarrow \infty} b_{j,k} \leq B+1/p \right\},$$

and

$$k_p^* = \min \left\{ k > k_{p-1}^* : \sup_{l \geq k} a_{j_p^*, l} \leq A+2/p \text{ and } \sup_{l \geq k} b_{j_p^*, l} \leq B+2/p \right\}.$$

For each $p \geq 1$ and each $k \in [k_p^*, k_{p+1}^*) \cap \mathbb{N}$, define $j_k = j_p^*$, then

$$a_{j_k, k} \leq \sup_{l \geq k_p^*} a_{j_p^*, l} \leq A+2/p, \quad b_{j_k, k} \leq \sup_{l \geq k_p^*} b_{j_p^*, l} \leq B+2/p.$$

□

4.2.4 Convergence of global minimizers

Theorem 4.11. \mathcal{E}_0 is the Gamma-limit of \mathcal{E}_ε as $\varepsilon \rightarrow 0$.

Proof. See Propositions 4.4 and 4.7 for the liminf and limsup inequalities. □

Proposition 4.12. \mathcal{E}_ε has a global minimizer.

Proof. We use the direct method in the calculus of variations. We can show that for any fixed ε , any minimizing sequence $\{(u_j, v_j)\}$ of \mathcal{E}_ε are uniformly bounded in $W^{1,2}(\Omega) \times L^2(\Omega)$, and thus possesses a subsequence (not relabeled) satisfying $u_j \rightharpoonup u_\infty$ in $W^{1,2}(\Omega)$ and $v_j \rightarrow v_\infty$ in $L^2(\Omega)$ for some $u_\infty \in W^{1,2}(\Omega)$ and $v_\infty \in L^2(\Omega)$. By the Rellich–Kondrachov theorem, $u_j \rightarrow u_\infty$ both in $L^2(\Omega)$ and pointwise (up to a further subsequence). Similar to Step 5 of the Proof of Proposition 4.3, we can show $W(u_\infty, v_\infty) \leq \liminf_{j \rightarrow \infty} W(u_j, v_j)$. Similar to Step 2 of Proposition 4.4, we can show $\mathcal{N}(u_\infty, v_\infty) = \lim_{j \rightarrow \infty} \mathcal{N}(u_j, v_j)$.

Finally, since $u_j \rightharpoonup u_\infty$ in $W^{1,2}(\Omega)$ and $u_j \rightarrow u_\infty$ in $L^2(\Omega)$, by the Cauchy–Schwarz inequality we know $\|\nabla u_\infty\|_{L^2(\Omega)} \leq \liminf_{j \rightarrow \infty} \|\nabla u_j\|_{L^2(\Omega)}$. Therefore, we have proven $\mathcal{E}_\varepsilon(u_\infty, v_\infty) \leq \liminf_{j \rightarrow \infty} \mathcal{E}_\varepsilon(u_j, v_j)$, and therefore (u_∞, v_∞) is a global minimizer of \mathcal{E}_ε . □

Theorem 4.13. *Let $(u_\varepsilon, v_\varepsilon) \in W^{1,2}(\Omega) \times L^2(\Omega)$ be a global minimizer of \mathcal{E}_ε with $\varepsilon \rightarrow 0$, then any subsequence of $\{(u_\varepsilon, v_\varepsilon)\}$ has a further subsequence (not relabeled) such that $u_\varepsilon \rightarrow u_0$ in $L^2(\Omega)$ and $v_\varepsilon \rightarrow v_0$ in $L^2(\Omega)$, where $(u_0, v_0) \in BV(\Omega; \{0, 1\}) \times L^2(\Omega; [0, 1])$ is a global minimizer of \mathcal{E}_0 , satisfying $\mathcal{E}_0(u_0, v_0) = \liminf_{\varepsilon \rightarrow 0} \mathcal{E}_\varepsilon(u_\varepsilon, v_\varepsilon)$.*

Proof. According to [61, Bottom of Page 18], $\{\mathcal{E}_\varepsilon\}$ is equi-coercive thanks to the compactness result (Proposition 4.3). Since \mathcal{E}_0 is the Gamma-limit of \mathcal{E}_ε as $\varepsilon \rightarrow 0$ (Theorem 4.11), according to [61, Theorem 1.4.5], \mathcal{E}_0 has a global minimizer (u_0, v_0) such that $\mathcal{E}_0(u_0, v_0) = \liminf_{\varepsilon \rightarrow 0} \mathcal{E}_\varepsilon(u_\varepsilon, v_\varepsilon)$. Thanks to the compactness result (Proposition 4.3) and the limsup inequality (Proposition 4.7), we know that the global minimizer sequence $\{(u_\varepsilon, v_\varepsilon)\}$ is precompact, and every cluster point of this sequence is a global minimizer of \mathcal{E}_0 [61, Theorem 1.4.5]. \square

4.3 Equivalence to the original problem

We are now left with some justifications to make in order to establish the equivalence between the Gamma-limit \mathcal{E}_0 and the original problem E . Recall that E given by (1) is a functional of two subsets of \mathbb{R}^n , with G being the fundamental solution. In the definition of $\mathcal{E}_0(u, v)$, the function v is allowed to take any value between 0 and 1. However, as we show in Section 4.3.1, the minimizer (u_*, v_*) of \mathcal{E}_0 satisfies $v_* \in \{0, 1\}$ a.e., which means that v_* can be regarded as an indicator function. Since \mathcal{E}_0 is the Gamma-limit of \mathcal{E}_ε , the boundary conditions on G should be inherited from \mathcal{E}_ε to \mathcal{E}_0 , which can be either no boundary conditions (i.e., G is the fundamental solution) or periodic boundary conditions. In Section 4.3.2, we show the equivalence between those two types of boundary conditions.

4.3.1 Justification for the relaxation

We can regard \mathcal{E}_0 as a relaxed version of E , since the second argument of \mathcal{E}_0 is allowed to take intermediate values between 0 and 1. As we now explain, such relaxation does not affect the energy minimizers.

Proposition 4.14. *For any fixed $u \in BV(\Omega; \{0, 1\})$, if v_* is a global minimizer of $\mathcal{N}(u, v)$ (given by (11)) among all the $v \in L^2(\Omega; [0, 1])$ such that $vu = 0$ a.e. and $\int_\Omega v = \zeta \int_\Omega u$, then v_* must be an indicator function, i.e., $v_* \in \{0, 1\}$ a.e.*

Proof. Our proof is very similar to [7, Equation (3.11)] (see also [62, Lemma 4]). Given any fixed $\tau > 0$, we want to prove $|S| = 0$, where $S = \{\vec{x} \in \Omega : v_*(\vec{x}) \in (\tau, 1-\tau)\}$. If $|S| > 0$, define the perturbation $\psi = (\varphi_* - c)\mathbf{1}_S$, where $\varphi_* = G * (u - v_*/\zeta)$ and $c = \int_S \varphi_*/|S|$. According to [27, Theorem 9.9], we have $\varphi_* \in W^{2,p}(\Omega)$ for all $1 < p < \infty$, and $\Delta\varphi_* = u - v_*/\zeta$ a.e. on Ω . In particular, we have $\Delta\varphi_* < -\tau/\zeta$ a.e. on S , because $v_* > \tau > 0$ a.e. on S and $u = 0$ a.e. on S (due to $v_*u = 0$ a.e. on Ω).

We compute the following first-order variation:

$$\left. \frac{d}{d\delta} \mathcal{N}(u, v_* - \psi\delta) \right|_{\delta=0} = \int_\Omega \psi \varphi_*/\zeta = \int_\Omega \varphi_*(\varphi_* - c)\mathbf{1}_S/\zeta = \int_S \varphi_*(\varphi_* - c)/\zeta = \int_S (\varphi_* - c)^2/\zeta.$$

Due to the minimality condition on v_* , the above left-hand side is zero, and thus φ_* is constant a.e. on S . According to [27, Lemma 7.7], which asserts that the weak derivatives of a Sobolev function are zero a.e. on its level set, we have $\nabla\varphi_* = \vec{0}$ a.e. on S , and consequently $\Delta\varphi_* = 0$ a.e. on S , which is a contradiction. \square

4.3.2 Justification for boundary conditions

4.3.2.1 Compactly supported minimizers We now establish that periodic boundary conditions and no boundary conditions on G are equivalent for the purpose of energy minimization in the sharp interface limit, as long as Ω is sufficiently large so that the minimizers are compactly supported in Ω . The key is the screening property satisfied by the energy minimizers [6, Corollary 3.3], i.e., different connected components of a minimizer do not interact with each other. So far we have been ambiguously using G for the Green's functions of $-\Delta$ under either periodic boundary conditions or no boundary conditions. From now on, we let \tilde{G} denote the former, and let G denote the latter. We use analogous notations for other symbols as well: e.g., E is given by (1) with the nonlocal kernel G being the fundamental solution, and \tilde{E} is the periodic counterpart with the nonlocal kernel being the Green's function under periodic boundary conditions.

Proposition 4.15. Let (U, V) be a global minimizer of E , and let (\tilde{U}, \tilde{V}) be a global minimizer of \tilde{E} , under the mass constraints $|U| = |\tilde{U}| = m$ and $|V| = |\tilde{V}| = \zeta m$. If Ω is large enough for U, V, \tilde{U} and \tilde{V} to be compactly supported in Ω with positive distance to $\partial\Omega$, then $E(U, V) = \tilde{E}(U, V) = E(\tilde{U}, \tilde{V}) = \tilde{E}(\tilde{U}, \tilde{V})$.

Proof.

Step 1: We first prove $E(U, V) = \tilde{E}(U, V) \geq \tilde{E}(\tilde{U}, \tilde{V})$. It suffices to prove $N(U, V) = \tilde{N}(U, V)$, where \tilde{N} is the periodic counterpart of N (i.e., \tilde{N} is the nonlocal term with the nonlocal kernel being the Green's function under periodic boundary conditions). According to Proposition 1.1-(3), we have $\phi_{U,V} = 0$ in $\Omega \setminus (U \cup V)$, where $\phi_{U,V}$ is the electrostatic potential ϕ associated with U and V , given by (2). Since $\phi_{U,V}$ satisfies periodic boundary conditions and the Poisson's equation $-\Delta\phi_{U,V} = \mathbf{1}_U - \mathbf{1}_V/\zeta$, we have $\tilde{\phi}_{U,V} = \text{constant} + \phi_{U,V}$, where $\tilde{\phi}_{U,V}$ is the solution to $-\Delta\tilde{\phi}_{U,V} = \mathbf{1}_U - \mathbf{1}_V/\zeta$ under periodic boundary conditions. According to (3), we have $2N(U, V) = \int_U \phi_{U,V} - \int_V \phi_{U,V}/\zeta = \int_U \tilde{\phi}_{U,V} - \int_V \tilde{\phi}_{U,V}/\zeta = 2\tilde{N}(U, V)$.

Step 2: We now prove $\tilde{E}(\tilde{U}, \tilde{V}) = E(\tilde{U}, \tilde{V}) \geq E(U, V)$. It suffices to prove $\tilde{N}(\tilde{U}, \tilde{V}) = N(\tilde{U}, \tilde{V})$. In Step 3 we will prove $\tilde{\phi}_{\tilde{U},\tilde{V}} = \text{constant}$ in $\Omega \setminus (\tilde{U} \cup \tilde{V})$, so we can extend $\tilde{\phi}_{\tilde{U},\tilde{V}}$ to be this constant in $\mathbb{R}^n \setminus \Omega$. Since $\phi_{\tilde{U},\tilde{V}}$ vanishes at infinity [7, Lemma 3.1], $\tilde{\phi}_{\tilde{U},\tilde{V}} - \phi_{\tilde{U},\tilde{V}}$ is harmonic and bounded in \mathbb{R}^n , therefore $\tilde{\phi}_{\tilde{U},\tilde{V}} - \phi_{\tilde{U},\tilde{V}} = \text{constant}$. Similar to Step 1, we can prove $\tilde{N}(\tilde{U}, \tilde{V}) = N(\tilde{U}, \tilde{V})$.

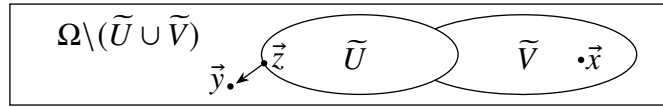


Figure 6: Step 3 in the Proof of Proposition 4.15.

Step 3: Now let us prove $\tilde{\phi}_{\tilde{U},\tilde{V}} = \text{constant}$ in $\Omega \setminus (\tilde{U} \cup \tilde{V})$. Our proof is similar to [7, Section 4]. According to [6, Top of Page 8], E is a volume perturbation of the perimeter, and U is a quasi-minimizer of the perimeter, so ∂U is of differentiability class C^∞ (Proposition 1.1-(2)). Similarly, \tilde{E} is also a volume perturbation of the perimeter, so we can assume that \tilde{U} and \tilde{V} are open, and that $\partial\tilde{U}$ is of differentiability class C^∞ . If \tilde{V} is not open, we can instead consider the points at which the Lebesgue density of \tilde{V} is positive, similar to [7, Page 1141]. See Figure 6 for visualization.

Using the optimality of \tilde{V} for $\tilde{N}(\tilde{U}, \cdot)$, we can prove the following by contradiction:

$$\tilde{\phi}_{\tilde{U},\tilde{V}}(\vec{x}) \geq \tilde{\phi}_{\tilde{U},\tilde{V}}(\vec{y}), \quad \text{for any } \vec{x} \in \tilde{V} \text{ and any } \vec{y} \in \Omega \setminus \overline{\tilde{U} \cup \tilde{V}}.$$

Otherwise, we can decrease the energy by moving some negative charge from a neighborhood of \vec{x} to a neighborhood of \vec{y} . More precisely, since $\tilde{\phi}_{\tilde{U},\tilde{V}}$ is continuous and $2\tilde{N}(\tilde{U},\tilde{V}) = \int_{\tilde{U}} \tilde{\phi}_{\tilde{U},\tilde{V}} - \int_{\tilde{V}} \tilde{\phi}_{\tilde{U},\tilde{V}}/\zeta$, we can define a competitor $\tilde{V}_r = B(\vec{y};r) \cup \tilde{V} \setminus B(\vec{x};r)$ where r is small enough, and $\tilde{N}(\tilde{U},\tilde{V}_r) < \tilde{N}(\tilde{U},\tilde{V})$.

On $\Omega \setminus (\tilde{U} \cup \tilde{V})$, since $\tilde{\phi}_{\tilde{U},\tilde{V}}$ is harmonic and satisfies the periodic boundary conditions, its minimum a and maximum b are attained on the boundary $\partial(\tilde{U} \cup \tilde{V})$. If $\tilde{\phi}_{\tilde{U},\tilde{V}}$ is non-constant in $\Omega \setminus (\tilde{U} \cup \tilde{V})$, then $a < b \leq \tilde{\phi}_{\tilde{U},\tilde{V}}(\vec{x})$ for any $\vec{x} \in \tilde{V}$, and the minimum a can only be attained on $\partial\tilde{U} \setminus \partial\tilde{V}$, because $\tilde{\phi}_{\tilde{U},\tilde{V}}$ is continuous in Ω . Let $\vec{z} \in \partial\tilde{U} \setminus \partial\tilde{V}$ such that $\tilde{\phi}_{\tilde{U},\tilde{V}}(\vec{z}) = a$. Without loss of generality, let us assume that \tilde{U} is connected. Because $\tilde{\phi}_{\tilde{U},\tilde{V}} \geq a$ on both $\partial\tilde{U} \setminus \partial\tilde{V}$ and $\partial\tilde{U} \cap \partial\tilde{V}$, and $-\Delta\tilde{\phi}_{\tilde{U},\tilde{V}} = 1$ on \tilde{U} , by the strong minimum principle for superharmonic functions, we have $\tilde{\phi}_{\tilde{U},\tilde{V}} > a$ on \tilde{U} . Since \tilde{U} satisfies the interior ball condition ($\partial\tilde{U}$ is of differentiability class C^∞), the Hopf boundary point lemma [27, Lemma 3.4] states that the outer normal derivative of $\tilde{\phi}_{\tilde{U},\tilde{V}}$ at \vec{z} is negative, which is a contradiction to the minimality of a , because there is \vec{y} outside of $\tilde{U} \cup \tilde{V}$ such that \vec{y} is very close to \vec{z} and $\tilde{\phi}_{\tilde{U},\tilde{V}}(\vec{y}) < a$. \square

4.3.2.2 Non-compactly supported minimizers Even if Ω is not large enough and the global minimizer of \tilde{E} is not compactly supported in Ω , we believe the asymptotics in Conjecture 4.16 to hold true. Our rationale is that according to [62, Theorem 8], any lower-dimensional structure with zero dipole moment can be extended to a higher dimension using a radially symmetric cutoff function, with asymptotically the same energy-to-mass ratio.

Conjecture 4.16. Assume that (\tilde{U},\tilde{V}) satisfies the mass constraints $|\tilde{U}| = m$ and $|\tilde{V}| = \zeta m$, but we no longer require (\tilde{U},\tilde{V}) to be a global minimizer or compactly supported in Ω . Additionally, we assume that (\tilde{U},\tilde{V}) has zero dipole moment, i.e., $\int_{\Omega} \vec{x}(1_{\tilde{U}}(\vec{x}) - 1_{\tilde{V}}(\vec{x})/\zeta) d\vec{x} = \vec{0}$, which can be achieved by selecting a suitable translational representative according to Lemma 4.19. Let $(\tilde{U}_j,\tilde{V}_j)$ denote the juxtaposition of j^n copies of (\tilde{U},\tilde{V}) (there are j cycles along the direction of each standard basis vector in \mathbb{R}^n , similar to the cubic crystal structure). Then $\tilde{E}(\tilde{U},\tilde{V}) = \lim_{j \rightarrow \infty} E(\tilde{U}_j,\tilde{V}_j)/j^n$.

Remark 4.17.

- ① For $n = 3$, Conjecture 4.16 has a well-known discrete variant in which \tilde{U} and \tilde{V} are replaced by Dirac delta functions representing point charges with zero surface area. When calculating the electrostatic potential energy-to-mass ratio of a crystal made up of many (but finite) unit cells, solid physicists and material scientists usually take a shortcut: they consider only one unit cell and use Ewald summation which implicitly assumes periodic boundary conditions on Poisson's equation [35, Left of Page 7888]. Such Ewald summation gives an asymptotically correct value for a large but finite crystal surrounded by vacuum as long as the dipole moment in the unit cell is zero [59, Equation (1.8)], in which case the net Coulomb interaction decays sufficiently fast so that the summation is absolutely convergent. In this sense, periodic boundary conditions and no boundary conditions are equivalent for zero dipole moment.
- ② For a nonzero dipole moment, the correct electrostatic energy-to-mass ratio is the sum of an intrinsic part and an extrinsic part. The intrinsic part is given by the above Ewald summation and is dependent on the unit cell but independent of the global shape of the crystal [33]. The extrinsic part depends on the shape of the crystal, and can be interpreted as the outcome of "effective" charges distributed on the surface of the crystal (those surface charges reproduce the total dipole moment produced by

the unit cells in the bulk) [38, 59]. In this sense, periodic boundary conditions and no boundary conditions are not equivalent for a nonzero dipole moment.

- ③ The above extrinsic part should produce a voltage across the crystal formed by polar unit cells. However, this voltage seems to be absent in everyday life except in pyroelectric materials (whose polarization depends on the temperature). After a sufficiently long time at a constant temperature, even pyroelectric materials will lose such a voltage, because external charges will build up on the surface of the crystal through leakage currents (conducted by the crystal itself or the ambient atmosphere), thus canceling out that voltage in a similar way to grounding or earthing. Therefore, it seems more realistic to assume that the electrostatic potential is zero on the surface of the crystal, which leads to the homogeneous Dirichlet boundary conditions. According to Lemma 4.18, the electrostatic potential energy is actually minimized by the homogeneous Dirichlet boundary conditions. Many physicists and chemists refer to homogeneous Dirichlet boundary conditions as “tin foil” or “conducting” boundary conditions (imagine a crystal wrapped in a tin foil, or submerged in a conducting medium). They also believe that periodic boundary conditions and homogeneous Dirichlet boundary conditions are equivalent (see [54, Bottom-right of Page 5024], [24, Top-left of Page 6134] and [33, Right of Page 124106-1]). Therefore, the physical reality may be better approximated by periodic boundary conditions than by no boundary conditions in certain scenarios [38, Page 6167].

The following lemma shows that within a bounded and connected domain, among all the electrostatic potentials that solve the same Poisson’s equation, the electrostatic potential energy is minimized by the one satisfying homogeneous Dirichlet boundary conditions.

Lemma 4.18. Assuming that Ω is connected. For any fixed $\phi \in W^{1,2}(\Omega)$, consider the functional $h \mapsto \|\nabla(\phi - h)\|_{L^2(\Omega)}$ defined on the set consisting of all harmonic functions on Ω . Its global minimizer h_* is unique (up to addition of a constant) and satisfies Dirichlet boundary conditions $h_* = \phi$ on $\partial\Omega$.

Proof. Let h_* be a global minimizer, we can consider a competitor $h_* + \delta h$, where $\delta \in \mathbb{R}$ and h is any harmonic function on Ω . Since h_* is stationary, we have

$$0 = \frac{d}{d\delta} \|\nabla(\phi - h_* - \delta h)\|_{L^2(\Omega)}^2 \Big|_{\delta=0} = 2 \int_{\Omega} \nabla h \cdot \nabla(h_* - \phi) = 2 \int_{\partial\Omega} (h_* - \phi) \frac{\partial h}{\partial \vec{n}} - 2 \int_{\Omega} (h_* - \phi) \Delta h.$$

On the one hand, if $h_* - \phi$ is constant on $\partial\Omega$, then the above right-hand side vanishes, because $\int_{\partial\Omega} \partial h / \partial \vec{n} = \int_{\Omega} \Delta h = 0$. On the other hand, if $h_* - \phi$ is non-constant on $\partial\Omega$, then we can find a solution to Laplace’s equation $\Delta h = 0$ under Neumann boundary conditions $\partial h / \partial \vec{n} = \text{constant} + \phi - h_*$ on $\partial\Omega$, so that h_* is not stationary against the small perturbations along the direction h . In summary, $h_* - \phi$ must be constant on $\partial\Omega$. \square

The following lemma shows that any \vec{U} and \vec{V} contained in Ω can be periodically (or circularly) shifted so that the dipole moment vanishes, thus satisfying the assumption in Conjecture 4.16. Without loss of generality, we only present the 2-D case ($n = 2$).

Lemma 4.19. For any fixed $g \in L^1([0, 1]^2)$, we extend it periodically in both directions. If $\int_{[0, 1]^2} g(\vec{x}) d\vec{x} = 0$, then there exists $\vec{t} = (t_1, t_2) \in [0, 1]^2$ such that $\int_{[0, 1]^2} \vec{x} g(\vec{x} + \vec{t}) d\vec{x} = \vec{0}$.

Proof. Define $\vec{h}(\vec{t}) = (h_1(t_1, t_2), h_2(t_1, t_2)) = \int_{[0, 1]^2} \vec{x} g(\vec{x} + \vec{t}) d\vec{x}$, then \vec{h} is continuous in \mathbb{R}^2 . Since g is periodic in both directions, \vec{h} is also periodic. Moreover, we have $h_1(t_1, t_2) = \int_0^1 \int_0^1 x_1 g(x_1 + t_1, x_2 +$

$t_2) dx_2 dx_1 = \int_0^1 \int_0^1 x_1 g(x_1+t_1, x_2) dx_2 dx_1 = h_1(t_1, 0)$, and

$$\begin{aligned} \int_0^1 h_1(t_1, 0) dt_1 &= \int_0^1 \int_0^1 \int_0^1 x_1 g(x_1+t_1, x_2) dx_2 dx_1 dt_1 \\ &= \int_0^1 \int_0^1 \int_0^1 x_1 g(x_1+t_1, x_2) dt_1 dx_2 dx_1 \\ &= \int_0^1 \int_0^1 \int_0^1 x_1 g(t_1, x_2) dt_1 dx_2 dx_1 \\ &= \frac{1}{2} \int_0^1 \int_0^1 g(t_1, x_2) dt_1 dx_2 = 0. \end{aligned}$$

Therefore, there exists $t_1^* \in [0, 1]$ such that for any $t_2 \in \mathbb{R}$, we have $h_1(t_1^*, t_2) = h_1(t_1^*, 0) = 0$. Similarly, there exists $t_2^* \in [0, 1]$ such that for any $t_1 \in \mathbb{R}$, we have $h_2(t_1, t_2^*) = 0$. In summary we have $\vec{h}(t_1^*, t_2^*) = \vec{0}$. \square

5 Phase-field simulations

In this section, we present some numerical simulations based on the phase-field reformulation proposed in Section 4.

The numerical methods used in the simulations are very similar to those adopted in a previous work for the liquid drop model [69, Section III]. The main difference is that two phase-field functions are used here, whereas only one was used in the previous work. Similar to [69, Section III.A], we use the following nonlinear function for the definition of \mathcal{E} in Section 4.1:

$$f(z) := 3z^2 - 2z^3.$$

For the time-marching scheme, we still use the convex splitting scheme, but our choice of the convex splitting is different from [69, Equation (8)]. For the potential well W defined by (10), our choice here is $W = W_1 + W_2$, where $W_1(u, v) = 87u^2/2 + 27uv + 27v^2$ and $W_2 = W - W_1$. It is easy to check the convexity of W_1 and the concavity of W_2 on $[-0.1, 1.1] \times [-0.1, 1.1]$, which are sufficient to stabilize our numerical scheme. Similar to [69, Equation (5)], in order to find the local minimizers, we use the following L^2 gradient flow which is called the penalized Allen–Cahn–Ohta–Kawasaki (pACOK) dynamics:

$$\frac{\partial u}{\partial t} = -L_1 \frac{\delta \mathcal{E}}{\delta u}, \quad \frac{\partial v}{\partial t} = -L_2 \frac{\delta \mathcal{E}}{\delta v},$$

where $L_1, L_2 > 0$ are called mobility coefficients. We use the semi-implicit time-marching scheme similar to [69, Equation (8)].

In most simulations, the phase-fields almost vanish near $\partial\Omega$. According to Section 4.3.2, no boundary conditions (i.e., G is the fundamental solution) and periodic boundary conditions on G are equivalent for the purpose of energy minimization. Therefore we only need to consider periodic boundary conditions, which allow us to use the Fourier spectral method similar to [69, Section III.D].

Although the perimeter of V is not penalized in (1), we may add a penalty term $\int_{\Omega} |\nabla v|^2$ to \mathcal{E} in order for v to converge faster. In practice, the penalty coefficient of $\int_{\Omega} |\nabla v|^2$ can be chosen to be around $1/1250000$ of that of $\int_{\Omega} |\nabla u|^2$. Note that doing so is optional, and it will not significantly alter the numerical results but only provide some regularization for v .

In Sections 5.1 and 5.2, we present some possible local minimizers as well as some snapshots taken from pACOK dynamics, in order to provide numerical evidence for our conjectures about the Gamma-expansion of the sharp interface energy in 2-D and 3-D for $\zeta < \zeta_1$ (see the first statement in Conjecture 3.7 and the first statement in Conjecture 3.8, respectively).

5.1 Simulations in 2-D

In our 2-D simulations, we choose $\zeta = 1$, $\gamma = 1500$, $\varepsilon = 5 \times 10^{-2}$, $K_1 = 3 \times 10^4$, $K_2 = 24 \times 10^3/5$, $L_1 = 1$, $L_2 = 5$, $\Delta t = 25 \times 10^{-5}/2$ (which is the time step), and the simulation domain is chosen to be $[0, 13/5] \times [0, 13/5]$ which is then discretized into 256×256 uniform grid points. We visualize the results using RGB images of 256×256 pixels, where the hydrophobic region U is drawn in purplish pink, and the hydrophilic region V is drawn in greenish yellow. More specifically, we assign an RGB triplet to every possible value of (u, v) . We assign $(211, 95, 183)$, $(220, 220, 98)$ and $(255, 255, 255)$ to $(1, 0)$, $(0, 1)$ and $(0, 0)$, respectively. For other values of (u, v) , the RGB triplet is linearly interpolated from the above three, and then truncated to $[0, 255]^3$. The color at the position \vec{x} is then determined by the RGB triplet assigned to $(u(\vec{x}), v(\vec{x}))$.

We present 13 local minimizers in Figure 7. Next to each local minimizer is $(m, \mathcal{E}/m)$. Each local minimizer is obtained by choosing a suitable initial value, and then numerically simulating the pACOK dynamics until the iteration converges. The reason we treat them as local minimizers is that they appear to be stable against random perturbations in our simulations. One could further investigate their stability by evaluating the second-order variation of the energy or using rigorously validated numerics (similar to [46]).

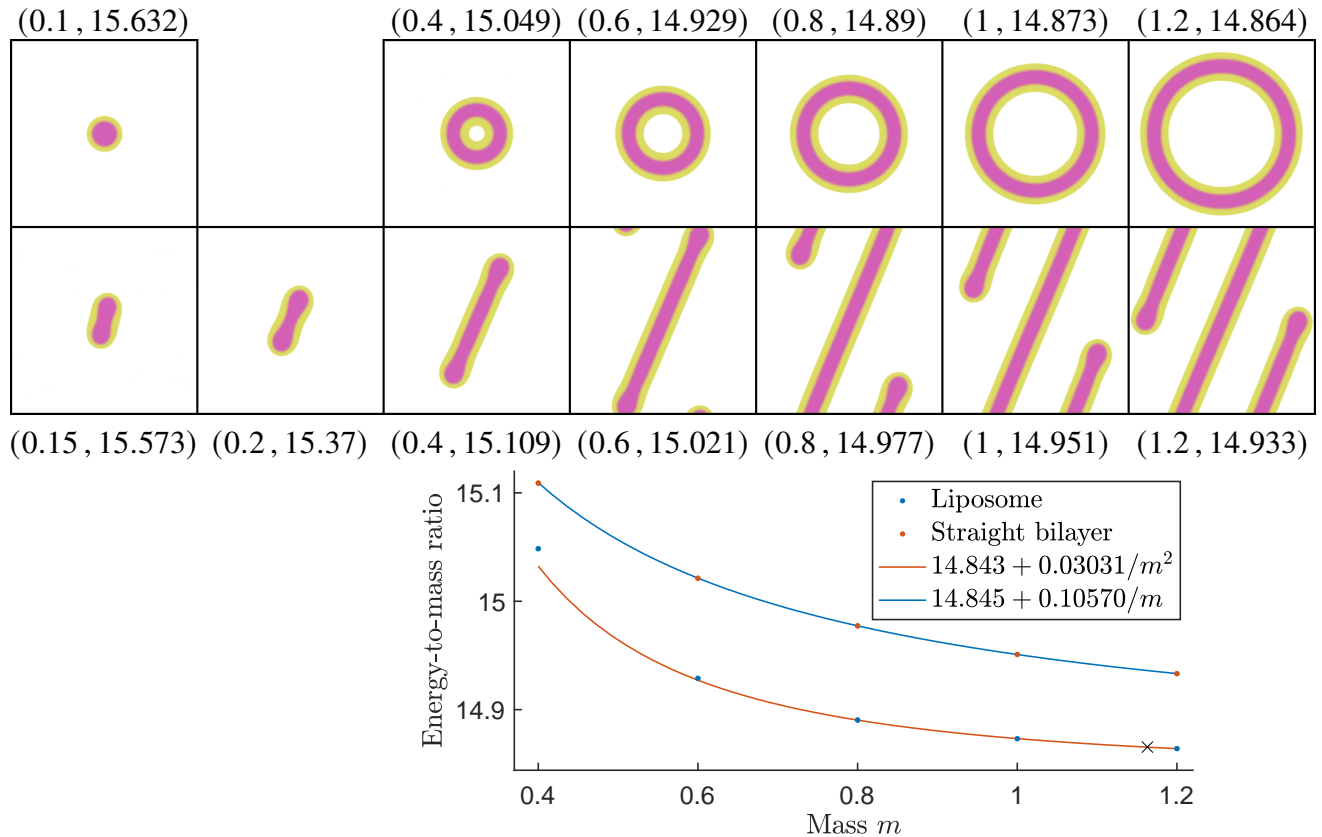


Figure 7: Top: local minimizers obtained in numerical simulations. Each square box represents the simulation domain containing a local minimizer. Next to each local minimizer are the mass and the energy-to-mass ratio. Bottom: curve fitting to the energy-to-mass ratios of the above local minimizers.

As we can see in Figure 7, the local minimizer is a micelle for $m = 0.1$, which is consistent with the 2-D generalization of Proposition 1.1-(4). As m increases to 0.15 and 0.2, the micelle is no longer stable and deforms into a shape that is similar to the eye-mask shaped local minimizers in [69, Figure 8]. As m further increases to 0.4 and beyond, as shown in the second row of Figure 7, the local minimizer becomes more and more elongated, resembling a straight bilayer of approximately uniform thickness, except that near the two ends the U layer is slightly thicker while the V layer is slightly thinner. The two open ends cause the straight bilayer to have slightly higher energy than the local minimizer shown in the first row of Figure 7, which resembles a liposome. The liposome and straight bilayer seem to prefer roughly the same thickness, which is consistent with Remark 2.4-(2). Their energy-to-mass ratios also seem to converge to roughly the same constant as $m \rightarrow \infty$, and the convergence rate for the liposome seems to be second-order, which is consistent with Corollary 2.2. The convergence rate for the straight bilayer seems to be first-order, indicating that the two open ends carry asymptotically constant energy penalties. Our numerical results therefore suggest a Gamma-expansion very similar to [50, Equation (1.6)] for $n = 2$ and $\zeta = 1$.

For the liposome local minimizers in Figure 7, we note that the inner V layer is slightly thicker than the outer V layer, and that such a difference becomes less noticeable as m increases, which are consistent with Remark 3.6-(1). Our numerical evidence indicates that for $n = 2$ and $\zeta = 1$, the optimal liposome candidate (whose asymptotics is given in Corollaries 2.2 and 3.4) is indeed a local minimizer, and might even be a global minimizer. In fact, if the first statement in Conjecture 3.7 is true, i.e., for $\zeta < \zeta_1$ the second-order

term in the Gamma-expansion of our energy is the elastica functional, then the global minimizer should be approximately (or exactly) circular according to Proposition 3.9.

In order to provide some numerical evidence for the first statement in Conjecture 3.7 and verify the resistance of the bilayer to bending, we carry out two simulations of the pACOK dynamics, as shown in Figure 8. In the first simulation, we choose $m = 1.163$, and we choose the initial value to be a bilayer of approximately uniform thickness, which resembles a random non-convex closed curve. We observe that over time, the bilayer becomes convex and resembles an ellipse, and eventually becomes circular after a sufficiently long time. The terminal value is shown in the top-right of Figure 8, and its energy-to-mass ratio is indicated by the black cross \times in the bottom-right of Figure 7. In the second simulation, we choose $m = 0.6$, and we choose the initial value by making a small hole in the liposome local minimizer shown in the top-middle of Figure 7. We observe that over time, the bilayer straightens and eventually converges to a straight bilayer, which is a rigid transformation of the straight bilayer shown in the middle of the second row in Figure 7. The convergence is relatively slow in both simulations, which is not surprising if the elastica functional is the second-order term in the Gamma-expansion.

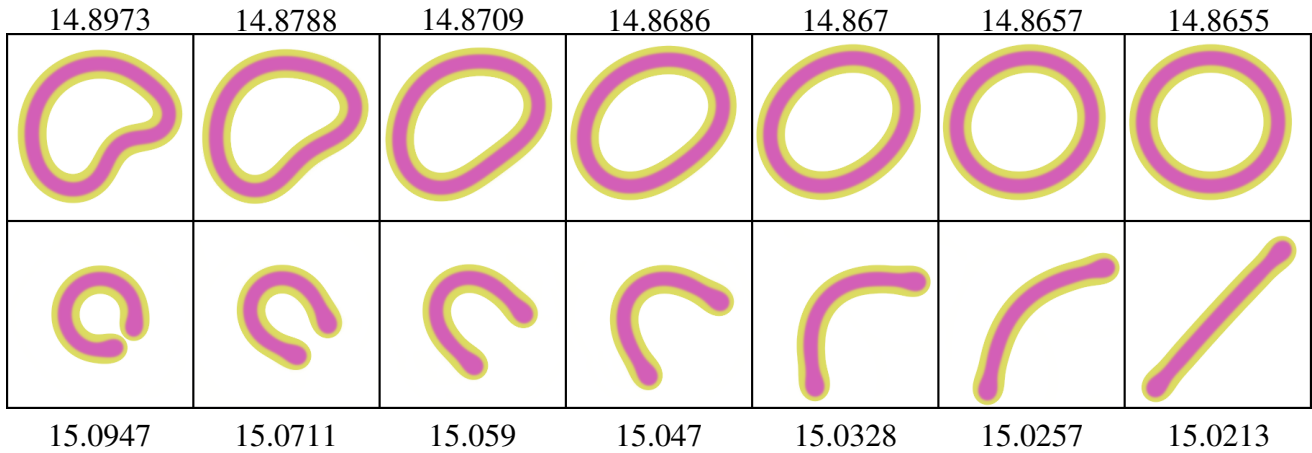


Figure 8: Numerical simulations of pACOK dynamics. Each square box represents a snapshot with t increasing from left to right. Next to each snapshot is the energy-to-mass ratio. Top: the first simulation with $m = 1.163$ and the initial value resembling a random curve. Bottom: the second simulation with $m = 0.6$ and the initial value resembling a perforated liposome.

5.2 Simulations in 3-D

In our 3-D simulations, we choose $\gamma = 500$, $L_1 = 1$, $L_2 = 4$, and the simulation domain $[0, X] \times [0, Y] \times [0, Z]$ is discretized into $N \times M \times P$ uniform grid points. We visualize the results using the following two MATLAB commands:

```
isosurface(u+v, 1/2); isosurface(u, 1/2);
```

where the former is set to be greenish yellow and transparent, representing the boundary of $\overline{U \cup V}$, while the latter is set to be purplish pink and opaque, representing the boundary of U . In order to visualize the inner structures, we also plot the cross-section with the cutting plane parallel to the front view and passing through the center of the simulation box.

We present 8 stationary points in Figure 9, each of which is the terminal value of the pACOK dynamics starting from a suitable initial value and evolving over a long period of time until the shape barely changes.

We present two simulations of the pACOK dynamics in Figure 10. In Figures 9 and 10, we choose $\zeta = 1$, $\varepsilon = 6 \times 10^{-2}$, $K_1 = 5/2 \times 10^4$, $K_2 = 4 \times 10^3$, and $\Delta t = 2.1 \times 10^{-5}$. In the top rows of Figures 9 and 10, we choose $X = Y = Z = 3.66$ and $M = N = P = 256$. In the last row in Figure 10 and in the left three columns of the last row in Figure 9, we choose $X = Y = 4Z = 3.66$ and $M = N = 4P = 256$. In the rightmost column of the last row in Figure 9, we choose $X/2 = Y/2 = 4Z = 3.66$ and $M/2 = N/2 = 4P = 256$.

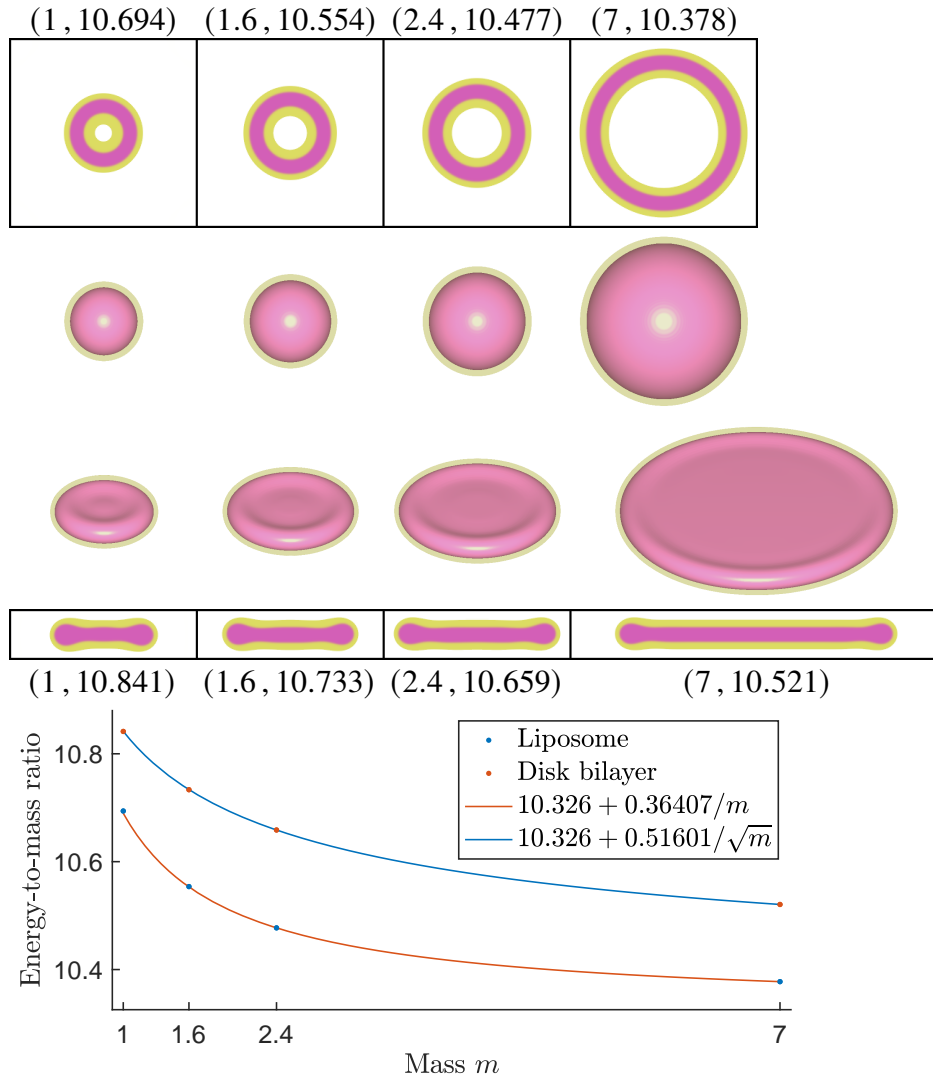


Figure 9: Top: stationary points obtained in numerical simulations. Each rectangle represents the cross-section of the simulation box. Next to each stationary point are the mass and the energy-to-mass ratio. Bottom: curve fitting to the energy-to-mass ratios of the above stationary points.

The stationary points in Figure 9 resemble liposomes and disk bilayers, and they prefer roughly the same thickness, which is consistent with Remark 2.4-②. Near the rim of a disk bilayer, the U layer is slightly thicker while the V layer is slightly thinner, which is a typical manifestation of frustration. Therefore, as $m \rightarrow \infty$, the disk bilayer should have a radius of order \sqrt{m} and a thickness of order 1. Its rim should have a perimeter of order \sqrt{m} and thus carry an energy penalty of order \sqrt{m} . Consequently, its energy-to-mass ratio should converge to a constant with order $1/2$, which is confirmed by the bottom of Figure 9. We can

also see that the energy-to-mass ratio of the liposome converges to roughly the same constant with order 1, which is consistent with Corollary 2.2. Our numerical calculations show that the liposome has lower energy than the disk bilayer, so that the latter cannot be a global minimizer. The liposome seems to be a local minimizer in our simulation. However, we are not confident that the disk bilayer is also a local minimizer, although its shape remains almost unchanged after 3.5×10^7 iterations. This is because the disk bilayer resembles an open surface, and we expect that the perimeter of its rim is penalized on the first order in the Gamma-expansion, and that the bending energy is only a second-order effect (see Section 3). Therefore, although the disk bilayer has zero bending energy, its priority should be to close in on itself and form a closed surface for sufficiently large m . In fact, we can see that for $m = 7$ the disk bilayer in Figure 9 has higher energy than the curved bilayer shown in the top-left of Figure 10, because the latter has smaller rim perimeter despite larger bending energy.

As mentioned above, for a bilayer resembling an open surface, we expect a first-order energy penalty associated with its rim. In order to gain more insights, we carry out two simulations in Figure 10. In the first and second simulations, the initial value is chosen by making a hole in the liposome ($m = 7$) and the disk bilayer ($m = 2.4$) that are obtained in Figure 9, respectively. We observe that the hole diminishes and vanishes over time (cf. Bottom of Figure 8 where the hole enlarges). Therefore, our numerical results demonstrate the self-healing property of lipid bilayers in 3-D, which is consistent with experimental observations [15] and is essential to biological membranes.

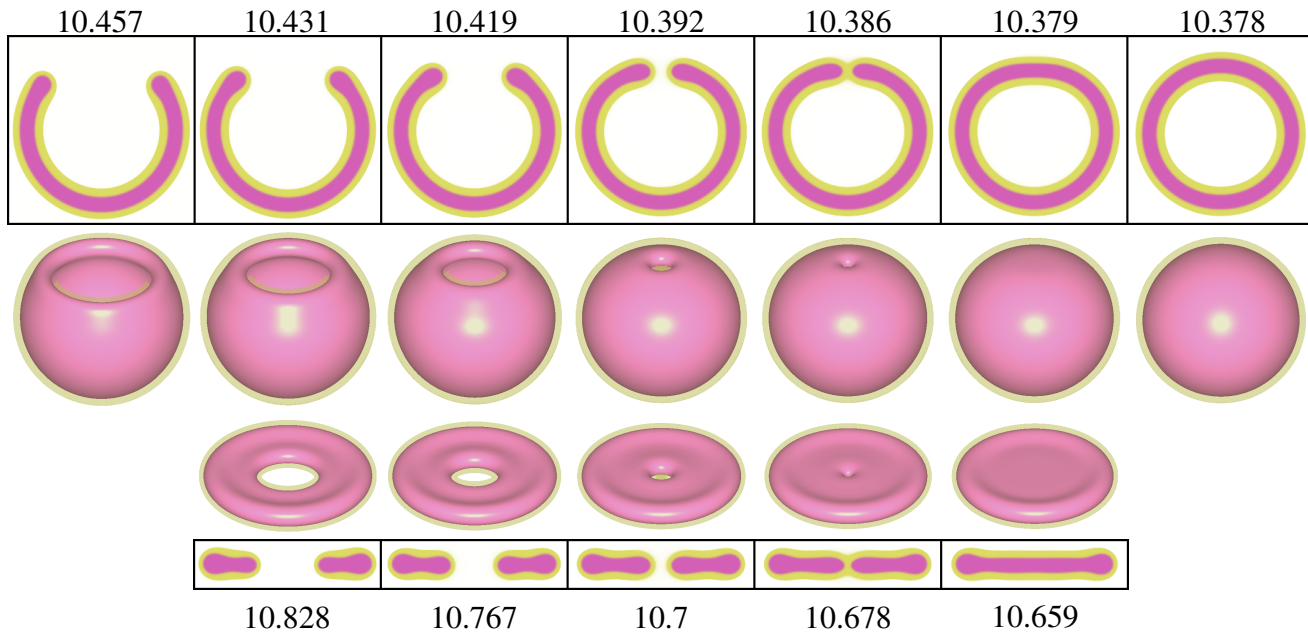


Figure 10: Numerical simulations of pACOK dynamics with t increasing from left to right. Next to each snapshot is the energy-to-mass ratio. Top: the first simulation with $m = 7$ and the initial value resembling a perforated liposome. Bottom: the second simulation with $m = 2.4$ and the initial value resembling a perforated disk bilayer.

In order to provide some numerical evidence for the first statement in Conjecture 3.8 (i.e., the Willmore energy appears in the second-order Gamma-expansion), we present two numerical simulations in Figure 11. Recall that the Clifford torus and its image under a conformal transformation are non-isolated local minimizers of the Willmore energy (see Figure 14). In the first and second simulations, we start from an

initial value resembling a torus and a deformed torus, respectively, let it evolve according to the pACOK dynamics over a long period of time until the shape barely changes, and plot the terminal value in the left and right of Figure 11, respectively. In both simulations we choose $m = 11.27$, $\zeta = 1$, $\varepsilon = 0.1$, $K_1 = 1.5 \times 10^4$, $K_2 = 2.4 \times 10^3$, $\Delta t = 9 \times 10^{-5}/8$, $X = Y = 2Z = 5.124$, and $\mathbb{M} = \mathbb{N} = 2\mathbb{P} = 256$. In Figure 11, the terminal values shown in the left and right resemble the Clifford torus and its image under a conformal map, respectively. The former seems to be a local minimizer, while the latter has slightly higher energy than the former and seems to be evolving very slowly in the direction of becoming the former. We think the reason why the latter is not a local minimizer is that diffuse interfaces are used in our phase-field simulations, or that the bilayer has nonzero thickness, so that higher-order terms in the Gamma-expansion destroy the non-isolated local minimality.

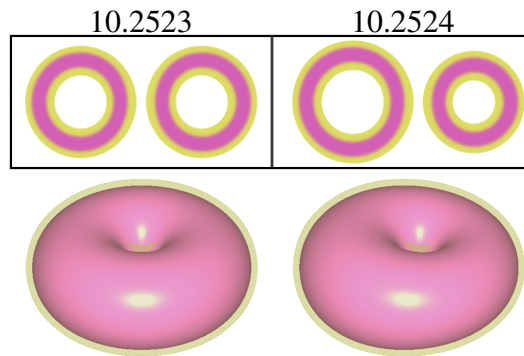


Figure 11: Terminal values of the pACOK dynamics after a sufficiently long time. Left: the first simulation with the initial value resembling a torus. Right: the second simulation with the initial value resembling a deformed torus.

In order to provide numerical evidence for Remark 3.11-② (i.e., triply periodic minimal surfaces may be preferred over planar bilayer for small ζ), we present four local minimizers shown in Figure 12. They are obtained as the terminal values of the pACOK dynamics starting from suitable initial values after a sufficiently long time. We choose $\varepsilon = 3.5 \times 10^{-2}$, $K_1 = 30 \times 10^4/7$, $K_2 = 48 \times 10^3/7$, $\Delta t = 21 \times 10^{-5}/40$, and $\mathbb{M} = \mathbb{N} = \mathbb{P} = 512$. We choose $\zeta = 0.6$ for the left two local minimizers, and choose $\zeta = 1$ for the right two local minimizers. We choose $X = Y = Z = 3.51$ for the left three local minimizers, and choose $X = Y = Z = 3.6855$ for the rightmost local minimizer. From left to right, we choose $m = 7.6886, 11.5742, 7.1262$ and 11.8021 , respectively, so that the respective energy-to-mass ratios are locally minimized with respect to m . From Figure 12 we can see that for $\zeta = 0.6$, the gyroid-like local minimizer has lower energy-to-mass ratio than the planar bilayer, and vice versa for $\zeta = 1$. This combined with Conjecture 4.16 is consistent with Remark 3.11-②.

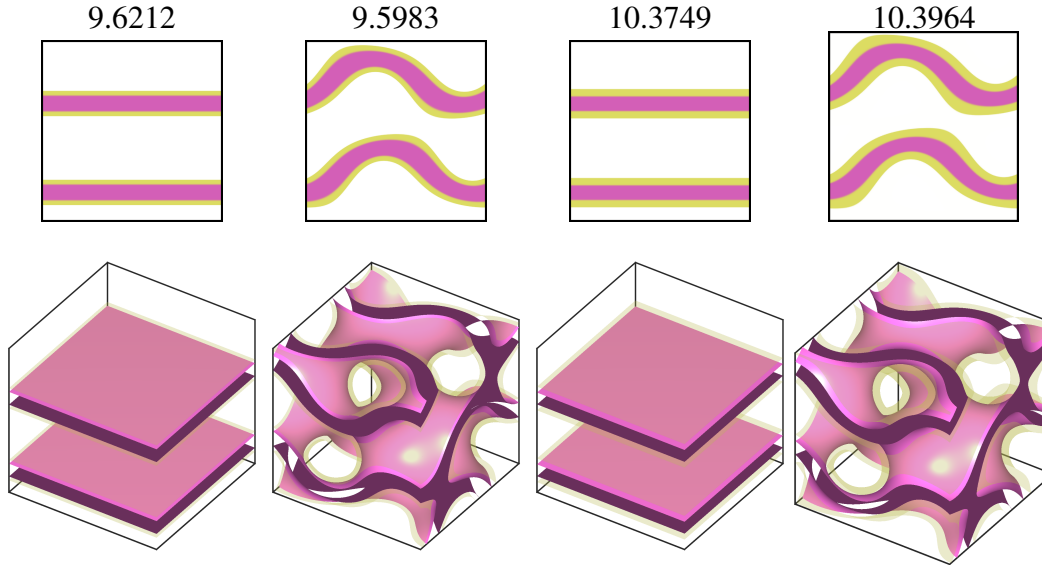


Figure 12: Four local minimizers. From left to right: $\zeta = 0.6, 0.6, 1, 1$. Next to each local minimizer is the energy-to-mass ratio.

In theory, the energy-to-mass ratio of the planar bilayer should equal that of the liposome in the limit of $m \rightarrow \infty$, which is given by $\sqrt[3]{9\gamma(\zeta+1)}/8$ in Corollary 2.2. With $\gamma = 500$, this constant equals 9.6549 and 10.4004 for $\zeta = 0.6$ and 1, respectively, which are slightly different than the respective numerical energy-to-mass ratios of the first and third local minimizers shown in Figure 12, with the relative error being -0.35% and -0.25% , respectively. We believe that this error is due to the diffuse interfaces used in our simulations. In fact, the initial values in this simulation are interpolated from the terminal values obtained in another simulation with a coarser grid, where we chose $\varepsilon = 7 \times 10^{-2}$ and $\mathbb{M} = \mathbb{N} = \mathbb{P} = 256$, with other parameters being the same. In the simulation with a coarser grid, we obtained four local minimizers similar to those shown in Figure 12, with their energy-to-mass ratios being 9.5211, 9.4955, 10.2989, and 10.3184, respectively from left to right. As $\varepsilon \rightarrow 0$ and $\mathbb{M}, \mathbb{N}, \mathbb{P} \rightarrow \infty$, we expect that the first and third energy-to-mass ratios converge to their respective theoretical values, and that the second and fourth ones maintain their relative differences to the first and third ones, respectively.

6 Discussion

In Figure 3, we can see that as ζ increases, the optimal morphology should transition from bilayer membrane to cylindrical micelle to spherical micelle. In the liquid drop model [69], a ball loses stability when its mass exceeds a threshold. Similarly, we expect that there exist two thresholds of ζ , beyond which the bilayer membrane and cylindrical micelle lose stability, respectively. For $\zeta = 1$, the straight bilayer membrane is stable on any 2-D periodic strip [63, Figure 1], and we think that the stability analysis therein can be generalized to any $\zeta \in (0, \infty)$, thus allowing us to determine the threshold of ζ beyond which the bilayer membrane is unstable. Note that such a threshold should be higher than ζ_1 in Figure 3.

As we mentioned in Remark 3.6, the inner V layer of the optimal liposome is slightly thicker but has slightly less mass compared to the outer V layer. We can intuitively explain this phenomenon in Figure 13-b, where a mismatch occurs as soon as a lipid bilayer membrane is curved. The inner monolayer becomes slightly more densely packed, while the outer monolayer becomes slightly less crowded. Those changes

will inevitably increase the energy. To alleviate such a problem, some lipids may be transferred from the inner monolayer to the outer monolayer, as shown in Figure 13-d. Our results indicate that when a closed bilayer membrane deforms (e.g., from a sphere to an ellipsoid), the lipids in the outer monolayer should flow from low curvature areas to high curvature areas, and vice versa for the inner monolayer. According to the fluid mosaic model [58], the lipids in a bilayer membrane can move easily within each monolayer, and they can also, albeit relatively slowly, move from one monolayer to the other (a movement known as flip-flop) [2, 51]. The flip-flop process can be facilitated by certain proteins known as flippase, floppase and scramblase. The flippase moves lipids from the outer monolayer to the inner monolayer (flipping), the floppase does the opposite (flopping), and the scramblase does both.

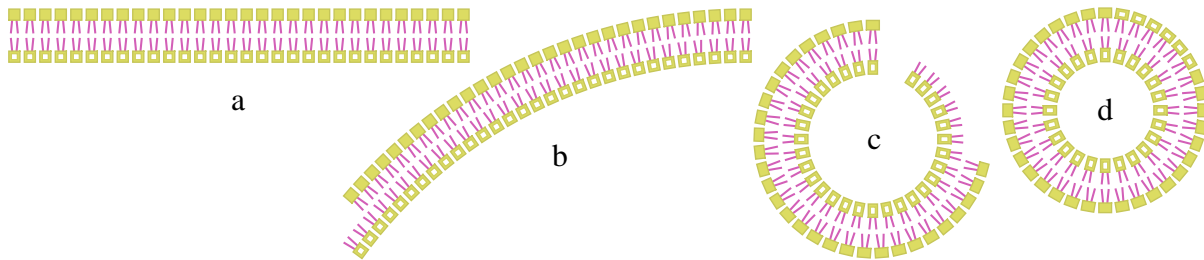


Figure 13: Mismatch of the two monolayers in a curved bilayer.

In this paper, we have studied a degenerate version of the Ohta–Kawasaki energy and demonstrated its remarkable ability to reproduce the fascinating phenomena exhibited by self-assembling amphiphiles. We have presented some asymptotic and numerical evidence for the partial localization property of our model. Partial localization is coined in [50, Section 1.2] and refers to the concentration to lower-dimensional structures. An important example is the bilayer membrane formed by lipids: it is thin along one direction, but relatively large along the other two. Such a structure is vital to the biological membranes of every living cell. Our study may help us better understand the formation of lipid bilayer membranes. In fact, there are only two terms in our energy: the perimeter term which models the immiscibility between water and hydrophobic tails, and a Coulombic nonlocal term which models the attractive force between the heads and tails. It turns out that our model still possesses similar properties even if this Coulombic term is replaced by the 1-Wasserstein distance [50, Section 9.5], which penalizes the heads for straying far from the tails. Neither our Coulombic term nor the 1-Wasserstein distance keeps track of which head is connected to which tail. Therefore, the specific structure of the lipid molecule (a head and a tail connected by a covalent bond) is not the essence of partial localization, although it is a practical way to enforce the long-range attractive force that is needed in our model.

For the variant model mentioned above (in which the nonlocal term is the 1-Wasserstein distance), only the case of $\zeta = 1$ has been considered in [50, 43]. In view of the rich complexity exhibited in our model for various ζ , it might be interesting to revisit this variant model in the general cases $\zeta > 0$. On this note, we also draw attention to the well-known linkage between the 2-Wasserstein distance and the nonlocal (negative) Sobolev space norm [23].

Our study is a step towards understanding the pattern formation phenomena from the viewpoint of energetic competition. It is the competition between the short- and long- range terms in the Ohta–Kawasaki energy that gives rise to various interesting mesoscopic periodic patterns that are commonly observed in block copolymers and many other systems [68, 11, 28, 48]. We show that in the degenerate case (i.e., only the interface of U is penalized), the Ohta–Kawasaki energy is capable of reproducing the partial localization

feature of self-assembling amphiphiles. It is natural to ask how far can our results be generalized. For example, it might be of mathematical interest to explore other variant models with the Euclidean perimeter replaced by the 1-perimeter [29], a fractional perimeter [19], or a general nonlocal perimeter [9], with the Coulomb potential replaced by a Yukawa potential [22], a Riesz potential [5], a fractional inverse Laplacian kernel [10, Appendix], or a general nonlocal kernel [42].

Acknowledgments

We would like to thank Xuenan Li, Johan Wärnegård, and Qi Zhang for helpful discussions. We thank the referee for helpful suggestions. This research is supported in part by US NSF DMS-1937254 and DMS-2309245. We acknowledge computing resources from Columbia University’s Shared Research Computing Facility project, which is supported by NIH Research Facility Improvement Grant 1G20RR030893-01, and associated funds from the New York State Empire State Development, Division of Science Technology and Innovation (NYSTAR) Contract C090171, both awarded April 15, 2010.

Data availability

The data that support the findings of this study are openly available in Open Science Framework at [DOI:10.17605/OSF.IO/U2896](https://doi.org/10.17605/OSF.IO/U2896).

Declarations of interest

None.

A Helfrich and Willmore energies

In this appendix we provide background on the Helfrich energy and Willmore energy. According to [30, Equation (2)], the Helfrich energy has been used to model a sheet-like membrane that resembles a regular closed surface S in \mathbb{R}^3 : $\int_S (\lambda_1(H - H_0)^2 + \lambda_2 K) dA$, where H is the mean curvature (mean of principal curvatures), H_0 is the spontaneous curvature, K is the Gaussian curvature, the bending modulus λ_1 is a positive constant, and the Gaussian (or saddle-splay) modulus λ_2 is a constant. For monolayers, H_0 is nonzero in general; for bilayers, H_0 is zero because of symmetry. By the Gauss–Bonnet formula, we have $\int_S K dA = 4\pi(1-g)$, where g is the genus of S , which is a constant as long as S does not undergo topological changes. In this way the Helfrich energy for bilayer membranes can be reduced to the Willmore energy $\int_S H^2 dA$, as long as no topological change happens.

The unique global minimizer of the Willmore energy is a sphere [66]. Under an additional constraint that S is of genus g , there exists a constrained global minimizer of the Willmore energy for any given $g \in \mathbb{N}_0$ [3]. For $g = 0$ (spherical topology), the sphere is the only minimizer of the Willmore energy, and the minimum energy is 4π . For $g = 1$ (toroidal topology), the Clifford torus [44] is the unique minimizer up to conformal transformations (this is because the Willmore energy is conformal invariant [57, Section 5.1]), and the minimum energy is $2\pi^2$. For $g \geq 2$, the minimizer is unknown but conjectured to be

Lawson's surfaces [34]. The minimum energy converges to 8π as g goes to infinity (and is conjectured to be monotonically increasing) [39].

The above-mentioned toroidal minimizer of the Willmore energy for $g = 1$ was conjectured in 1965 [66] and proved in 2014 [44]. Such a long-held conjecture was partly supported by the experimental observation of toroidal structures formed by artificial membranes [47, Figures 3 and 4] (see also [49, 26]), as shown in Figure 14. In addition, there were some numerical evidence from phase-field simulations of the Willmore energy [20, Section 4.3.2]. This result is also manifested in our numerical simulations (see Figure 11), thus providing support for the first statement in Conjecture 3.8.

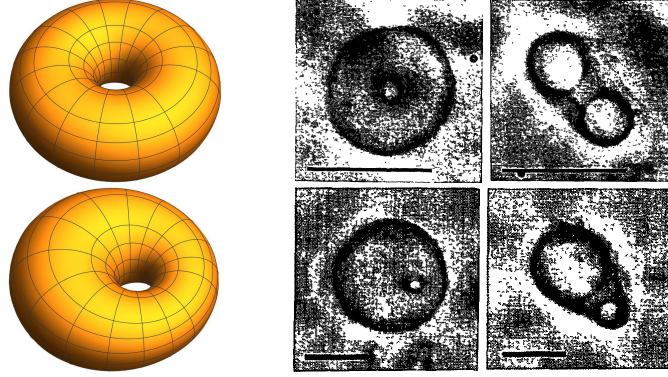


Figure 14: Top-left: Clifford torus given by [57, Equation (5.3)]. Bottom-left: Its image under a conformal transformation. Top-right: Clifford torus observed in [47, Figure 3]. Bottom-right: Deformed Clifford torus observed in [47, Figure 4]. Bar indicates $10 \mu\text{m}$. The right part is reproduced from [47].

B Calculations of radially symmetric candidates

In this appendix we derive the asymptotic results presented in Section 2.1.

Proposition B.1. The energy (1) of a liposome candidate is $E(U, V) = \text{Per } U + \gamma N(U, V)$, where

$$\text{Per } U = \begin{cases} 2\pi(R_1 + R_2), & n = 2, \\ 4\pi(R_1^2 + R_2^2), & n = 3. \end{cases}$$

For $n = 2$, we have

$$16\zeta^2 N(U, V)/\pi = (1 - \zeta^2)(R_2^4 - R_1^4) + R_0^4 - R_3^4 + 4\left(R_3^4 \ln R_3 - R_0^4 \ln R_0\right. \\ \left. + (\zeta + 1)(2R_0^2 R_1^2 - (\zeta + 1)R_1^4) \ln R_1 - (\zeta + 1)(2R_3^2 R_2^2 - (\zeta + 1)R_2^4) \ln R_2\right). \quad (12)$$

For $n = 3$, we have

$$15\zeta^2 N(U, V)/\pi = 6(R_0^5 - R_3^5) + (\zeta + 1)\left(10R_2^2 R_3^3 - (6\zeta + 4)R_2^5 + (6\zeta + 4)R_1^5 - 10R_0^3 R_1^2\right). \quad (13)$$

Proposition B.2. Any minimizer of $E(U, V)$ among the liposome candidates must satisfy the following conditions if $n = 2$,

$$\begin{aligned} R_3^2 \ln R_3^2 - R_0^2 \ln R_0^2 &= (\zeta + 1)(R_2^2 \ln R_2^2 - R_1^2 \ln R_1^2), \\ 4\zeta^2(\zeta + 1)^{-1}\gamma^{-1}(R_1^{-1} + R_2^{-1}) &= \zeta(R_2^2 - R_1^2) + (R_0^2 - (\zeta + 1)R_1^2) \ln(R_2^2/R_1^2), \end{aligned}$$

and satisfy the following equations if $n = 3$ (see also [7, Equation (A.1)]),

$$\begin{aligned} R_3^2 - R_0^2 &= (\zeta + 1)(R_2^2 - R_1^2), \\ 12\zeta^2\gamma^{-1}(R_1^{-1} + R_2^{-1}) &= (3\zeta + 2)(R_3^2 - R_0^2) + 2(\zeta + 1)(R_0^3/R_1 - R_3^3/R_2). \end{aligned}$$

Theorem B.3. With ζ and γ fixed, as $m \rightarrow \infty$, the minimizer of $E(U, V)$ among the liposome candidates has the following asymptotics if $n = 2$,

$$\begin{aligned} \frac{E(U, V)}{m} &= \sqrt[3]{\gamma \frac{\zeta + 1}{8/9}} + \frac{8\pi^2}{5} \frac{\zeta^2 + 4\zeta + 1}{\gamma(\zeta + 1)m^2} + O\left(\frac{1}{m^3}\right), & R_2 - R_1 &= \sqrt[3]{\frac{24/\gamma}{\zeta + 1}} + O\left(\frac{1}{m^2}\right), \\ (R_3^2 - R_2^2) - (R_1^2 - R_0^2) &= \frac{4\zeta(\zeta + 2)}{\sqrt[3]{3(\gamma\zeta + \gamma)^2}} + O\left(\frac{1}{m^2}\right), & \frac{R_1 + R_2}{2} &= \frac{m}{4\pi} \sqrt[3]{\gamma \frac{\zeta + 1}{3}} + O\left(\frac{1}{m}\right), \\ R_1 - R_0 &= \sqrt[3]{\frac{3}{\gamma} \frac{\zeta^3}{\zeta + 1}} + \frac{2\pi\zeta}{\gamma m} \frac{\zeta + 2}{\zeta + 1} + O\left(\frac{1}{m^2}\right), & R_3 - R_2 &= \sqrt[3]{\frac{3}{\gamma} \frac{\zeta^3}{\zeta + 1}} - \frac{2\pi\zeta}{\gamma m} \frac{\zeta + 2}{\zeta + 1} + O\left(\frac{1}{m^2}\right), \end{aligned}$$

and has the following asymptotics if $n = 3$,

$$\begin{aligned} \frac{E(U, V)}{m} &= \sqrt[3]{\gamma \frac{\zeta + 1}{8/9}} + \frac{4\pi}{15m} \frac{\zeta^2 + 4\zeta + 16}{(\gamma(\zeta + 1)/3)^{2/3}} + O\left(\frac{1}{m^{3/2}}\right), & R_2 - R_1 &= \sqrt[3]{\frac{24/\gamma}{\zeta + 1}} + O\left(\frac{1}{m}\right), \\ (R_3^3 - R_2^3) - (R_1^3 - R_0^3) &= \frac{\sqrt{6m\zeta(\zeta + 2)}}{\sqrt{\pi\gamma(\zeta + 1)}} + O\left(\frac{1}{m^{1/2}}\right), & \frac{R_1 + R_2}{2} &= \frac{\sqrt[6]{\gamma(\zeta + 1)/3}}{2\sqrt{2\pi/m}} + O\left(\frac{1}{m^{1/2}}\right), \\ R_1 - R_0 &= \sqrt[3]{\frac{3}{\gamma} \frac{\zeta^3}{\zeta + 1}} + \frac{(\zeta + 2)\sqrt{8\pi/m}}{\sqrt[6]{3(\gamma\zeta + \gamma)^5/\zeta}} + O\left(\frac{1}{m}\right), & R_3 - R_2 &= \sqrt[3]{\frac{3}{\gamma} \frac{\zeta^3}{\zeta + 1}} - \frac{(\zeta + 2)\sqrt{8\pi/m}}{\sqrt[6]{3(\gamma\zeta + \gamma)^5/\zeta}} + O\left(\frac{1}{m}\right). \end{aligned}$$

Proposition B.4. Under the additional assumption that the inner and outer V layers have the same mass [61, Equation (5.16)], i.e.,

$$R_3^n - R_2^n = R_1^n - R_0^n, \quad (14)$$

with ζ and γ fixed, as $m \rightarrow \infty$, the minimizer of $E(U, V)$ among the liposome candidates (satisfying (14)) has the following asymptotics if $n = 2$,

$$\begin{aligned} \frac{E(U, V)}{m} &= \sqrt[3]{\gamma \frac{\zeta + 1}{8/9}} + 24\pi^2 \frac{2\zeta^2 + 8\zeta + 7}{5\gamma(\zeta + 1)m^2} + O\left(\frac{1}{m^3}\right), \\ R_1 - R_0 &= \sqrt[3]{\frac{3}{\gamma} \frac{\zeta^3}{\zeta + 1}} + \frac{6\pi\zeta}{m\gamma} \frac{\zeta + 2}{\zeta + 1} + O\left(\frac{1}{m^2}\right), & R_2 - R_1 &= \sqrt[3]{\frac{24/\gamma}{\zeta + 1}} + O\left(\frac{1}{m^2}\right), \\ R_3 - R_2 &= \sqrt[3]{\frac{3}{\gamma} \frac{\zeta^3}{\zeta + 1}} - \frac{6\pi\zeta}{m\gamma} \frac{\zeta + 2}{\zeta + 1} + O\left(\frac{1}{m^2}\right), & \frac{R_1 + R_2}{2} &= \frac{\sqrt[3]{\gamma(\zeta + 1)/3}}{4\pi/m} + O\left(\frac{1}{m}\right), \end{aligned}$$

and has the following asymptotics if $n = 3$,

$$\begin{aligned}\frac{E(U, V)}{m} &= \sqrt[3]{\gamma \frac{\zeta+1}{8/9}} + \frac{4\pi}{5m} \frac{7\zeta^2+28\zeta+32}{(\gamma(\zeta+1)/3)^{2/3}} + O\left(\frac{1}{m^{3/2}}\right), \\ R_1 - R_0 &= \sqrt[3]{\frac{3}{\gamma} \frac{\zeta^3}{\zeta+1}} + \frac{\zeta(\zeta+2)\sqrt{8\pi/m}}{((\gamma\zeta+\gamma)/3)^{5/6}} + O\left(\frac{1}{m}\right), & R_2 - R_1 &= \sqrt[3]{\frac{24/\gamma}{\zeta+1}} + O\left(\frac{1}{m}\right), \\ R_3 - R_2 &= \sqrt[3]{\frac{3}{\gamma} \frac{\zeta^3}{\zeta+1}} - \frac{\zeta(\zeta+2)\sqrt{8\pi/m}}{((\gamma\zeta+\gamma)/3)^{5/6}} + O\left(\frac{1}{m}\right), & \frac{R_1+R_2}{2} &= \frac{\sqrt[6]{\gamma(\zeta+1)/3}}{2\sqrt{2\pi/m}} + O\left(\frac{1}{m^{1/2}}\right).\end{aligned}$$

Proof. [of Proposition B.1] Similar to [62, Page 106], we compute the electrostatic potential ϕ and then use (3) to obtain $N(U, V)$. We know that $\phi(\vec{x})$ is radially symmetric and can be written as $\phi(r)$ with $r = |\vec{x}|$, satisfying

$$-r^{1-n} \frac{d}{dr} (r^{n-1} \phi'(r)) = [R_1 \leq r \leq R_2] - \frac{[R_0 \leq r \leq R_1 \text{ or } R_2 \leq r \leq R_3]}{\zeta},$$

where the left-hand side is due to Laplacian expressed in spherical coordinates, and $[\cdot]$ on the right-hand side is the Iverson bracket. Since ϕ is a continuously differentiable even function, we have $\phi'(0) = 0$. We further require $\phi(\infty) = 0$.

For $n = 2$, we obtain

$$4\zeta\phi(r) = \begin{cases} 0, & R_3 < r < \infty, \\ 2(R_3^2 \ln R_3) - R_3^2 + r^2 - 2R_3^2 \ln r, & R_2 < r < R_3, \\ 2(R_3^2 \ln R_3 - (\zeta+1)R_2^2 \ln R_2) - R_3^2 + (\zeta+1)R_2^2 - \zeta r^2 - 2(R_3^2 - (\zeta+1)R_2^2) \ln r, & R_1 < r < R_2, \\ 2(R_3^2 \ln R_3 - (\zeta+1)R_2^2 \ln R_2 + (\zeta+1)R_1^2 \ln R_1) - R_0^2 + r^2 - 2R_0^2 \ln r, & R_0 < r < R_1, \\ 2(R_3^2 \ln R_3 - (\zeta+1)R_2^2 \ln R_2 + (\zeta+1)R_1^2 \ln R_1 - R_0^2 \ln R_0), & 0 < r < R_0. \end{cases}$$

For $n = 3$, we obtain

$$6\zeta\phi(r) = \begin{cases} 0, & R_3 < r < \infty, \\ -3(R_3^2) + 2R_3^3/r + r^2, & R_2 < r < R_3, \\ -3(R_3^2 - (\zeta+1)R_2^2) + 2(R_3^3 - (\zeta+1)R_2^3)/r - \zeta r^2, & R_1 < r < R_2, \\ -3(R_3^2 - (\zeta+1)R_2^2 + (\zeta+1)R_1^2) + 2R_0^3/r + r^2, & R_0 < r < R_1, \\ -3(R_3^2 - (\zeta+1)R_2^2 + (\zeta+1)R_1^2 - R_0^2), & 0 < r < R_0. \end{cases}$$

Notice that we have used (4) to simplify the expressions for ϕ . □

Proof. [of Proposition B.2] We minimize $E(U, V)$ given by Proposition B.1 with constraints (4) and (5).

For $n = 2$, we obtain

$$\begin{aligned}R_3^2 \ln R_3 - (\zeta+1)R_2^2 \ln R_2 &= \lambda = R_0^2 \ln R_0 - (\zeta+1)R_1^2 \ln R_1, \quad \text{and} \\ R_0^2 \left(\ln R_1 + \frac{1}{2}\right) - R_1^2 \left((\zeta+1) \ln R_1 + \frac{1}{2}\right) + \frac{2\zeta^2 R_1^{-1}}{\gamma(\zeta+1)} &= \lambda - \frac{\mu}{\zeta+1} \\ &= R_3^2 \left(\ln R_2 + \frac{1}{2}\right) - R_2^2 \left((\zeta+1) \ln R_2 + \frac{1}{2}\right) - \frac{2\zeta^2 R_2^{-1}}{\gamma(\zeta+1)},\end{aligned}$$

where λ and μ are Lagrange multipliers. From the last two equalities, we obtain

$$\begin{aligned}
\frac{4\zeta^2(R_1^{-1}+R_2^{-1})}{\gamma(\zeta+1)} &= R_3^2(\ln R_2^2 + 1) - R_2^2((\zeta+1) \ln R_2^2 + 1) + R_1^2((\zeta+1) \ln R_1^2 + 1) - R_0^2(\ln R_1^2 + 1) \\
&= R_3^2 - R_0^2 + R_1^2 - R_2^2 + (\zeta+1)(R_1^2 \ln R_1^2 - R_2^2 \ln R_2^2) + R_3^2 \ln R_2^2 - R_0^2 \ln R_1^2 \\
&= \zeta(R_2^2 - R_1^2) + (\zeta+1)(R_1^2 \ln R_1^2 - (R_1^2 + m/\pi) \ln R_2^2) + (R_0^2 + (\zeta+1)m/\pi) \ln R_2^2 - R_0^2 \ln R_1^2 \\
&= \zeta(R_2^2 - R_1^2) + (R_0^2 - (\zeta+1)R_1^2) \ln(R_2^2/R_1^2).
\end{aligned}$$

where the third equality is due to (4) and (5).

For $n = 3$, we obtain

$$\begin{aligned}
(\zeta+1)R_1^2 - R_0^2 &= \lambda/3 = (\zeta+1)R_2^2 - R_3^2, \quad \text{and} \\
2\frac{R_0^3}{R_1} - (3\zeta+2)R_1^2 - \frac{12\zeta^2 R_1^{-1}}{(\zeta+1)\gamma} &= \mu - \lambda = 2\frac{R_3^3}{R_2} - (3\zeta+2)R_2^2 + \frac{12\zeta^2 R_2^{-1}}{(\zeta+1)\gamma},
\end{aligned}$$

where μ and λ are Lagrange multipliers. □

Proof. [of Theorem B.3]

The 2-D case ($n = 2$)

We assume that ζ and γ are fixed. To obtain the asymptotics of R_i as $m \rightarrow \infty$, we use the change of variables $r_i = R_i^2 \pi/m$ and $\Gamma^{-1} = 4\zeta^2(\zeta+1)^{-1}(\pi/m)^{3/2}/\gamma$, therefore transforming (4), (5) and Proposition B.2 into the following

$$\begin{aligned}
r_3 - r_0 &= \zeta + 1 = (\zeta + 1)(r_2 - r_1), \\
r_3 \ln r_3 - r_0 \ln r_0 &= (\zeta + 1)(r_2 \ln r_2 - r_1 \ln r_1), \\
\Gamma^{-1}(1/\sqrt{r_1} + 1/\sqrt{r_2}) &= \zeta(r_2 - r_1) + (r_0 - (\zeta + 1)r_1) \ln(r_2/r_1),
\end{aligned}$$

or equivalently,

$$\begin{aligned}
r_3 &= r_0 + \zeta + 1, \quad r_2 = r_1 + 1, \\
\frac{r_3}{r_1} \ln \frac{r_3}{r_1} - \frac{r_0}{r_1} \ln \frac{r_0}{r_1} &= (\zeta + 1) \left(\frac{r_2}{r_1} \ln \frac{r_2}{r_1} - \frac{r_1}{r_1} \ln \frac{r_1}{r_1} \right), \\
\Gamma^{-1}(1/\sqrt{r_1} + 1/\sqrt{r_2})/r_1 &= \zeta(r_2/r_1 - 1) + (r_0/r_1 - (\zeta + 1)) \ln(r_2/r_1).
\end{aligned}$$

Using the change of variables $a = 1/r_1$ and $b = 1 - r_0/r_1$, we obtain

$$(1+a(\zeta+1)-b) \ln(1+a(\zeta+1)-b) - (1-b) \ln(1-b) = (\zeta+1)(1+a) \ln(1+a), \quad (15)$$

$$\Gamma^{-1}(\sqrt{a} + \sqrt{a/(1+a)})a = a\zeta - (b+\zeta) \ln(1+a). \quad (16)$$

Using the ansatz that $a, b \rightarrow 0$ as $\Gamma \rightarrow \infty$, by Taylor-expanding (15) around $a, b = 0$, we obtain

$$O(a^7 + b^7) = a(\zeta+1) \left(\frac{a\zeta}{2} - b - \zeta \frac{\zeta+2}{6} a^2 + \frac{\zeta+1}{2} ab - \frac{b^2}{2} + \dots \right).$$

Assuming $b = p_1 a + p_2 a^2 + p_3 a^3 + p_4 a^4 + p_5 a^5 + O(a^6)$ and plugging it into the above equation, we obtain

$$O(a^7) = a^2(\zeta+1) \left(\frac{\zeta}{2} - p_1 \right) - a^3(\zeta+1) \left(\zeta \frac{\zeta+2}{6} - \frac{\zeta+1}{2} p_1 + \frac{p_1^2}{2} + p_2 \right) + \dots,$$

from which we obtain the following solution

$$p_1 = \frac{\zeta}{2}, \quad p_2 = -\zeta \frac{\zeta+2}{24}, \quad p_3 = \zeta \frac{\zeta+2}{48}, \quad p_4 = -\zeta \frac{3\zeta^2+6\zeta+76}{5760/(\zeta+2)}, \quad p_5 = \zeta \frac{\zeta^2+2\zeta+12}{1280/(\zeta+2)}. \quad (17)$$

By plugging (17) into (16) and Taylor-expanding it around $a = 0$, we obtain

$$\Gamma^{-1} = \frac{\zeta^2}{48} \sqrt{a^3} - \frac{\zeta^2}{64} \sqrt{a^5} + \frac{\zeta^2+4\zeta+46}{3840/\zeta^2} \sqrt{a^7} - 7 \frac{\zeta^2+4\zeta+21}{15360/\zeta^2} \sqrt{a^9} + O(\sqrt{a^{11}}),$$

from which we obtain

$$\begin{aligned} a &= \frac{4}{(\Gamma \zeta^2/6)^{2/3}} + \frac{8}{(\Gamma \zeta^2/6)^{4/3}} - 4 \frac{2\zeta^2+8\zeta-43}{15(\Gamma \zeta^2/6)^2} - 16 \frac{2\zeta^2+8\zeta-13}{15(\Gamma \zeta^2/6)^{8/3}} + O\left(\frac{1}{\Gamma^{10/3}}\right) \\ &= \frac{2^4 \pi/m}{(\gamma(\zeta+1)/3)^{2/3}} + \frac{2^7 \pi^2/m^2}{(\gamma(\zeta+1)/3)^{4/3}} - \frac{2^8 \pi^3 (2\zeta^2+8\zeta-43)}{15m^3 (\gamma(\zeta+1)/3)^2} - \frac{2^{12} \pi^4 (2\zeta^2+8\zeta-13)}{15m^4 (\gamma(\zeta+1)/3)^{8/3}} + O\left(\frac{1}{m^5}\right), \end{aligned}$$

where the second equality is due to $\Gamma^{-1} = 4\zeta^2(\zeta+1)^{-1}(\pi/m)^{3/2}/\gamma$. According to the definition of a and b , we have

$$R_0 = \sqrt{m/\pi} \sqrt{(1-b)/a}, \quad R_1 = \sqrt{m/\pi} \sqrt{1/a}, \quad R_2 = \sqrt{m/\pi} \sqrt{1+1/a}, \quad R_3 = \sqrt{m/\pi} \sqrt{(1-b)/a+\zeta+1},$$

which allow us to compute the asymptotics of $E(U, V)$, $R_{i+1}-R_i$, $(R_1+R_2)/2$, and $(R_3^2-R_2^2) - (R_1^2-R_0^2)$.

The 3-D case ($n = 3$)

Similar to the 2-D case, we use the rescaling $r_i = R_i \sqrt[3]{4\pi/(3m)}$ and $\Gamma = 3m\gamma/(4\pi)$. Using the change of variables $a = r_0^{-3}$ and $b = r_1/r_0 - 1$, we transform (4), (5) and Proposition B.2 into the following

$$d^2 - 1 = (\zeta+1)(c^2 - (b+1)^2), \quad (18)$$

$$12\zeta^2 \Gamma^{-1} ((b+1)^{-1} + c^{-1}) a = (3\zeta+2)(d^2-1) + 2(\zeta+1)((b+1)^{-1} - d^3/c), \quad (19)$$

where $c = \sqrt[3]{a+(b+1)^3}$ and $d = \sqrt[3]{a(\zeta+1)+1}$. Using the ansatz that $a, b \rightarrow 0$ as $\Gamma \rightarrow \infty$, by Taylor-expanding (18) around $a, b = 0$, we obtain

$$O(a^7+b^7) = a(\zeta+1) \left(\frac{2b}{3} - \frac{a\zeta}{9} - \frac{2b^2}{3} - \frac{4ab}{9} + 4\zeta \frac{\zeta+2}{81} a^2 + \dots \right).$$

Assuming $b = p_1 a + p_2 a^2 + p_3 a^3 + p_4 a^4 + p_5 a^5 + O(a^6)$ and plugging it into the above equation, we obtain

$$O(a^7) = (\zeta+1) \frac{a^2}{9} (6p_1 - \zeta) + (\zeta+1) \frac{2a^3}{81} (2\zeta(\zeta+2) - 9p_1(3p_1+2) + 27p_2) + \dots,$$

from which we obtain the following solution

$$\begin{aligned} p_1 &= \frac{\zeta}{6}, \quad p_2 = -\zeta \frac{5\zeta+4}{108}, \quad p_3 = \zeta \frac{15\zeta^2+26\zeta+12}{648}, \quad p_4 = \frac{167\zeta^3+452\zeta^2+424\zeta+136}{-11664/\zeta}, \\ p_5 &= \frac{693\zeta^4+2561\zeta^3+3644\zeta^2+2348\zeta+576}{69984/\zeta}. \end{aligned} \quad (20)$$

By plugging (20) into (19) and Taylor-expanding it around $a = 0$, we obtain

$$\Gamma^{-1} = \frac{\zeta+1}{648}a^2 - \frac{(\zeta+1)^2}{648}a^3 + \frac{187\zeta^2+376\zeta+196}{139968/(\zeta+1)}a^4 - \frac{79\zeta^2+160\zeta+88}{69984/(\zeta+1)^2}a^5 + O(a^6).$$

from which we obtain

$$\begin{aligned} a &= \frac{18\sqrt{2/\Gamma}}{\sqrt{\zeta+1}} + \frac{324}{\Gamma} + \sqrt{2} \frac{83\zeta^2+164\zeta+74}{(\Gamma(\zeta+1))^{3/2}/27} + \frac{29\zeta^2+56\zeta+20}{\Gamma^2(\zeta+1)/972} + O\left(\frac{1}{\Gamma^{5/2}}\right) \\ &= \frac{12\sqrt{6\pi/m}}{\sqrt{\gamma(\zeta+1)}} + \frac{432\pi}{\gamma m} + 24\sqrt{6} \frac{83\zeta^2+164\zeta+74}{(\gamma(\zeta+1)m/\pi)^{3/2}} + 1728 \frac{29\zeta^2+56\zeta+20}{\gamma^2(\zeta+1)m^2/\pi^2} + O\left(\frac{1}{m^{5/2}}\right), \end{aligned}$$

where the second equality is due to $\Gamma = 3m\gamma/(4\pi)$. According to the definition of a and b , we have

$$R_0 = \sqrt[3]{\frac{3m}{4\pi a}}, \quad R_1 = (1+b)\sqrt[3]{\frac{3m}{4\pi a}}, \quad R_2 = \sqrt[3]{a+(1+b)^3} \sqrt[3]{\frac{3m}{4\pi a}}, \quad R_3 = \sqrt[3]{1+a(\zeta+1)} \sqrt[3]{\frac{3m}{4\pi a}},$$

which allow us to compute the asymptotics of $E(U, V)$, $R_{i+1}-R_i$, $(R_1+R_2)/2$, and $(R_3^3-R_2^3) - (R_1^3-R_0^3)$. \square

Proof. [of Proposition B.4] Our proof is similar to [62, Proof of Theorem 11]. Define $\kappa > 0$ via $\kappa^{-n} = (R_1^n + R_2^n)/2$, then according to (14), (4) and (5), we obtain

$$\begin{aligned} (R_0^2, R_1^2, R_2^2, R_3^2) &= \kappa^{-2} + (-\zeta-1, -1, 1, \zeta+1) m/(2\pi), \quad \text{for } n = 2, \\ (R_0^3, R_1^3, R_2^3, R_3^3) &= \kappa^{-3} + (-\zeta-1, -1, 1, \zeta+1) (3m)/(8\pi), \quad \text{for } n = 3. \end{aligned}$$

The 2-D case ($n = 2$)

Using a change of variables $\kappa = 2\pi t/m$, we obtain the following asymptotics for $E(U, V)$ given by Proposition B.1:

$$\frac{E(U, V)}{m} = \left(\frac{\zeta+1}{24}\gamma t^2 + \frac{2}{t}\right) + \pi^2 t^3 \frac{\gamma(\zeta+1)(\zeta^2+4\zeta+6)t^3-60}{60m^2} + O\left(\frac{1}{m^4}\right). \quad (21)$$

Minimizing $\gamma(\zeta+1)t^2/24+2/t$ with respect to t ($t > 0$) yields $t = 2\sqrt[3]{3/(\gamma\zeta+\gamma)}$ and

$$\frac{E(U, V)}{m} = \sqrt[3]{\gamma \frac{\zeta+1}{8/9}} + 24\pi^2 \frac{2\zeta^2+8\zeta+7}{5\gamma(\zeta+1)m^2} + O\left(\frac{1}{m^4}\right).$$

In order to obtain a more detailed asymptotics of t , we differentiate (21) with respect to t and find its root. Using the ansatz $t = 2\sqrt[3]{3/(\gamma\zeta+\gamma)} + Cm^{-2} + O(m^{-4})$, where C is independent of m , we obtain

$$\frac{1}{20m^2} \left(48\pi^2 \frac{4\zeta^2+16\zeta+19}{(\gamma(\zeta+1)/3)^{2/3}} + 5\gamma(\zeta+1)C \right) = O\left(\frac{1}{m^4}\right),$$

from which we can solve for C ,

$$C = -\frac{16}{5}\pi^2 \frac{4\zeta^2+16\zeta+19}{(\gamma(\zeta+1)/3)^{5/3}}.$$

We are then able to compute the asymptotics of $R_{i+1} - R_i$ and $(R_1 + R_2)/2$.

The 3-D case ($n = 3$)

Using a change of variables $\kappa = \sqrt{4\pi t/m}$, we obtain the following asymptotics for $E(U, V)$ given by Proposition B.1:

$$\frac{E(U, V)}{m} = \left(\frac{\zeta+1}{24} \gamma t^2 + \frac{2}{t} \right) + \pi t^2 \frac{7\gamma(\zeta+1)(\zeta^2+4\zeta+6)t^3 - 240}{120m} + O\left(\frac{1}{m^2}\right). \quad (22)$$

Minimizing $\gamma(\zeta+1)t^2/24 + 2/t$ with respect to t ($t > 0$) yields $t = 2\sqrt[3]{3/(\gamma\zeta+\gamma)}$ and

$$\frac{E(U, V)}{m} = \sqrt[3]{\gamma \frac{\zeta+1}{8/9}} + \frac{4\pi}{5m} \frac{7\zeta^2+28\zeta+32}{(\gamma(\zeta+1)/3)^{2/3}} + O\left(\frac{1}{m^2}\right).$$

In order to obtain a more detailed asymptotics of t , we differentiate (22) with respect to t and find its root. Using the ansatz $t = 2\sqrt[3]{3/(\gamma\zeta+\gamma)} + Cm^{-1} + O(m^{-2})$, where C is independent of m , we obtain

$$\frac{1}{4m} \left(8\pi \frac{7\zeta^2+28\zeta+38}{(\gamma(\zeta+1)/3)^{1/3}} + \gamma(\zeta+1)C \right) = O\left(\frac{1}{m^2}\right),$$

from which we can solve for C ,

$$C = -\frac{8}{3}\pi \frac{7\zeta^2+28\zeta+38}{(\gamma(\zeta+1)/3)^{4/3}}.$$

We are then able to compute the asymptotics of $R_{i+1} - R_i$ and $(R_1 + R_2)/2$. □

C Asymptotics with 1-Wasserstein distance

In this appendix we make some clarification of Remark 3.6-③. We are interested in $(R_1 - R_0) - (R_3 - R_2)$, which is the difference in the thickness between the inner and outer V layers. For $n = 2$, such a difference is $4\pi\rho^2(\zeta+2)\zeta/(\zeta m+m)$ in Corollary 3.4, and is $12\pi\rho^2(\zeta+2)\zeta/(\zeta m+m)$ in Corollary 3.5. The latter is exactly three times the former. Such a relation is also true for $n = 3$. As we explain below, this is still true for $n = 2$ in a variant model, where the Coulombic nonlocal term is replaced by the 1-Wasserstein distance (the case of $n = 3$ in this variant model is unclear to us since the thickness of V layers is not explicitly provided in [43]).

For this variant model, a candidate is constructed for the lim-sup inequality in [50, Section 8.1]. Using the notation in [50], $\kappa(s)$ in [50, Figure 8] is negative. The V layers is given by the following [50, Section 8.1]:

$$\text{supp}(v_\varepsilon) = \{\psi_+(q, t) : 0 \leq t \leq t_+(q, 1)\} \cup \{\psi_-(q, t) : t_-(q, -1) \leq t \leq 0\},$$

where

$$\begin{aligned} \psi_+(q, t) &:= \tilde{\gamma}_+(q) + t\tilde{v}_+(q), & \psi_-(q, t) &:= \tilde{\gamma}_-(q) + t\tilde{v}_-(q), \\ t_+(q, m) &= \left(1 - \sqrt{1 - 2\varepsilon\tilde{\kappa}_+m}\right) / \tilde{\kappa}_+, & t_-(q, m) &= \left(1 - \sqrt{1 - 2\varepsilon\tilde{\kappa}_-m}\right) / \tilde{\kappa}_-, \\ \tilde{\kappa}_+ &= \kappa/(1 - \varepsilon\kappa), & \tilde{\kappa}_- &= \kappa/(1 + \varepsilon\kappa). \end{aligned}$$

Therefore, the thickness of the inner V layer is

$$(1/|\kappa|-\varepsilon)\left(1 - \sqrt{3-2/(1-\varepsilon|\kappa|)}\right) = \varepsilon + \frac{\varepsilon^2|\kappa|}{2} + O(\varepsilon^3),$$

and the thickness of the outer V layer is

$$(1/|\kappa|+\varepsilon)\left(\sqrt{3-2/(1+\varepsilon|\kappa|)} - 1\right) = \varepsilon - \frac{\varepsilon^2|\kappa|}{2} + O(\varepsilon^3).$$

If we require the inner and outer V layers to have the same mass, then their thickness would be $\varepsilon+3|\kappa|\varepsilon^2/2+O(\varepsilon^3)$ and $\varepsilon-3|\kappa|\varepsilon^2/2+O(\varepsilon^3)$, respectively, with the difference being exactly three times that of the above lim-sup candidate.

References

- [1] Alama, S., Bronsard, L., Lu, X., and Wang, C. (2023). Core shells and double bubbles in a weighted nonlocal isoperimetric problem. *arXiv preprint [arXiv:2212.06381v4](https://arxiv.org/abs/2212.06381v4)*. Accepted by SIAM Journal on Mathematical Analysis.
- [2] Allhusen, J. S. and Conboy, J. C. (2017). The ins and outs of lipid flip-flop. *Accounts of Chemical Research*, 50(1):58–65.
- [3] Bauer, M. and Kuwert, E. (2003). Existence of minimizing Willmore surfaces of prescribed genus. *International Mathematics Research Notices*, 2003(10):553–576.
- [4] Ben-Shaul, A. and Gelbart, W. M. (1994). Statistical thermodynamics of amphiphile self-assembly: structure and phase transitions in micellar solutions. In *Micelles, Membranes, Microemulsions, and Monolayers*, pages 1–104. Springer.
- [5] Bonacini, M. and Cristoferi, R. (2014). Local and global minimality results for a nonlocal isoperimetric problem on \mathbb{R}^N . *SIAM Journal on Mathematical Analysis*, 46(4):2310–2349.
- [6] Bonacini, M. and Knüpfer, H. (2016). Ground states of a ternary system including attractive and repulsive Coulomb-type interactions. *Calculus of Variations and Partial Differential Equations*, 55:1–31.
- [7] Bonacini, M., Knüpfer, H., and Röger, M. (2016). Optimal distribution of oppositely charged phases: perfect screening and other properties. *SIAM Journal on Mathematical Analysis*, 48(2):1128–1154.
- [8] Brandt, E. G. (2011). *Molecular dynamics simulations of fluid lipid membranes*. PhD thesis, KTH Royal Institute of Technology.
- [9] Cesaroni, A. and Novaga, M. (2017). The isoperimetric problem for nonlocal perimeters. *Discrete and Continuous Dynamical Systems-S*, 11(3):425–440.
- [10] Chan, H., Nejad, M. J., and Wei, J. (2019). Lamellar phase solutions for diblock copolymers with nonlocal diffusions. *Physica D: Nonlinear Phenomena*, 388:22–32.

- [11] Choksi, R. (2012). On global minimizers for a variational problem with long-range interactions. *Quarterly of Applied Mathematics*, pages 517–537.
- [12] Choksi, R. and Peletier, M. A. (2010). Small volume fraction limit of the diblock copolymer problem: I. sharp-interface functional. *SIAM Journal on Mathematical Analysis*, 42(3):1334–1370.
- [13] Choksi, R. and Ren, X. (2003). On the derivation of a density functional theory for microphase separation of diblock copolymers. *Journal of Statistical Physics*, 113:151–176.
- [14] Choksi, R. and Ren, X. (2005). Diblock copolymer/homopolymer blends: derivation of a density functional theory. *Physica D: Nonlinear Phenomena*, 203(1-2):100–119.
- [15] Creasy, M. A. and Leo, D. J. (2008). Self-healing bilayer lipid membranes formed over synthetic substrates. In *Smart Materials, Adaptive Structures and Intelligent Systems*, volume 43321, pages 601–606.
- [16] Damodaran, K., Merz Jr, K. M., and Gaber, B. P. (1992). Structure and dynamics of the dilauroylphosphatidylethanolamine lipid bilayer. *Biochemistry*, 31(33):7656–7664.
- [17] Delfour, M. C. and Zolésio, J.-P. (2011). *Shapes and Geometries*, chapter 7. Metrics via oriented distance functions, pages 335–408. [Society for Industrial and Applied Mathematics](#), 2 edition.
- [18] Deng, Y. and Mieczkowski, M. (1998). Three-dimensional periodic cubic membrane structure in the mitochondria of amoebae *chaos carolinensis*. *Protoplasma*, 203:16–25.
- [19] Dipierro, S., Novaga, M., and Valdinoci, E. (2017). Rigidity of critical points for a nonlocal Ohta–Kawasaki energy. *Nonlinearity*, 30(4):1523.
- [20] Du, Q., Liu, C., and Wang, X. (2006). Simulating the deformation of vesicle membranes under elastic bending energy in three dimensions. *Journal of Computational Physics*, 212(2):757–777.
- [21] Evans, L. C. and Gariepy, R. F. (2015). *Measure Theory and Fine Properties of Functions, Revised Edition*. [Chapman and Hall/CRC](#).
- [22] Fall, M. M. (2018). Periodic patterns for a model involving short-range and long-range interactions. *Nonlinear Analysis*, 175:73–107.
- [23] Figalli, A. and Glaudo, F. (2021). *An Invitation to Optimal Transport, Wasserstein Distances, and Gradient Flows*. [EMS Press](#).
- [24] Figueirido, F., Del Buono, G. S., and Levy, R. M. (1995). On finite-size effects in computer simulations using the Ewald potential. *The Journal of Chemical Physics*, 103(14):6133–6142.
- [25] Fonseca, I. and Leoni, G. (2007). *Modern Methods in the Calculus of Variations: L^p Spaces*. Springer Science & Business Media.
- [26] Fourcade, B., Mutz, M., and Bensimon, D. (1992). Experimental and theoretical study of toroidal vesicles. *Physical Review Letters*, 68(16):2551.

- [27] Gilbarg, D. and Trudinger, N. S. (2001). *Elliptic Partial Differential Equations of Second Order, Reprint of the 1998 Edition*. Springer Science & Business Media.
- [28] Glasner, K. and Orizaga, S. (2018). Multidimensional equilibria and their stability in copolymer-solvent mixtures. *Physica D: Nonlinear Phenomena*, 373:1–12.
- [29] Goldman, M. and Runa, E. (2019). On the optimality of stripes in a variational model with non-local interactions. *Calculus of Variations and Partial Differential Equations*, 58(3):103.
- [30] Guckenberger, A. and Gekle, S. (2017). Theory and algorithms to compute Helfrich bending forces: a review. *Journal of Physics: Condensed Matter*, 29(20):203001.
- [31] Han, L. and Che, S. (2018). An overview of materials with triply periodic minimal surfaces and related geometry: from biological structures to self-assembled systems. *Advanced Materials*, 30(17):1705708.
- [32] Han, Y., Xu, Z., Shi, A.-C., and Zhang, L. (2020). Pathways connecting two opposed bilayers with a fusion pore: a molecularly-informed phase field approach. *Soft Matter*, 16(2):366–374.
- [33] Hecce, H. D., Garcia, A. E., and Darden, T. (2007). The electrostatic surface term: (I) periodic systems. *The Journal of Chemical Physics*, 126(12).
- [34] Hsu, L., Kusner, R., and Sullivan, J. (1992). Minimizing the squared mean curvature integral for surfaces in space forms. *Experimental Mathematics*, 1(3):191–207.
- [35] Hummer, G., Pratt, L. R., and García, A. E. (1998). Molecular theories and simulation of ions and polar molecules in water. *The Journal of Physical Chemistry A*, 102(41):7885–7895.
- [36] Ingólfsson, H. I., Melo, M. N., van Eerden, F. J., Arnarez, C., Lopez, C. A., Wassenaar, T. A., Periole, X., De Vries, A. H., Tieleman, D. P., and Marrink, S. J. (2014). Lipid organization of the plasma membrane. *Journal of the American Chemical Society*, 136(41):14554–14559.
- [37] Jia, W., Wang, H., Chen, M., Lu, D., Lin, L., Car, R., Weinan, E., and Zhang, L. (2020). Pushing the limit of molecular dynamics with ab initio accuracy to 100 million atoms with machine learning. In *SC20: International Conference for High Performance Computing, Networking, Storage and Analysis*, pages 1–14. IEEE.
- [38] Kantorovich, L. and Tupitsyn, I. (1999). Coulomb potential inside a large finite crystal. *Journal of Physics: Condensed Matter*, 11(32):6159.
- [39] Kuwert, E., Li, Y., and Schätzle, R. (2010). The large genus limit of the infimum of the Willmore energy. *American Journal of Mathematics*, 132(1):37–51.
- [40] Leoni, G. (2013). Gamma convergence and applications to phase transitions. Lecture notes from 2013 CNA Summer School “Topics in Nonlinear PDEs and Calculus of Variations, and Applications in Materials Science”, Center for Nonlinear Analysis, Carnegie Mellon University. Accessible at <https://www.mat.univie.ac.at/~stefanelli/cv/paper1.pdf> or https://www.iam.uni-bonn.de/fileadmin/user_upload/stinson/leoni-modicaMortola.pdf. A different version is available at https://www.math.cmu.edu/~tblass/CNA-PIRE/Leoni_modica-mortola-lecture-2012-02-17.pdf. Last accessed on 2024/01/01.

- [41] Lin, Z., Liu, S., Mao, W., Tian, H., Wang, N., Zhang, N., Tian, F., Han, L., Feng, X., and Mai, Y. (2017). Tunable self-assembly of diblock copolymers into colloidal particles with triply periodic minimal surfaces. *Angewandte Chemie*, 129(25):7241–7246.
- [42] Luo, W. and Zhao, Y. (2022). Nonlocal effect on a generalized Ohta-Kawasaki model. *arXiv preprint arXiv:2204.05394v1*.
- [43] Lussardi, L., Peletier, M. A., and Röger, M. (2014). Variational analysis of a mesoscale model for bilayer membranes. *Journal of Fixed Point Theory and Applications*, 15:217–240.
- [44] Marques, F. C. and Neves, A. (2014). Min-max theory and the Willmore conjecture. *Annals of Mathematics*, pages 683–782.
- [45] Marrink, S. J., Corradi, V., Souza, P. C., Ingolfsson, H. I., Tieleman, D. P., and Sansom, M. S. (2019). Computational modeling of realistic cell membranes. *Chemical Reviews*, 119(9):6184–6226.
- [46] Martine-La Boissoniere, G., Choksi, R., and Lessard, J.-P. (2022). Microscopic patterns in the 2d phase-field-crystal model. *Nonlinearity*, 35(3):1500.
- [47] Michalet, X. and Bensimon, D. (1995). Vesicles of toroidal topology: observed morphology and shape transformations. *Journal de Physique II*, 5(2):263–287.
- [48] Muratov, C. B. (2002). Theory of domain patterns in systems with long-range interactions of Coulomb type. *Physical Review E*, 66(6):066108.
- [49] Mutz, M. and Bensimon, D. (1991). Observation of toroidal vesicles. *Physical Review A*, 43(8):4525.
- [50] Peletier, M. A. and Röger, M. (2009). Partial localization, lipid bilayers, and the elastica functional. *Archive for Rational Mechanics and Analysis*, 193:475–537.
- [51] Porcar, L. and Gerelli, Y. (2020). On the lipid flip-flop and phase transition coupling. *Soft Matter*, 16(33):7696–7703.
- [52] Porte, G. (1994). Micellar growth, flexibility and polymorphism in dilute solutions. In *Micelles, Membranes, Microemulsions, and Monolayers*, pages 105–151. Springer.
- [53] Ren, X. and Wei, J. (2003). Triblock copolymer theory: free energy, disordered phase and weak segregation. *Physica D: Nonlinear Phenomena*, 178(1-2):103–117.
- [54] Roberts, J. E. and Schnitker, J. (1994). How the unit cell surface charge distribution affects the energetics of ion–solvent interactions in simulations. *The Journal of Chemical Physics*, 101(6):5024–5031.
- [55] Sadeghi, M. and Noé, F. (2020). Large-scale simulation of biomembranes incorporating realistic kinetics into coarse-grained models. *Nature Communications*, 11(1):2951.
- [56] Schwarz, U. and Gompper, G. (2002). Bicontinuous surfaces in self-assembling amphiphilic systems. In *Morphology of Condensed Matter: Physics and Geometry of Spatially Complex Systems*, volume 600, pages 107–151. Springer.

- [57] Seifert, U. (1997). Configurations of fluid membranes and vesicles. *Advances in Physics*, 46(1):13–137.
- [58] Singer, S. J. and Nicolson, G. L. (1972). The fluid mosaic model of the structure of cell membranes: cell membranes are viewed as two-dimensional solutions of oriented globular proteins and lipids. *Science*, 175(4023):720–731.
- [59] Smith, E. R. (1981). Electrostatic energy in ionic crystals. *Proceedings of the Royal Society of London. A. Mathematical and Physical Sciences*, 375(1763):475–505.
- [60] Sternberg, P. (1988). The effect of a singular perturbation on nonconvex variational problems. *Archive for Rational Mechanics and Analysis*, 101:209–260.
- [61] van Gennip, Y. (2008). *Partial Localisation in a Variational Model for Diblock Copolymer-homopolymer Blends*. PhD thesis, [Technische Universiteit Eindhoven](#).
- [62] van Gennip, Y. and Peletier, M. A. (2008). Copolymer–homopolymer blends: global energy minimisation and global energy bounds. *Calculus of Variations and Partial Differential Equations*, 33:75–111.
- [63] van Gennip, Y. and Peletier, M. A. (2009). Stability of monolayers and bilayers in a copolymer-homopolymer blend model. *Interfaces and Free Boundaries*, 11(3):331–373.
- [64] van Gennip, Y. and Peletier, M. A. (2011). The H^{-1} -norm of tubular neighbourhoods of curves. *ESAIM: Control, Optimisation and Calculus of Variations*, 17(1):131–154.
- [65] Wang, X., Li, S., and Cai, Y. (2021). Analytical calculation of the elastic moduli of self-assembled liquid-crystalline bilayer membranes. *The Journal of Physical Chemistry B*, 125(20):5309–5320.
- [66] Willmore, T. J. (1965). Note on embedded surfaces. *An. Sti. Univ. “Al. I. Cuza” Iasi Sect. I a Mat.(NS) B*, 11(493-496):20.
- [67] Willmore, T. J. (1993). *Riemannian Geometry*. [Oxford University Press](#).
- [68] Xu, Z. and Du, Q. (2022). On the ternary Ohta–Kawasaki free energy and its one-dimensional global minimizers. *Journal of Nonlinear Science*, 32:61.
- [69] Xu, Z. and Du, Q. (2023). Bifurcation and fission in the liquid drop model: a phase-field approach. *Journal of Mathematical Physics*, 64(7):071508.